

**Dynamics, regulation and function
of macrophages in skin repair**

Inaugural-Dissertation

zur
Erlangung des Doktorgrades
der Mathematisch-Naturwissenschaftlichen Fakultät
der Universität zu Köln

vorgelegt von

Tina Lucas
aus Krefeld

Köln, 2011

Berichtersteller:

Prof. Dr. Matthias Hammerschmidt

PD Dr. Roswitha Nischt

Tag der mündlichen Prüfung: 05. Juli 2011

Summary

Tissue repair is a highly dynamic process comprising the sequential phases of inflammation, tissue formation, and maturation. The mechanisms that orchestrate the natural sequence of the wound healing response remain elusive. Influx of macrophages plays a crucial role in tissue repair. However, the precise function of macrophages during the healing response has remained a subject of debate due to their functional dichotomy as effectors of both, tissue injury and repair. In this study the hypothesis was examined whether macrophages recruited during the diverse phases of skin repair after mechanical injury exert specific functions to restore tissue integrity. For this purpose a mouse model was developed that allows conditional depletion of macrophages during the sequential stages of the repair response by using the inducible diphtheria toxin receptor mouse model in combination with a myeloid cell-specific *Cre* mouse line. Depletion of macrophages restricted to the early stage of the repair response (inflammatory phase) significantly reduced the formation of a vascularized granulation tissue and showed impaired re-epithelialization. However, recruitment of macrophages during the mid phase of repair, after macrophage depletion was stopped, rescued the impaired healing response and resulted in minimized scar formation. In contrast, depletion of macrophages restricted to the mid stage of the repair response (phase of tissue formation) resulted in severe hemorrhages within the wound tissue. Under these conditions, transition into the subsequent phase of tissue maturation and wound closure did not occur. Finally, macrophage depletion restricted to the late stage of repair (phase of tissue maturation) did not significantly impact the outcome of the repair response. Taken together, these results demonstrate that macrophages exert distinct functions during the different phases of skin repair, which are crucial to control the natural sequence of repair events. Furthermore, the effect of macrophages on endothelial cell function and wound angiogenesis appeared to be critical. Therefore the impact of macrophage-derived vascular endothelial growth factor-A (VEGF-A) on the outcome of the wound healing response was analyzed, by using conditional gene targeting to specifically deplete VEGF-A expression in myeloid cells. It could be shown that during the early phase of repair, myeloid cell-derived VEGF-A is essential to induce the angiogenic response, in contrast, at later stages of the wound healing response epidermal-derived VEGF-A controls vascular growth. We further showed that myeloid cell-derived VEGF-A is critical for tip cell formation, a process fundamental for vascular sprouting. Collectively, our findings propose novel mechanistic insights on macrophage-mediated repair events after skin injury and potentially might identify new therapeutic targets that can promote wound angiogenesis in impaired wound healing conditions.

Zusammenfassung

Wundheilung ist ein komplexer und dynamischer Prozess, der mehrere Phasen umfasst: Entzündung, Gewebebildung und -reifung. Die Mechanismen, die diese Abfolge der Wundheilung kontrollieren sind bisher wenig verstanden. Auf der Grundlage bereits bekannter Untersuchungen ist davon auszugehen, dass Makrophagen eine wichtige Funktion im Heilungsprozess übernehmen. Dennoch ist ihre genaue Aufgabe noch ungeklärt. Zum einen sind Makrophagen bedeutend für die Immunabwehr in offenen kutanen Wunden, zum anderen spielen sie aber auch eine entscheidende Rolle bei der Gewebeheilung. In dieser Arbeit wurde der Hypothese nachgegangen, dass Makrophagen in den individuellen Phasen der Wundheilung unterschiedliche Funktionen ausüben. Um dieser Fragestellung nachgehen zu können, wurde ein Mausmodell entwickelt, in dem spezifisch und induzierbar Makrophagen depletiert werden können. Dazu wurde eine transgene Mauslinie verwendet in der der humane Diphtherietoxinrezeptor nur in myeloiden Zellen exprimiert wird. Makrophagendepletion in der frühen Entzündungsphase der Wundheilung resultierte in einer signifikant verringerten Bildung von Granulationsgewebe und einer verzögerten Reepithelisierung. Dahingegen bewirkte eine Makrophagendepletion in der folgenden Phase der Gewebeneubildung massive Hämorrhagien im Wundgewebe, so dass eine Reifung der Wunde zu einem stabilen Narbengewebe nicht stattfinden konnte und es zu keinem Wundschluss kam. Eine Makrophagendepletion in der späten Phase der Wundheilung, der Phase der Gewebereifung, hatte keinen wesentlichen Effekt auf den Verlauf der Heilung. Die bisherigen Ergebnisse zeigen deutlich, dass Makrophagen unterschiedliche Funktionen in den individuellen Phasen der Wundheilung ausüben, welche für den physiologischen Ablauf der Heilung entscheidend sind. Darüber hinaus scheinen Makrophagen einen wichtigen Einfluss auf die Funktion von Endothelzellen auszuüben. Aus diesem Grund wurde die Bedeutung von Makrophagen-spezifischem vaskulären endotheliale Wachstumsfaktor-A (VEGF-A) in der Wundheilung analysiert, indem VEGF-A spezifisch in myeloiden Zellen deletiert wurde. Es konnte gezeigt werden, dass speziell von myeloiden Zellen sezerniertes VEGF-A in der frühen Phase der Wundheilung die Angiogenese stimuliert. Im Gegenzug gewinnt epidermales VEGF-A in den späteren Phasen der Wundheilung an Bedeutung. Darüber hinaus erscheint myeloid Zell-spezifisches VEGF-A wichtig für die Bildung von neusprießenden Gefäßen in der frühen Phase der Wundheilung zu sein, ein fundamentaler Prozess der Wundangiogenese. Zusammenfassend liefern diese Daten neue mechanistische Einblicke in die Makrophagen-vermittelte Wundheilung und bieten möglicherweise neue therapeutische Angriffspunkte zur Unterstützung der Wundangiogenese bei Ischämie und chronischen Wundheilungsstörungen.

Table of contents

1 Introduction.....	1
1.1 Skin morphology and function	1
1.2 Physiological skin repair	2
1.2.1 The inflammatory phase	2
1.2.2 The tissue formation phase	3
1.2.3 The tissue maturation phase	4
1.3 Macrophages.....	5
1.3.1 Macrophage origin.....	5
1.3.2 Macrophage activation and function.....	7
1.3.3 The role of macrophages in wound healing	8
1.4 Vascular endothelial growth factor-A.....	9
1.4.1 VEGF function in angiogenesis	11
1.4.2 The role of VEGF and macrophage-derived VEGF in wound repair.....	13
2 Specific aims.....	15
3 Results.....	16
3.1 Cell type specific and timely restricted depletion of macrophages in LysMCre/iDTR mice	16
3.2 Macrophage function during the different stages of repair	19
3.2.1 Macrophage function during the early stage of repair	19
3.2.1.1 Macrophages recruited during the inflammatory phase of repair induce granulation tissue formation, which results in scar formation.....	19
3.2.1.2 Macrophage depletion in wounds of LysMCre/iDTR mice receiving DT injections following regimen A	24
3.2.1.3 Wound vascularization and contraction is controlled by macrophage influx during the inflammatory phase of repair	26
3.2.1.4 Macrophage recruitment during the inflammatory phase of repair promotes alternative activation.....	28
3.2.2 Analysis of macrophage depletion during the mid stage of repair	30
3.2.2.1 Macrophages recruited during the inflammatory phase of tissue formation control vascular stability and the transition of granulation tissue into scar tissue	30
3.2.2.2 Endothelial cell damage and apoptosis in macrophage-depleted granulation tissue ...	33
3.2.3 Analysis of macrophage depletion during the late stage of repair	35
3.2.3.1 Macrophages present at the late stage of repair do not impact tissue maturation	35
3.3 The impact of myeloid cell-derived VEGF-A on the outcome of the wound healing response.....	38
3.3.1 Macrophages are the prevailing VEGF-A source in the early phase of tissue repair	38
3.3.2 VEGF expressing macrophages reveal a pro-inflammatory M1 phenotype	41
3.3.3 Efficient VEGF gene deletion in macrophages.....	41
3.3.4 VEGF synthesis by myeloid cells is critical for the induction of wound angiogenesis and tissue growth during the early phase of repair	45
3.3.5 Epidermal-derived VEGF is critical for wound angiogenesis during the late phase of tissue repair.....	48
3.3.6 Myeloid cell-derived VEGF controls tip cell formation and the spatial association between macrophages and sprouting vessels during the early phase of tissue repair	55
4 Discussion	58

4.1 Eligible mouse model for inducible and timely-restricted depletion of macrophages	58
4.2 Macrophage functions during the early phase of repair	59
4.2.1 Macrophages recruited during the inflammatory phase of repair induce a highly vascularized granulation tissue, which results in scar formation.....	59
4.2.2 Myeloid cell-derived VEGF initiates the angiogenic response in the early phase of the wound healing response.....	60
4.2.2.1 Myeloid cell-derived VEGF controls tip cell formation and the spatial association between macrophages and sprouting vessels during the early phase of tissue repair.....	62
4.2.3 Macrophage depletion during the early phase of repair attenuates alternative activation ...	63
4.3 Macrophage depletion during the mid stage of repair abrogates transition into scar tissue and causes vessel instability	65
4.4 Macrophages present at the late stage of repair do not impact tissue maturation	67
4.5 Model: Macrophages as sentinels directing the quality of skin repair.....	67
5 Material and Methods	69
5.1 Material	69
5.1.1 Chemicals and enzymes	69
5.1.2 Buffers used.....	69
5.1.3 Kits.....	69
5.1.4 Oligonucleotides	70
5.1.5 Antibodies	71
5.1.6 Special technical equipment.....	72
5.1.7 Software.....	72
5.2 Standard molecular biology methods	72
5.2.1 RNA extraction, RT PCR and quantitative real time PCR	72
5.2.1.1 Mouse angiogenesis real time PCR array.....	73
5.2.2 RNA quantification.....	73
5.2.3 Isolation of genomic DNA	73
5.2.4 Polymerase chain reaction (PCR)	74
5.2.5 VEGF-specific ELISA	74
5.3 Mice.....	74
5.3.1 Mouse strains	74
5.3.2 Genotyping	75
5.3.3 Administration of diphtheria toxin	75
5.3.4 Thioglycolate-induced peritonitis	76
4.3.5 Wounding.....	76
5.4 Flow cytometrie.....	77
5.4.1 Single cell suspensions	77
5.4.1.1 Peritoneal lavage.....	77
5.4.1.2 Blood leukocyte cell suspension	77
5.4.1.3 Wound cell suspension.....	77
5.4.2 FACS staining.....	78
5.4.2.1 FDG staining.....	78
5.5 Cultivation of macrophages	79
5.6 Histology	79
5.6.1 Histochemistry.....	79

5.6.2 Immunohistochemistry.....	80
5.6.3 X-Gal staining	80
5.6.4 Morphometric analysis.....	82
5.6.4.1 Quantification of wound healing parameters	82
5.6.4.2 Quantification of histochemical stainings	83
5.6.4.3 Quantification of immunohistochemical stainings.....	83
5.7 Statistical analysis	83
6 References	84
7 Abbreviations.....	89

1 Introduction

1.1 Skin morphology and function

The skin is the largest organ in mammals and protects the organism from the surrounding environment. This anatomical barrier protects the inside from pathogens and UV-damage, but it is also a water resistant barrier protecting from liquid and nutrient loss. Furthermore, this organ is an important storage compartment for water and lipids, and the place of vitamin D synthesis. The skin contains nerve endings sensing heat and cold, touch, pressure and pain and protects the organism in this way passively from mechanical damage. It is highly vascularized and therefore important in thermoregulation by controlled vascular contraction and dilatation, respectively.

Structurally, the skin is divided into three layers, the cell-rich epidermis, the collagen-rich dermis and the subcutis, consisting of fat tissue. The epidermis is a stratified squamous epithelium and consists mainly of keratinocytes, but also hosts Langerhans cells, melanocytes and merkel cells. The epidermis is renewed constantly [1]. Keratinocytes originate from stem cells in the basal cell layer and differentiate on their way through the different epidermal layers until they reach the *stratum corneum*, where they undergo apoptosis and build up this layer. The layers between the *stratum basale* and the *stratum corneum* are named *stratum spinosum* and *stratum granulosum* and are characterized by the different differentiation states and a specific expression pattern of keratinocytes. The epidermis itself is anchored via hemidesmosomes to the basement membrane, which is a thin sheet of fibers and mediates the contact to the dermis (for review see [2]). The dermis predominantly consists of connective tissue characterized by a strong tensile strength. Its major constituent are cross-linked collagen bundles, with collagen type I being the major collagen found, and elastin fibers. Embedded in this network the most common cell type found in the dermis is the fibroblast, but also cells from the innate immune system, such as mast cells or macrophages are located there. Both collagen and elastin fibers as well as the cells are embedded in a basic substance consisting of glycosaminoglycans and proteoglycans, which are produced by fibroblasts [3]. Furthermore, although coming from and anchored in the epidermis, the dermis hosts appendages of the skin, namely hair follicles, sebaceous glands and sweat glands. It also carries many blood and lymphatic vessels. Without a defined border the dermis merges into the subcutis. This subcutaneous fat layer is less elastic, but rich in blood vessels and lipocytes and is directly lying on the muscle fascia. A cartoon illustrating skin structure is shown in figure 1 A.

1.2 Physiological skin repair

Restoration of skin integrity and homeostasis following injury is a vital process, because the skin serves as a protective barrier against pathogens and water loss and any break in it must be rapidly and efficiently mended [4]. Across different species this event requires a complex and dynamic interplay of epithelial and mesenchymal cells in concert with tissue resident and recruited hematopoietic cells to accomplish the sequential phases of the repair response: inflammation, tissue formation and maturation [5-8].

1.2.1 The inflammatory phase

Skin injury causes blood vessel damage. To prevent blood loss, a clot is formed which consists of platelets embedded in a fibrin-fibronectin network. The clot further serves as a provisional matrix over and into which cells can migrate, and in the same time it is also a reservoir for cytokines and growth factors released by activated platelets [4]. These factors are important to recruit inflammatory cells from the circulation to the site of injury, which initiate the subsequent wound healing steps. Within a few hours post injury, polymorphonuclear leukocytes (PMN, neutrophils) transmigrate across the endothelial cell wall of blood vessels by adhesion to P- and E-selectin as well as to the inter-cellular adhesion molecules 1 and 2 (ICAM-1 and -2). Bacterial compounds such as lipopolysaccharides (LPS) and formyl-methionyl peptides can accelerate the directed neutrophil locomotion. Recruited neutrophils begin the debridement of devitalized tissue and phagocytosis of infectious agents. For this purpose they release reactive oxygen species (ROS) and a cocktail of different proteases such as elastase, proteinase 3 and cathepsin G [9]. Under physiological situations, neutrophils normally disappear after a few days of healing as they become phagocytosed by macrophages, appearing at the wound site around two days post injury. Besides some tissue-resident macrophages already present at the site of injury, the main portion of macrophages is recruited from the blood. Macrophage infiltration is regulated by gradients of different chemotactic factors, such as macrophage inflammatory protein-1 α (MIP-1 α) and chemokine (C-C motif) ligand 2 (CCL2, also known as monocyte chemoattractant protein-1, MCP-1) [10, 11], which are secreted by platelets, hyperproliferative keratinocytes, fibroblasts and leukocyte-subsets themselves. Monocytes leave the blood stream via adhesion to selectins, ICAMs or integrins, which are expressed by endothelial cells. After leaving the circulation, they differentiate in the wound environment to become mature and activated tissue macrophages due to different stimuli. Besides their immunological functions as antigen presenting cells and phagocytes, they are important sources of growth factors, such as transforming growth factor- β (TGF- β), basic fibroblast growth factor (bFGF, FGF2), platelet-derived growth factor (PDGF) and vascular endothelial

Introduction

growth factor-A (VEGF-A), which promote directly or indirectly angiogenesis, cell proliferation and the synthesis of extracellular matrix (ECM) molecules by resident skin cells [12]. In contrast to neutrophils, macrophages stay at the wound site for the subsequent healing phases. The cartoon in figure 1 B illustrates the critical events of the inflammatory phase.

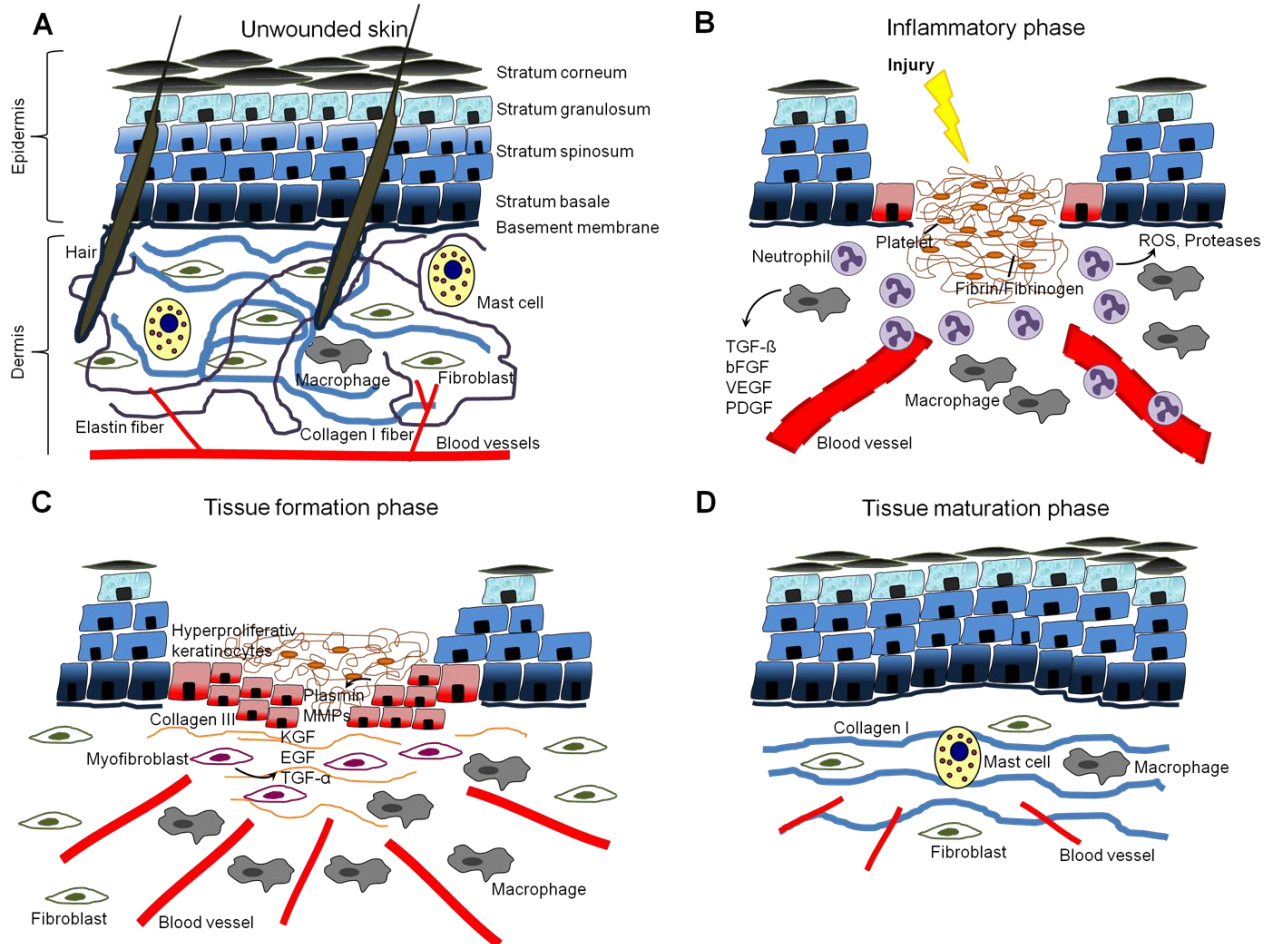


Figure 1: Skin morphology and the physiological sequence of wound healing. (A) Cartoon of normal unwounded skin, divided into in the keratinocyte-rich epidermis and the collagen-rich dermis. **(B)** The inflammatory response three days post injury. A fibrin/fibrinogen-rich clot is formed and a lot of inflammatory cells are recruited. **(C)** The tissue formation phase five to seven days post injury. Keratinocytes start to proliferate in order to reach wound closure. Myofibroblasts and new blood vessels are present to support wound healing. **(D)** Late phase of the tissue maturation phase resulting in a remaining scar tissue.

1.2.2 The tissue formation phase

The mid stage of the repair response consists of the phase of tissue formation, which is characterized by the development of granulation tissue, refilling the dermal wound space, and keratinocyte proliferation that closes the epidermal gap. Granulation tissue formation

Introduction

encompasses the invasion of endothelial cells and angiogenesis, the influx of fibroblasts, differentiating into myofibroblasts, and the accumulation of additional macrophages.

During neo-angiogenesis, new vessels sprout out of existing vessels and along growth factor gradients, mainly consisting of VEGF-A and bFGF secreted by keratinocytes, macrophages, and other cell types [4]. To mediate this outgrowth, endothelial cells have to degrade the basement membrane and the surrounding ECM, which is accomplished by the expression of proteases, mainly matrix metalloproteases (MMPs), serin, and cystein proteases [13]. Furthermore, they have to alternate their integrin expression for the adhesion to the provisional ECM and successful migration [14]. Contemporaneous resident dermal fibroblasts start to proliferate and migrate from the adjacent unwounded skin area into the provisional matrix of the wound bed, in response to secreted TGF- β . Once arrived, they produce a new collagen-rich matrix, mostly consisting of collagen type III. Besides of collagen deposition, some fibroblasts transform into myofibroblasts, which express α -smooth muscle actin (α -SMA) and promote wound contraction [15]. Wound contraction is a concerted action mediated by cell-cell and cell-matrix contacts as well as by tractional forces generated by migrating cells within the collagen matrix [16]. This contractile force supports the contemporaneously keratinocyte hyperproliferation and migration at the wound edge in order to restore the epidermal barrier, finally leading to wound closure. Growth factors which support proliferation and migration of keratinocytes are mainly epidermal growth factor (EGF), transforming growth factor- α (TGF- α) and keratinocyte growth factor (KGF) expressed by keratinocytes and dermal fibroblasts. As mentioned above in unwounded skin keratinocytes are attached to the basement membrane. This contact has to be dissolved and the integrin expression profile needs to be changed to allow crawling over the provisional fibrin-fibronectin wound matrix [17]. By expression of proteases, mainly plasmin and MMPs, keratinocytes carve path through the fibrin clot and the underlying dermal granulation tissue. Once the wound area has been covered by a layer of keratinocytes their migration stops, and a new basal lamina is synthesized, to which both keratinocytes and fibroblasts contribute [17], followed by reestablishment of the stratified epithelium starting at the wound margins [18]. Granulation tissue formation continues until the wound space is refilled and the overlaying epidermis is restored. The critical events of the tissue formation phase are illustrated in figure 1 C.

1.2.3 The tissue maturation phase

Upon completion of the epidermal barrier, the repair response enters the last and longest stage, which is characterized by tissue maturation. During the phase of tissue maturation

Introduction

granulation tissue transforms into scar tissue, characterized by attenuated cell proliferation, inflammation, neovascularization as well as replacement of the provisional matrix by deposition of collagen. Remaining vessels mature by recruitment of pericytes and the network re-organizes by pruning [19]. Most endothelial cells, macrophages and myofibroblasts undergo apoptosis or exit the wound, leaving a cell-poor and ECM-rich scar tissue [5]. Collagen type III, predominating in the wound matrix, is exchanged by a collagen type I network which is re-arranged, cross-linked and aligned along tension lines to increase tensile strength [20]. This process is supported by MMPs secreted by fibroblasts, macrophages and endothelial cells and strengthens the remaining scar tissue. However, tensile strength of uninjured skin is never re-established [21]. Also skin appendages like hairs and sweat glands are not regenerated. Figure 1 D illustrates the remaining scar tissue after wounding.

1.3 Macrophages

1.3.1 Macrophage origin

Organisms are exposed to many different pathogens in their environment. Besides physical barriers like the skin protecting the inner organism from pathogen infection passively, multi-cellular organisms developed additional immune host defense mechanisms against pathogens which are carried out by specialized cells and proteins. Vertebrates use two types of immune defense, first the rapid but pathogen-unspecific innate immune response and second the more effective and pathogen-specific adaptive immune response. The innate immune system is the first line of defense against invading pathogens. It is composed of different cell types including mast cells, dendritic cells (DCs), natural killer cells (NK cells), neutrophils and macrophages. Mast cells spontaneously degranulate upon infection and release different pro-inflammatory cytokines which in turn recruit other innate immune cells for phagocytosis and degradation of the invaded pathogens. Macrophages and DCs further link the innate and the adaptive immune response by presenting antigens to the corresponding T helper cells, effector cells of the adaptive immune system. Macrophages and many other leukocytes do not normally divide or reproduce by themselves. They develop from multipotent hematopoietic stem cells (HSCs) in the bone marrow. Two cell lineages originate from HSCs, the lymphoid lineage, containing T-, B-, and NK cells and the myeloid lineage, containing macrophages, neutrophilic granulocytes, and DCs among others.

The first developing stadium of macrophages is the highly proliferative monoblast which resides in the bone marrow and develops to the promonocyte stadium. The promonocytic

Introduction

stadium is mainly found in the bone marrow as well, but can also enter the blood circulation, which is the main location for the following maturation state the monocytic stadium (Figure 2). Monocytes share already some typical features of macrophages such as phagocytic capacity and adhesion to specific endothelial cell molecules. They are a systemic reservoir for the renewal of tissue macrophages and DCs [22, 23]. Monocyte development depends on the availability of the growth factor colony-stimulating factor-1 (Csf-1, also known as macrophage colony-stimulating factor, M-CSF, and CD115) [24]. Different subpopulations of monocytes have been described in the circulation of mouse and humans, which are distinguishable by a different expression pattern of cell surface marker proteins [25, 26]. It is speculated that in mouse the Ly-6C^{high} expressing monocyte subset is related to inflammatory conditions whereas the Ly-6C^{low} subset takes part in the renewal of tissue macrophages [26]. The majority of macrophages are stationed at critical points to police the respective organ in case of emergency. These so called tissue resident macrophages are found in skin, lung (alveolar macrophages), liver (Kupffer cells), bone (osteoclasts), neural tissue (microglia) and spleen (Figure 2). Without a specified stimulus or activation, macrophages have a vital homeostatic role by phagocytosis of erythrocytes, tissue debris and apoptotic cells. In contrast, in case of inflammation or tissue damage, monocytes adhere to endothelial cells via selectins or ICAMs. They transmigrate through the endothelial wall into the destination tissue where they mature and become activated macrophages.

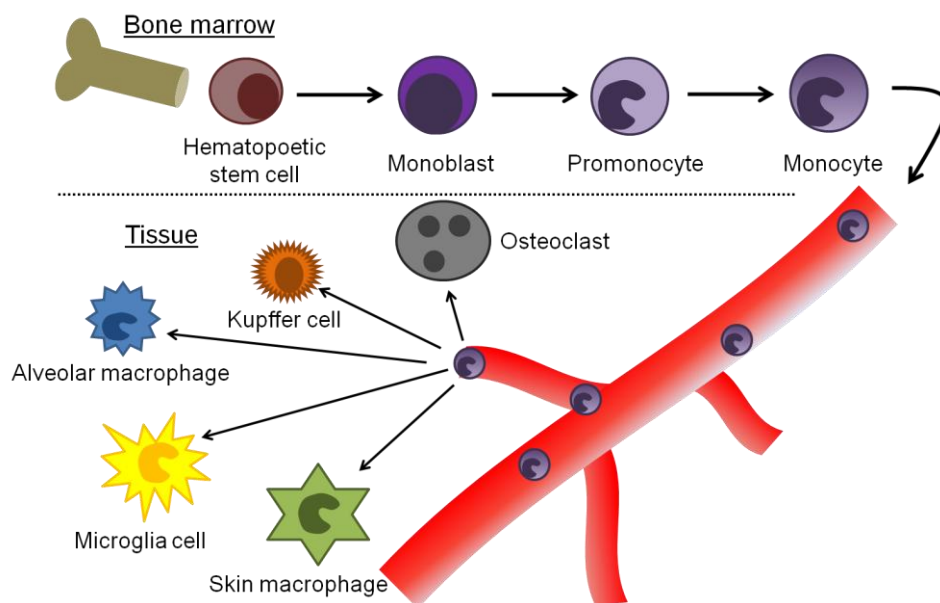


Figure 2: Macrophage development and diversity. Multipotent hematopoietic stem cells in the bone marrow pass through different maturation states until they are released into the circulation as blood monocytes and differentiate into macrophages when entering the tissue. Monocytes represent a reservoir for the renewal of tissue resident macrophages, such as alveolar macrophages in the lung, Kupffer cells in the liver, osteoclasts in the bone, microglia cells in neural tissues and skin macrophages.

1.3.2 Macrophage activation and function

Classically macrophages become activated by bacterial compounds such as LPS, recognized by Toll-like receptors (TLR), and by T helper 1 cells (Th1) via interferon- γ (INF- γ) and the corresponding receptor, which both trigger a harsh pro-inflammatory response, required to kill intracellular pathogens, such as *Mycobacterium tuberculosis*, *Leishmania* spp. or HIV [27] (Figure 3). Certainly, macrophages are plastic cells and they can adopt to different stimuli in the environment, leading to the concept of pro-inflammatory “classically activated M1” macrophages versus anti-inflammatory “alternatively activated M2” macrophages. In contrast to the classically M1 activation state, the alternative activation state is T helper 2 cell (Th2) –mediated in response to the two cytokines interleukin-4 (IL-4) and interleukin-13 (IL-13) [28] (Figure 3). The M2 phenotype is in contrast to M1 macrophages described to be important for the immune response to extracellular pathogens, such as nematodes or helminths. In addition, M2 macrophages are thought to have an important role in tissue repair and homeostasis. They function as immunoregulator and contribute to the production of ECM [29]. But alternatively activated M2 macrophages can also be detrimental to the host when their matrix-enhancing activity is dysregulated, similarly to the dysregulated activity of classically activated macrophages in autoimmunity [29]. Besides their substantial role in innate immunity and homeostasis, macrophages are important player in tumor biology. On the one hand, they are involved in antitumor immunity (rather M1 macrophages), but on the other hand, there is substantial evidence that in the majority of tumors these tumor-associated macrophages (TAMs) enhance tumor progression to malignancy by supporting tumor-associated angiogenesis, promoting tumor cell invasion, migration, and intravasation, as well as suppressing antitumor immune responses [30]. TAMs are thought to resemble the M2 phenotype and to support tumor progression by secreting growth factors like VEGF-A, TGF- β and PDGF [31].

M1 and M2 macrophages can be distinguished by the expression of different proteins. M1 macrophages highly up-regulate pro-inflammatory cytokines such as interleukin-6 (IL-6), interleukin-1 β (IL-1 β) and tumor necrosis factor- α (TNF- α) as well as inducible nitric oxide synthase (iNOS), regarding their function in host defense and bacterial killing. By contrast, the M2 macrophage phenotype is characterized by the expression of arginase 1 (antagonist of iNOS), mannose receptor (CD206), found in inflammatory zone-1 (Fizz1, also known as resistin like molecule- α , Relm- α), eosinophil chemotactic factor (Ecf, also known as Ym1) and selected chemokines [32] (Figure 3). The expression of the intracellular enzyme arginase is implicated in cell recruitment and granuloma formation, whereas the mannose receptor stimulates endocytosis [33]. Most of the work studying the importance and the phenotype of M2 macrophages was done in mouse and cannot be directly translated to

humans. Arginase 1 for instances cannot be used as a marker for human M2 macrophages because it is also induced by other pathways [28]. It is discussed that both activation stadia are not terminal and that they can switch from one to the other due to environmental stimuli.

1.3.3 The role of macrophages in wound healing

Numerous studies in the past revealed functional consequences of the innate immune response of resident cells as well as of recruited inflammatory cells during skin repair [34]. They combat invading microbes and contribute to debris scavenging, but may also critically support the repair process by releasing a spectrum of growth factors. However, due to the release of pro-inflammatory and cytotoxic mediators, the uncontrolled activity of macrophages may also be detrimental to tissue repair. Indeed, imbalanced inflammation characterized by increased numbers of macrophages is a hallmark of an attenuated repair response in human diseases including diabetes mellitus, vascular disease as well as aging [9, 35]. Neutrophils and macrophages represent the major fraction of inflammatory cells recruited to the wound site. Within a few hours post injury neutrophils transmigrate across the endothelial cell wall and begin the debridement of devitalized tissue and infectious agents as described above. Whereas the presence of neutrophils at the wound site is timely restricted to the early stage of the wound healing response, macrophages persist through all stages of the repair response. Their number increases during the phase of inflammation, peaks during the phase of tissue formation and gradually declines during the maturation phase [36].

Experiments in the 1970's established the concept, that under sterile conditions, the influx of macrophages is essential for efficient healing of incisional skin wounds, whereas the influx of neutrophils might not be crucial [37, 38]. This dogma has been challenged by recent reports, thereby arguing against an essential role of inflammatory cells in wound repair: early fetal wounds heal with minimal scarring, which is associated with little inflammation [39]. Furthermore, wounds in the neonatal PU.1 null mouse, which lacks macrophages and neutrophils (but also B cells, mast cells, eosinophils), heal without scarring and, surprisingly, with a similar time course as wild-type siblings [40]. However, the need of macrophage and neutrophil influx for physiological repair in adults is supported by different studies using murine knock out models deficient for specific endothelial cell or leukocyte adhesion molecules (E-, P- selectins, ICAM-1, β -1,4-galactosyltransferase, CD18) [41-44] or individual inflammatory mediators or their receptors (IL-6, CX3CR1) [11, 45]. These mouse mutants showed a dramatic delay in wound closure and a significantly reduced infiltration of neutrophils and macrophages.

Introduction

Although these studies emphasize that leukocytes clearly affect the quality of the healing response, validity of these models is limited, because they either do not target pathways mediated exclusively by macrophages or neutrophils or they address a neonate repair response, which is known to differ from healing in the adult organism [46]. Furthermore, it is hypothesized that both macrophage phenotypes, M1 and M2 are present in wounds during physiological repair. The classically activated M1 differentiation state is thought to mediate apoptosis of damaged cells, killing of bacteria and destruction of matrix and extracellular structures, whereas the alternatively activated M2 phenotype seems to rather play an immunomodulatory role and to induce cell proliferation and angiogenesis (Figure 3). As both macrophage types are necessary at the inflamed site, the right balance between these two populations is required for healing and resolution of inflammation [47-49]. However, experiments proving this concept of the importance of M1 and M2 macrophages in skin repair are still missing.

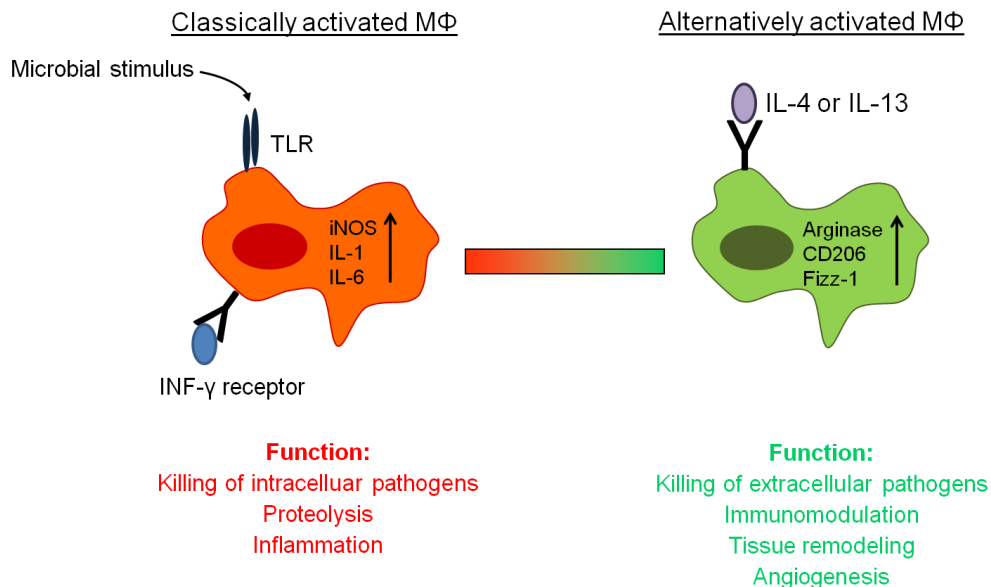


Figure 3: Model of macrophage activation. Macrophages can either be activated by a microbial stimulus and INF- γ to function as a classically activated macrophage or by IL-4/IL-13 to act as an alternatively activated macrophage. TLR, toll-like receptor; iNOS, inducible nitric oxide synthase; IL, interleukin; INF- γ , interferon- γ ; CD206, mannose receptor; Fizz-1, found in inflammatory zone; MΦ, macrophage.

1.4 Vascular endothelial growth factor-A

The vascular endothelial growth factor-A (VEGF-A) was discovered around thirty years ago, first as an inducer of vascular permeability in tumors, the reason why it is also known as

Introduction

vascular permeability factor (VPF), and later as a strong endothelial cell specific mitogen [50, 51]. Since its discovery VEGF-A has been one of the most studied angiogenic growth factors and is thought to be of singular importance in vascular biology. The essential role of VEGF-A during developmental vasculogenesis (mobilization of bone marrow-derived endothelial stem cells) and angiogenesis (sprouting of capillaries from existing blood vessels) was shown by different knock out models, which unraveled that already a heterozygous knock out of VEGF-A is embryonically lethal [52, 53]. Further, it was shown in adults, that endothelial cells require an autocrine VEGF-A-mediated survival signal [54]. Meanwhile, the VEGF family in mammals consists of five members, VEGF-A, VEGF-B, VEGF-C, VEGF-D and placenta growth factor (PlGF). Furthermore, structurally related proteins were also found in parapoxvirus (VEGF-E) and snake venom (VEGF-F). All VEGF members are homodimeric glycoproteins and share a common structure of eight characteristically spaced cysteine residues in a VEGF-homology domain. They have different physiological functions and exert them by binding in an overlapping fashion to three receptor tyrosine kinases, known as VEGFR-1 (also known as Fms-related tyrosine kinase-1, Flt-1), -2 (also known as kinase insert domain receptor, KDR or fetal liver kinase, Flk-1), and -3 (also known as Flt-4), as well as to co-receptors, including neuropillins (Nrp) and heparan sulfate proteoglycans [12, 55, 56] (Figure 4).

VEGF-A is the most prominent member of the VEGF family and is henceforth referred to as VEGF. VEGF is encoded by eight exons. Exon one to five encodes for the VEGFR-binding domains, whereas exons six and seven encode for two separate heparin binding domains [51]. Currently, eight alternative splice variants are described and named by their corresponding amino acid length (VEGF₁₂₁, VEGF₁₄₅, VEGF₁₄₈, VEGF₁₆₂, VEGF₁₆₅, VEGF₁₈₃, VEGF₁₈₉, and VEGF₂₀₆). Their relative abundance varies among different tissues [57]. All VEGF isoforms differ in their capability to bind to cell surfaces, the ECM and the corresponding receptors and have therefore their own biological significance [12]. VEGF₁₂₁, VEGF₁₆₅ and VEGF₁₈₉ are the major isoforms expressed in VEGF expressing cells. VEGF₁₂₁ lacks both exons encoding for heparin binding domains and represents therefore a soluble isoform. VEGF₁₆₅ comprises the heparin binding domain encoded by exon 6 which mediates a moderate binding to heparin, and VEGF₁₈₉ contains both heparin binding domains and has therefore a strong affinity to ECM structures. Due to alternate capabilities of different VEGF isoforms to bind ECM proteins VEGF gradients can be formed [12]. Among the different isoforms, VEGF₁₆₅ is the major gene product found in human tissues. In mice, VEGF-isoforms are one amino acid shorter than in humans, and therefore denoted as VEGF₁₂₀, VEGF₁₆₄, VEGF₁₈₈ and so on.

The major VEGF functions are mediated in binding to VEGFR-2 which is mostly expressed on endothelial cells but also on neuronal cells and hematopoietic stem cells [58]. VEGFR-2 is

Introduction

a type III transmembrane receptor tyrosine kinase. The extracellular domain of the receptor comprises seven immunoglobulin-like domains, of which the second and third interact with VEGF. A single transmembrane domain connects the outer domain to the intracellular two tyrosine kinase domains (Figure 4). Binding of VEGF to VEGFR-2 leads to enhanced proliferation, migration, cell survival and permeability by the induction of various complex signaling pathways (for review see [58]). Besides, VEGF is also able to bind to VEGFR-1, but VEGFR-1 signaling is less well understood. Strong experimental evidence indicates that VEGFR-1 on the vasculature may act primarily as a ligand-binding molecule during angiogenesis, rather than as a signaling tyrosine kinase [12]. Furthermore, *in vitro* studies revealed that VEGFR-1 on monocytes/macrophages promotes chemotaxis [59].

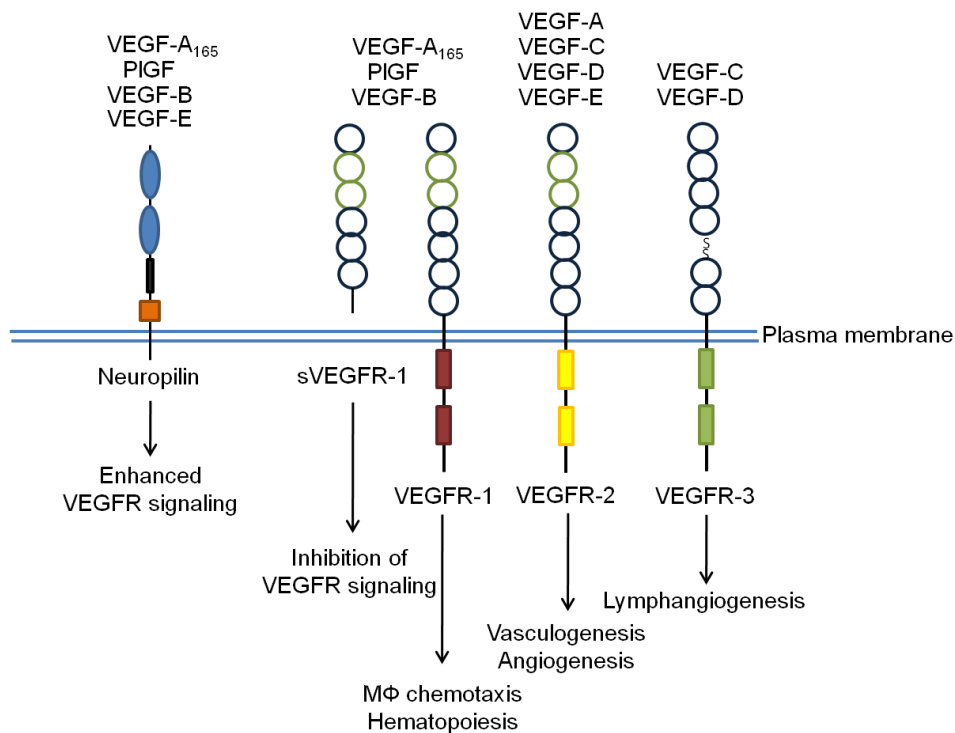


Figure 4: VEGF members and their receptors. Schematic representation of interactions between VEGF ligands and their transmembrane or soluble receptors (sVEGFR-1) as well as co-receptors (Modified: Erming et al., 2007, [12]).

1.4.1 VEGF function in angiogenesis

Almost all tissues depend on blood supply, which in turn depends on endothelial cells, which form the inner linings of the blood vessels. Endothelial cells originate in the early embryo during development from bone marrow-derived stem cells. Early embryonic endothelial cells migrate, proliferate, and differentiate to form the first rudimental blood vessels in a process

Introduction

termed vasculogenesis. Subsequent growth and branching of the vessels throughout the embryo and later in adults during tissue repair is mainly mediated by proliferation and migration of endothelial cells of pre-existing vessels, in a process termed angiogenesis. New vessels originate as a capillary sprout from the side of an existing capillary. Under physiological situations, endothelial cells are in a quiescent state, thus, they need to be activated and re-programmed during the early stages of angiogenesis [60]. Hypoxia is a strong stimulator for angiogenesis by leading to stabilization of the transcription factor hypoxia-induced factor-1 α (HIF-1 α) which in turn induces the expression of a wide range of pro-angiogenic mediators such as angiopoietins, TGF- β , bFGF and VEGF (Figure 5). VEGF then stimulates endothelial cell proliferation and directed migration. For endothelial cell migration, cell-cell contacts have to be disrupted, an additional function of VEGF activity [61]. The impaired cell barrier leads furthermore to vascular leakage and extravasation of plasma proteins, forming a provisional matrix constituting an anchorage point for migrating cells via integrins. In addition, VEGF stimulates the expression of different proteases to digest the basal membrane and the surrounding matrix to allow cell invasion. The outgrowing vascular sprout is guided by a single specialized endothelial cell, distinctive by tip structures with potential functions in guidance and migration [62] (Figure 5). The endothelial cells following the tip cell, named stalk cells, are hyperproliferative, while the tip cell is not. The tip cell guides the way by expressing VEGFR-2 and recognizing extracellular VEGF gradients released by nearby oxygen-deficient tissue [63] (Figure 5). Tip cells meet and fuse, forming blood vessel loops in a process termed anastomosis, to develop a new vascular network; though the precise mechanism remains unclear [64]. It is speculated that macrophages might function as bridge cells between two sprouting vessels in order to prepare them for fusion [65, 66]. Lateral inhibition prevents overgrowth of blood vessels during angiogenesis by a precise selection of tip cells. This inhibition is mediated by delta/notch signaling. The delta like-4 ligand (Dll4) is up-regulated in tip cells and inhibits via signaling through the notch receptor, expressed by stalk cells, the same cell fate in neighboring cells [67] (Figure 5). Dll4 expression in turn is induced by VEGF, indicating not only a stimulatory, but also a modulatory role of VEGF in angiogenesis [68]. The newly formed blood vessels are highly instable, leaky and, dependent of VEGF signaling for their survival. Vessels mature by the recruitment of pericytes, which cover the outside of the vessels and help to build a novel basal membrane [69]. Besides of the pro-angiogenic effects of VEGF in developmental and postnatal angiogenesis, there is substantial evidence that implicates VEGF as a mediator of pathological angiogenesis [55]. VEGF is highly up-regulated in the vast majority of human tumors, expressed by tumor and stromal cells, in order to supply the tumor environment with blood vessels. Anti-VEGF therapy in humans and VEGF knock out mouse models could substantiate the supporting effect of VEGF on tumor growth.

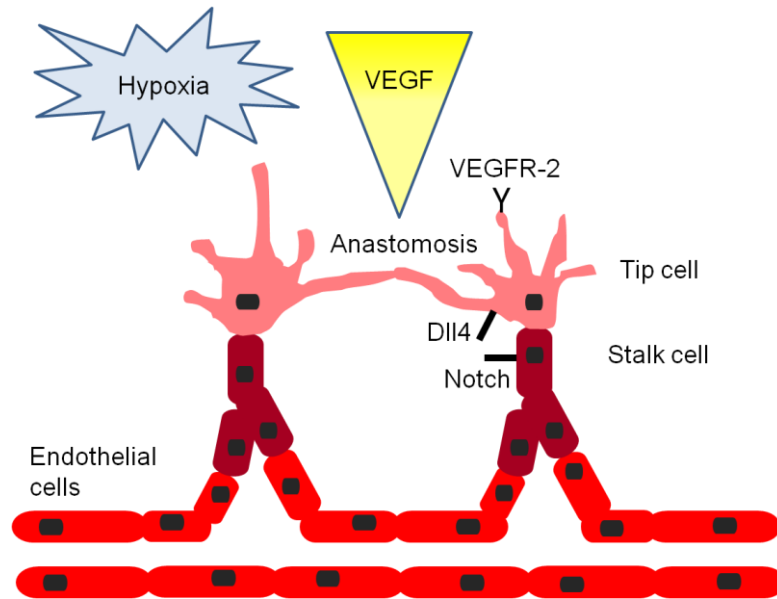


Figure 5: Model of vascular sprouting. Induced by a VEGF gradient, specialized tip cells guide the expanding sprout by exploring the environment for tissue gradients of guiding cues. They are followed by proliferating stalk cells, which form the sprout and generate lumen. Tip cell fate is determined by lateral inhibition, mediated by Dll4/Notch signaling.

1.4.2 The role of VEGF and macrophage-derived VEGF in wound repair

Angiogenesis is a central event during wound healing because the restoration of blood flow to the site of injured tissue is necessary to mount the initial immune response to pathogens, and at the same time to initiate repair of wounded tissue. Thus, VEGF, as a key regulator of angiogenesis represents an important mediator in skin repair. VEGF expression is nearly absent in unwounded skin, but highly induced after injury, mainly by hypoxia but also in response to different pro-inflammatory cytokines and growth factors [70].

A central function of VEGF during skin wound healing is supported by different studies in which reduced expression or activity of VEGF caused severe wound healing defects [11, 70]. The first study indicating VEGF as an important factor in wound healing was done in the wound healing impaired diabetic mouse model (db/db). It was shown that VEGF amounts were dramatically decreased, directly linking the reduced angiogenic response observed in this mouse model to the subsequent impaired healing response [70]. In another study it was shown that under the pathological healing conditions in the db/db mouse model, VEGF is a target for increased proteolytic activity, probably causing in the wound healing defects in diabetic mice [71]. Furthermore, these impaired healing conditions can be rescued or improved by applying a mutant protease resistant VEGF variant [72, 73].

Introduction

Mechanistically, during the early phase of repair release of VEGF into the wound is likely to contribute to increased vascular permeability, which mediates extravasation and extravascular deposition of plasma proteins (fibrinogen, fibronectin), a process central for the formation of the provisional wound matrix [74]. During the phase of tissue formation, VEGF provokes wound angiogenesis. Further, it is discussed that VEGF serves as a chemoattractant for monocytes and macrophages. Both express VEGFR-1 and can therefore answer to VEGF signals [75].

Initial studies of wound healing demonstrated that VEGF is mainly expressed by keratinocytes at the wound edge and by recruited macrophages [71, 74]. Some *in vitro* studies could further show that also platelets, mast cells, pericytes and fibroblasts are able to secrete VEGF. Additional wound healing studies with two different reporter mouse lines for VEGF expression gave contradictive results with regard to the sites of VEGF expression during repair. One model revealed VEGF expression mainly in wound fibroblasts, whereas in the other model keratinocytes were the main source for VEGF supply [12, 76, 77]. These different results can be explained by different promoter regions used and by the fact that the human VEGF promoter was used in these mouse models. However, the contribution of different cell compartments of VEGF expression during skin repair is not well understood. The importance of one specific cellular compartment releasing VEGF in wounds was shown by a *Cre*-mediated knock out for VEGF in keratinocytes, which results in an impaired healing response and decreased susceptibility to chemically-induced skin carcinogenesis [78]. Surprisingly, however, in wound repair consequences of VEGF depletion in keratinocytes became only apparent after wound closure had been completed, whereas granulation tissue formation and angiogenesis during the early phase occurred normally. This study suggests that keratinocyte-derived VEGF is dispensable for the early healing response, but plays a role in the later phases, indicating that during the phase of inflammation, other or additional cells must be a source for VEGF. Macrophages for example are the dominant cell type during the early steps of repair and they express VEGF [71]. Important stimuli for macrophage activation and induction of VEGF expression are hallmarks of microenvironmental conditions found in injured tissues, including hypoxia and lactate [79]. Furthermore, the importance of macrophage-derived VEGF on angiogenesis was shown by two recently published articles. A *Cre*-mediated knock out for VEGF exclusively in macrophages was analyzed in a mouse model for breast cancer and lung fibrosis [80, 81]. In both cases, the macrophage-specific knock out for VEGF had fundamental influences on the outcome of the angiogenic response, which was diminished.

2 Specific aims

Skin injury leads to an acute phase response, which is characterized by activation of the innate immune system, resulting in the activation of various repair mechanisms. Physiologically, when timely limited, the inflammatory response is beneficial for wound closure. However, when the acute inflammation persists and a chronic inflammatory response develops, it leads to severely impaired healing conditions. Therefore, it can be speculated that the inflammatory response is a crucial target to impact the outcome of the healing response. Currently, it is not completely understood how macrophages exactly influence the physiology of the repair response and how they may contribute to the pathology of healing in diseased conditions. Therefore, a more thorough understanding of macrophage-specific functions during the diverse phases of the repair response might broaden the understanding of this cell type in skin physiology and pathology. So far it is not examined how different cellular compartments contribute to VEGF-A supply in wounds. Macrophages could be an eminent source releasing significant amounts of this growth factor into wounds.

The specific aims of this study are:

- 1.) To test the hypothesis that macrophages present at the wound site during the different stages of skin repair exert specific functions. To this end, a mouse model is needed that allows the conditional depletion of macrophages in a timely restricted fashion during the distinct phases of the repair response in skin to delineate repair mechanisms dependent or independent from macrophage function.
- 2.) To determine the time course of VEGF-A expression in wounds and to identify different cellular compartments of VEGF-A expression by using a VEGF-lacZ reporter mouse, in which both proteins, VEGF-A and β -galactosidase are expressed under the control of the murine VEGF-A promoter.
- 3.) To analyze the specific functional impact of macrophage-derived VEGF-A on the outcome of the healing response by using conditional gene targeting to specifically deplete VEGF-A expression in myeloid cells.

3 Results

3.1 Cell type specific and timely restricted depletion of macrophages in LysMCre/iDTR mice

To analyze the functional impact of macrophages during diverse phases of skin repair, mice were generated in which macrophages can be inducibly ablated, using a model of *Cre*-inducible diphtheria toxin receptor-mediated cell ablation. This system is based on a *Cre*-inducible human diphtheria toxin receptor transgenic mouse line (*iDTR*) in which *Cre*-mediated excision of a STOP cassette, downstream of the ubiquitous active Rosa26 promotor, renders naturally diphtheria toxin (DT)-resistant mouse cells DT sensitive (kindly provided by Ari Waisman [82]). To generate mice in which macrophages can be inducibly ablated, the *iDTR* mouse line was crossed to lysozyme M *Cre* (*LysMCre*) mice, reported to express the *Cre* recombinase in cells of myeloid origin (macrophages and neutrophils) (kindly provided by Irmgard Förster [83], Figure 6).

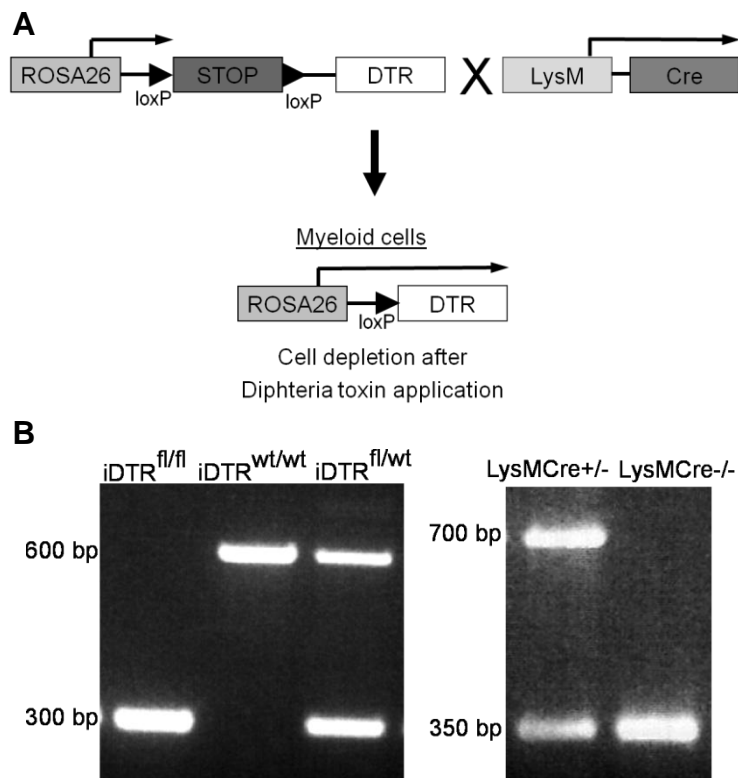
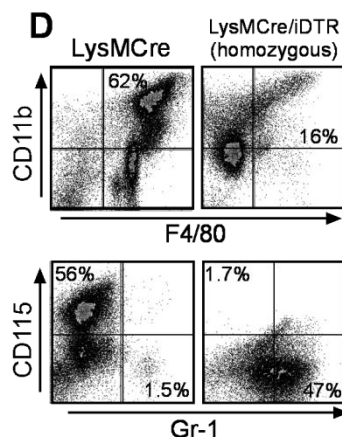
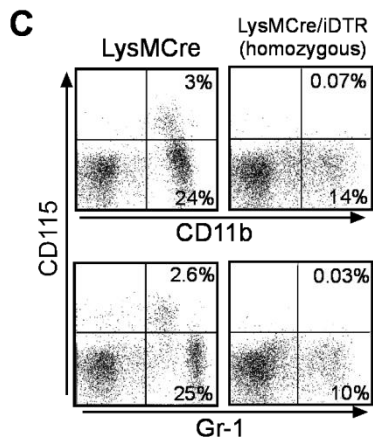
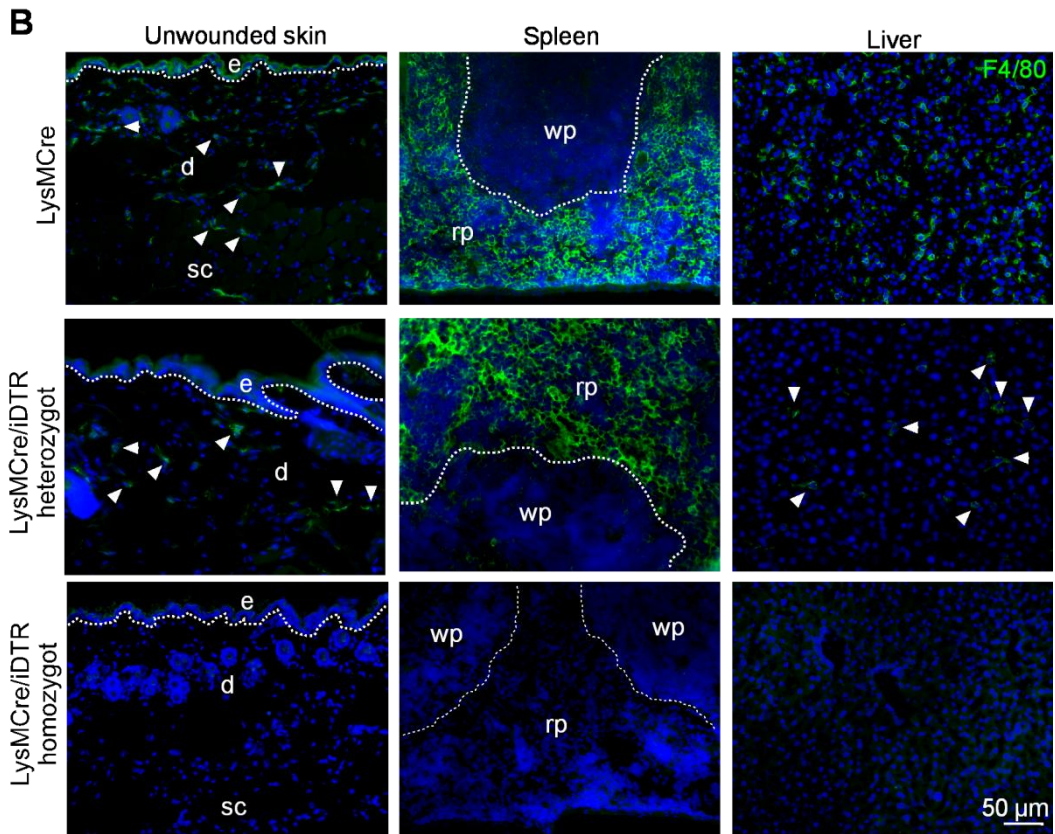
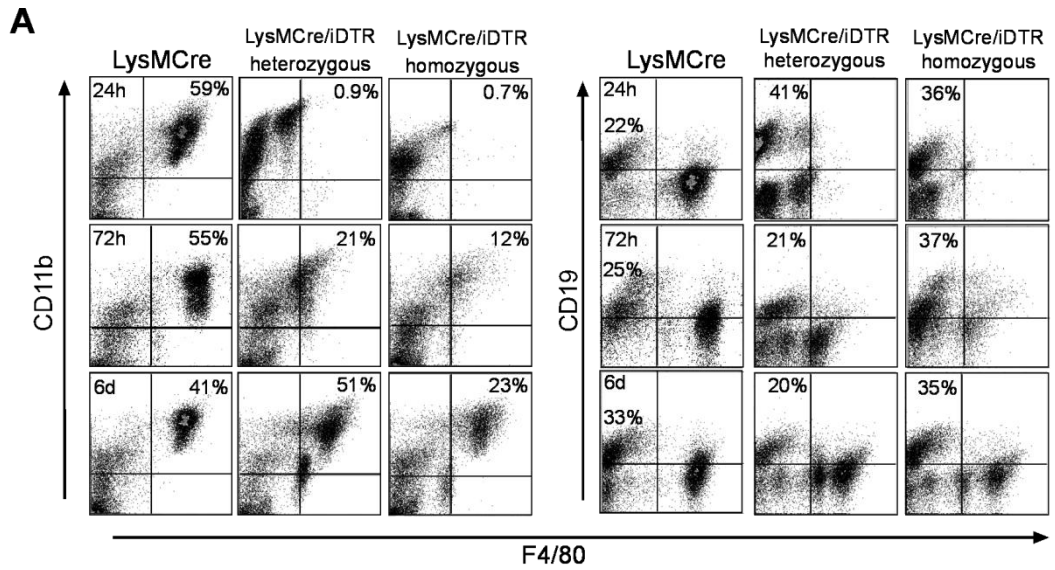


Figure 6: Mouse model for inducible myeloid cell depletion. (A) To generate mice in which myeloid cells can be inducibly ablated the *iDTR* mouse line, in which the expression of the DT receptor is under control of the Rosa26 promotor after *Cre*-mediated excision of a stop cassette, was crossed to the *LysMCre* mouse line. **(B)** Genotyping of *iDTR* (left) and *LysMCre* (right) mice by PCR. The 300 bp fragment represents the *iDTR* gene, whereas the 600 bp fragment shows the wild type allele in the *iDTR* PCR. For *LysMCre*, a 700 bp fragment indicates the presence of the gene encoding the *Cre* recombinase. The 350 bp fragment indicates the wild type allele. bp, base pairs; DTR, diphtheria toxin receptor; LysM, lysozyme M; wt, wild type; fl, loxP site.

Results

First, it was investigated how macrophage depletion can be controlled by the dose, kinetics, and route of diphtheria toxin (DT) application (intraperitoneal versus intravenous), as well as the *DTR* gene dose (heterozygous versus homozygous). As revealed by flow cytometry for macrophages (F4/80 and CD11b), a single intraperitoneal (i.p.) injection of DT (25 ng/g bodyweight) in *LysMCre/iDTR*(heterozygous) mutants resulted in complete depletion of peritoneal macrophages 24 hours later, that persisted approximately for 3 days (Figure 7 A). In contrast, total numbers of peritoneal B cells (CD19) as identified by flow cytometry were similar in *LysMCre* (control) and *LysMCre/iDTR*(heterozygous) mice, demonstrating the specificity of macrophage depletion following DT injection. By contrast, depletion of tissue resident macrophages in skin, liver and spleen was not achieved by a single i.p. injection of DT in *LysMCre/iDTR*(heterozygous) mice, as revealed by immunohistochemical staining for F4/80 (Figure 7 B, mid panel). Also repetitive i.p. DT injections did not result in efficient depletion of resident macrophages in these tissues. Therefore, it was investigated whether increasing the *DTR* gene dose and intravenous (i.v.) DT application affects the efficacy of tissue resident macrophage depletion. In fact, repetitive i.v. injections of DT (25 ng/g bodyweight) at two consecutive days in *LysMCre/iDTR*(homozygous) mice resulted in efficient depletion of both peritoneal and tissue resident macrophages in skin, spleen and liver one day after DT injection (Figure 7 A, B). Furthermore, the same regimen of DT application resulted in efficient depletion of circulating monocytes (CD115, CD11b) 24 hours later (Figure 7 C). Interestingly, although the lysozyme M gene is also expressed in polymorphonuclear leukocytes, DT injection did not result in efficient depletion of neutrophils (Gr-1) in the circulation (Figure 7 C). To investigate whether myeloid cells can be efficiently depleted under inflammatory conditions, *LysMCre/iDTR*(homozygous) and *LysMCre* mice received two i.v. injections of DT at consecutive days, which 24 hours later was followed by a single i.p injection with thioglycolate. This substance is standardly used to induce a sterile peritonitis characterized by a strong infiltration of macrophages and neutrophils into the peritoneal cavity. After thioglycolate injection, mice received DT injections i.p. for 3 consecutive days, and at day 4 post thioglycolate application, peritoneal lavage cells were analyzed. As revealed by flow cytometry for macrophages (F4/80, CD11b) and neutrophils (Gr-1) only macrophages were efficiently ablated, while the treatment did not affect neutrophil populations (Figure 7 D). Whether increased neutrophil number in *LysMCre* mice is simply the result of reduced phagocytosis by macrophages or results from the lack of different macrophage-mediated control mechanisms, is currently unknown. For the subsequent wound healing studies *LysMCre/iDTR*(homozygous) and *LysMCre* (control) mice were used.

Results



Results

Figure 7: Selective depletion of macrophages in LysMCre/iDTR mice. (A) Analysis of macrophage depletion by peritoneal lavage following a single i.p. injection of DT (25 ng/g bodyweight) in LysMCre/iDTR(heterozygous) or LysMCre/iDTR(homozygous) mice resulted in efficient depletion of peritoneal macrophages (F4/80, CD11b) 24 hours after DT injection that lasted for 3 days. Specificity of macrophage depletion was identified by normal B cell numbers (CD19). DT injection in LysMCre (control) mice had no effect on macrophage numbers. **(B)** Tissue resident macrophages (stained by F4/80) in skin, spleen and liver were efficiently depleted in LysMCre/iDTR(homozygous) mice 24 hours following i.v. DT injections (25 ng/g bodyweight) at two consecutive days. Tissue resident macrophages were not affected by DT injection in LysMCre mice and partially depleted in LysMCre/iDTR(heterozygous) mice. **(C)** Efficient depletion of monocytes (CD11b, CD115) and partial depletion of neutrophils (Gr-1) in the circulation 24 hours after two i.v. DT injections at consecutive days. **(D)** Effective depletion of macrophages (F4/80, CD11b) but not neutrophils (Gr-1) in LysMCre/iDTR(homozygous) mice after thioglycolate induced peritonitis. e, epidermis; d, dermis; sc, subcutaneous fat layer; wp, white pulp; rp, red pulp.

3.2 Macrophage function during the different stages of repair

To analyze macrophage function during the different phases of tissue repair, the above described mouse model was used and a cell depletion scheme in which macrophages were inducibly depleted in a timely restricted manner during the different phases of repair was developed (Figure 8). To this end, injections were performed on specific days prior or post wounding to achieve macrophage depletion during the inflammation, the tissue formation or the maturation phase (Figure 8 regimen A to C).

3.2.1 Macrophage function during the early stage of repair

3.2.1.1 Macrophages recruited during the inflammatory phase of repair induce granulation tissue formation, which results in scar formation

First, the impact of macrophages recruited during the early inflammation phase was analyzed by cell depletion following injection scheme A (Figure 8). For this purpose, mice were first injected with DT twice prior wounding to prevent an initial influx of macrophages after injury, which was followed by two i.p. DT injections at day two and four post injury. Macroscopic assessment of wound closure showed that depletion of macrophages during the inflammatory phase resulted in a significant delay of the early repair response compared with control (LysMCre) mice. While at day 5 post injury, the wound area was reduced to 50% of the original wound size in control mice, in macrophage-depleted wounds of LysMCre/iDTR mice the wound size was reduced by only 25%. However, at later time points, when DT

Results

injections were discontinued, wounds in LysMCre/iDTR mice demonstrated rapid wound closure comparable to control wounds (Figure 9).

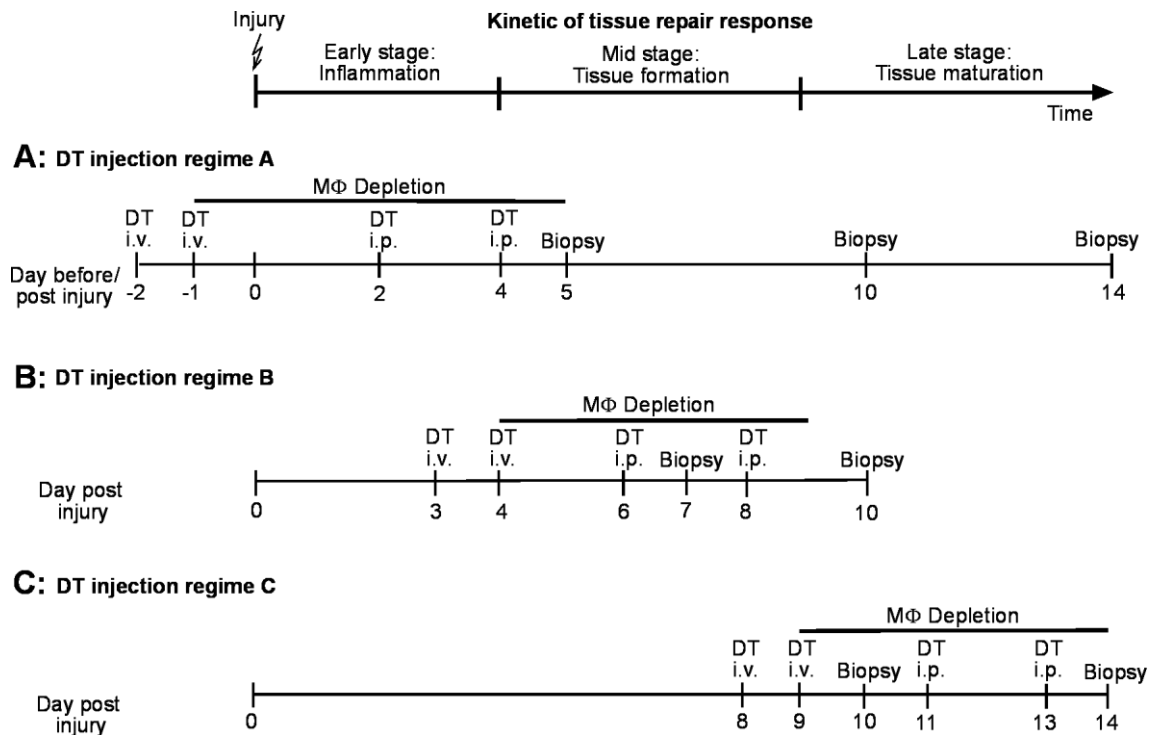


Figure 8: Schematic representation of DT-mediated macrophage depletion in distinct stages of the repair response. To achieve wound-phase-restricted depletion of macrophages LysMCre/iDTR and LysMCre mice were injected with DT (intravenously, i.v. or intraperitoneally, i.p.) according to three regimens: **(A)** DT injection regimen A, macrophage depletion during the inflammatory phase: DT injections 2 and 1 days prior wounding as well as at day 2 and 4 post wounding; **(B)** DT injection regimen B, macrophage depletion during the tissue formation phase: DT injections at day 3, 4, 6 and 8 post injury; **(C)** DT injection regimen C, macrophage depletion during the maturation phase: DT injections at days 8, 9, 11, and 13 post injury. At time points indicated mice were sacrificed and the wound tissue was excised for analysis. MΦ, macrophages; DT, diphtheria toxin.

Results

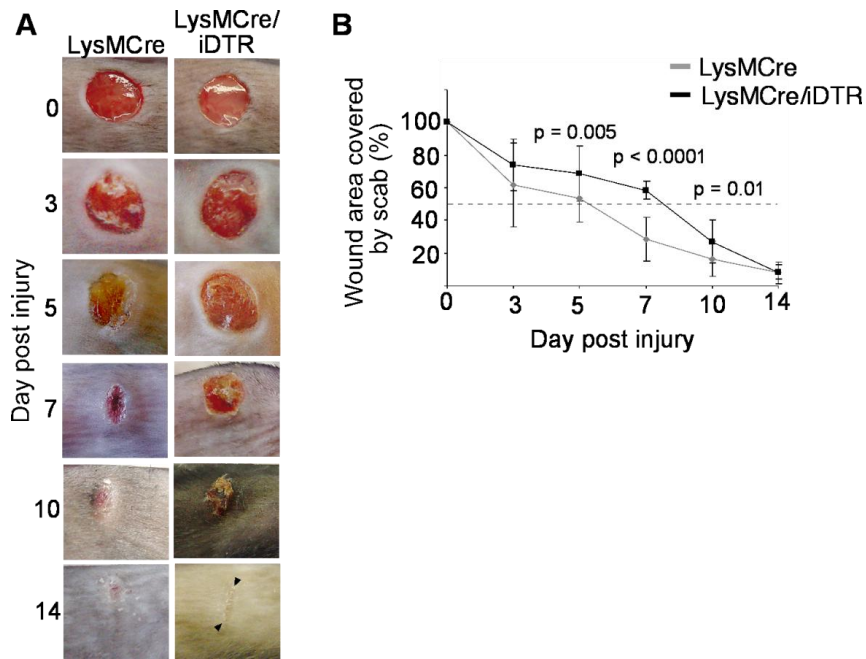


Figure 9: Macrophage depletion during the early stage of repair results in a delayed wound closure rate. (A) Macroscopic appearance of wounds in LysMCre/iDTR and LysMCre (control) mice after DT injection following regimen A; whereas wounds of control mice had already lost their scab, macrophage-depleted wounds in LysMCre/iDTR mice still carry a firmly adherent scab 7 days post wounding. **(B)** At the time points indicated, the wound area was determined using image analysis and expressed as percentage of the wound area immediately after injury ($n = 12$ wounds on 6 mice for each time point and genotype). Data are expressed as mean \pm SD.

The macroscopic findings were confirmed by histological assessment. For this purpose LysMCre/iDTR and control mice were sacrificed on day 5, 10 and 14 after injury and the wound tissue (5-12 wounds on 3-6 mice per time point for each group) was excised and analyzed. For histological quantification, the amount of granulation tissue, the distance between the two ends of the epithelial tips and the distance between the ends of the panniculus carnosus were measured on H&E stained paraffin sections (see overview in Figure 10 A).

At day 5 post injury, a significantly shorter distance between the tips of the epithelial tongues, representing the longitudinal diameter of the wound, was measured for the control wounds compared to macrophage-depleted wounds (Figure 10 B, C). Furthermore, as revealed by expression of the cell proliferation marker Ki67, the epidermal margins in control wounds were hyperproliferative, whereas the epidermal wound edge in macrophage-depleted wounds was short and showed few proliferating keratinocytes (Figure 10 B, G). To analyze dermal repair the amount of granulation tissue formation in wound tissue of macrophage-depleted and control mice was determined. Differences in the quantity of granulation tissue were analyzed in H&E-stained sections and were shown to be significantly reduced at all time points in macrophage-depleted wounds compared to controls (Figure 10 E). Whereas at

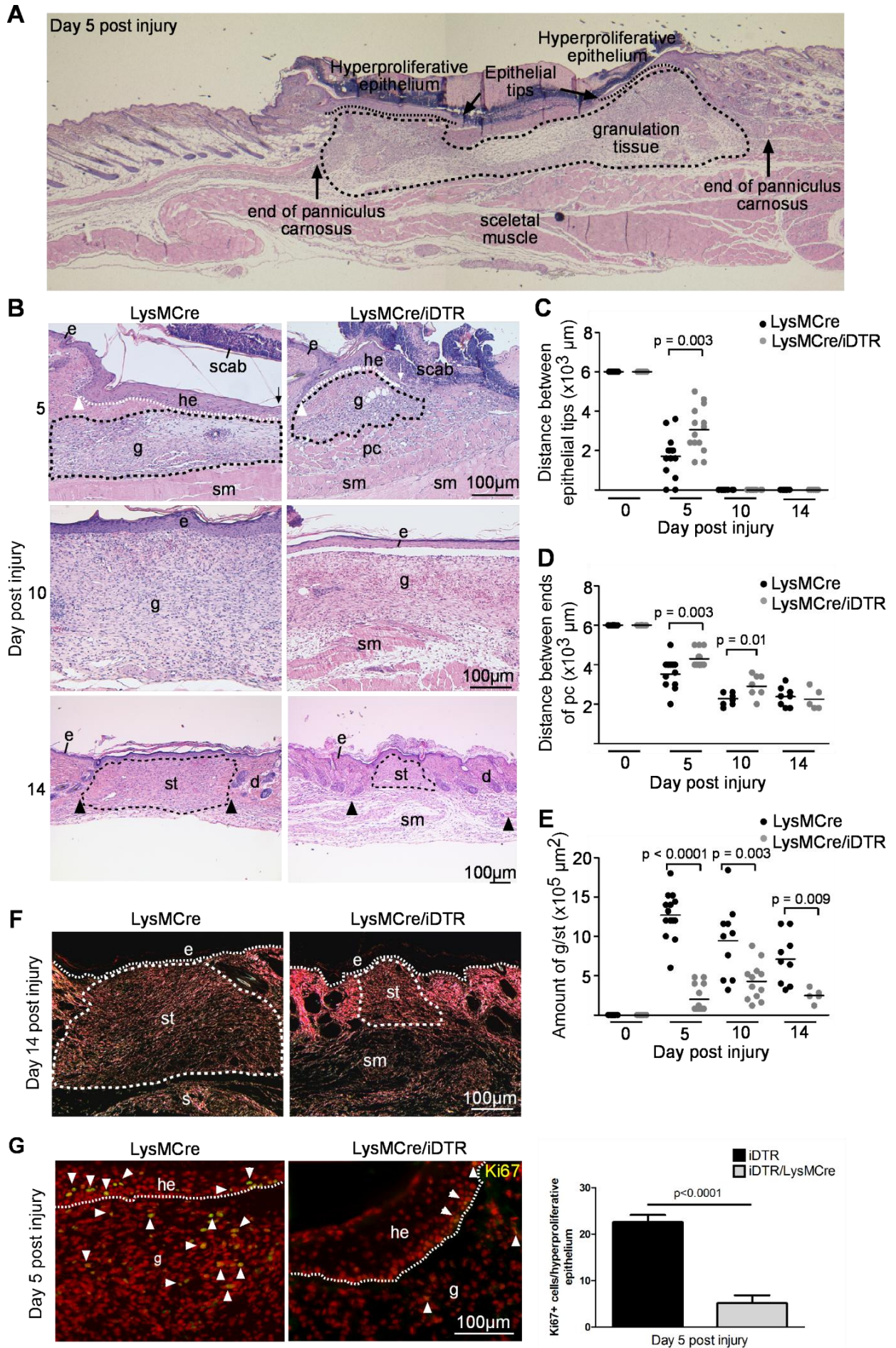
Results

day 5 post injury control wounds showed a highly vascularized, cellular and proliferative granulation tissue, in macrophage-depleted wounds granulation tissue was scarcely vascularized and showed few proliferating cells (Figure 10 B, G). Wound contraction was significantly reduced in LysMCre/iDTR mice when compared to controls (Figure 10 D).

At day 10 post injury, wounds in LysMCre/iDTR and control mice were still covered by eschar (Figure 9 A) and histological analysis revealed that in both a complete neo-epithelium had formed beneath the eschar (Figure 10 B). However, in LysMCre/iDTR mice, the epithelium appeared fragile, was thinner, and partially detached from the dermis, when compared to control mice, indicating immature anchorage and basement membrane formation. Furthermore, although in these wounds the quantity of granulation tissue increased when compared to day 5 post injury, it was significantly reduced compared to control wounds (Figure 10 B, E). Also wound contraction remained reduced in LysMCre/iDTR mice when compared to controls (Figure 10 D).

At day 14 post injury both wounds in LysMCre/iDTR and control mice had lost their eschar and were similar in their macroscopic appearance (Figure 9 A). In contrast, major differences between wounds in LysMCre/iDTR and control mice became apparent regarding the extent of scar tissue formation. As revealed by H&E (Figure 10 B) and Sirius red staining analyzed in polarized light (Figure 10 F), fine collagen bundles characteristic for scar tissue were almost absent in wounds of LysMCre/iDTR mice. Morphometric quantification of scar tissue revealed a significant reduction in LysMCre/iDTR mice when compared to controls (Figure 10 E). Morphological analysis of the epidermis overlaying the scar tissue revealed a slightly hyperproliferative, closed epithelium which was similar in mutant and control wounds (Figure 10 B).

Results



Results

Figure 10: Macrophage depletion during the early stage of repair attenuates epithelialization, granulation tissue formation and wound contraction. (A) H&E stained wild type wound section 5 days following injury. **(B)** H&E stainings of wounds in LysMCre (control) and LysMCre/iDTR mice at indicated time points after injury. Whereas in LysMCre mice, the day-5 wound is filled with a vascularized granulation tissue in LysMCre/iDTR mice only scarce granulation tissue has formed (black hatched line outlines granulation tissue, white dotted line outlines hyperproliferative epithelial tongue); in day-10 wounds of LysMCre and LysMCre/iDTR mice the granulation tissue is covered by a complete epithelium; however the epithelium is detached; day-14 wounds of LysMCre and LysMCre/iDTR are closed, scar tissue is minimal in LysMCre/iDTR mice (hatched line outlines scar tissue). **(C-E)** Morphometric analysis of wound tissue at different time points post injury: **(C)** Distance between the epithelial tips; **(D)** Distance between the edges of the panniculus carnosus; **(E)** Amount of granulation tissue (day 5 and 10 post injury) or scar tissue (day 14 post injury). Each dot represents one wound (day 5: two wounds on one mouse, day 10 and 14: one wound per mouse); horizontal bar represents the mean. **(F)** Sirius red staining and examination with polarized light revealed increased scar formation in control wounds when compared to LysMCre/iDTR wounds 14 days post injury. **(G)** Left: day 5 wounds of LysMCre and LysMCre/iDTR mice stained for Ki67 (green) and propidium iodide (red), arrowheads indicate Ki67 positive cells (yellow). Right: quantification of Ki67 positive cells in the hyperproliferative epithelium. Data are expressed as mean \pm SD, $n = 3$ wounds on 3 mice for each time point and group. Hatched line indicates basement membrane. e, epidermis; he, hypertrophic epidermal wound edge; d, dermis; sm, subcutaneous muscle layer; pc, panniculus carnosus; g, granulation tissue; st, scar tissue; arrows point to the tips of epithelial tongue, white arrowheads indicate wound edges, black arrowheads indicate edges of panniculus carnosus.

3.2.1.2 Macrophage depletion in wounds of LysMCre/iDTR mice receiving DT injections following regimen A

To analyze whether changes observed in the tissue repair response between LysMCre/iDTR and control (LysMCre) mice correlated with macrophage depletion, wound tissue was stained for the macrophage marker F4/80. In control wounds 5, 10 and 14 days post injury, F4/80 positive cells were present throughout the entire granulation tissue (Figure 11 A, B). Quantification of F4/80 positive macrophages revealed that their number was highest at day 5 post injury and subsequently declined to approximately 1/3 until 14 days post injury (Figure 11 B). In contrast, in LysMCre/iDTR mice receiving DT injections following regimen A (Figure 8), F4/80 positive cells were absent at day 5 post injury but appeared at the wound site at day 10 and 14 post injury (Figure 11 A, B). Thus, in LysMCre/iDTR mice, the absence of macrophages during the early stage of repair corresponded to the time course of DT injections. Furthermore, the data revealed that after DT injections were abolished, newly generated macrophages were recruited into the wound site during the consecutive phases of tissue formation and maturation. Finally and most importantly, the results demonstrate that macrophages recruited during the inflammatory phase impact repair mechanisms not only in the early stage of the repair response, but also in the consecutive mid and late stages of repair. As revealed by staining for the neutrophil marker Gr-1 (Figure 11 C) 5 days post injury neutrophils were not effectively depleted at the wound site by DT injections in this model, which is in agreement with the data presented in figure 6 D after thioglycolate-induced

Results

peritonitis. Of note, whereas in controls neutrophils are scattered throughout the granulation tissue, in LysMCre/iDTR wounds neutrophils are clustered at the wound surface (Figure 11 C).

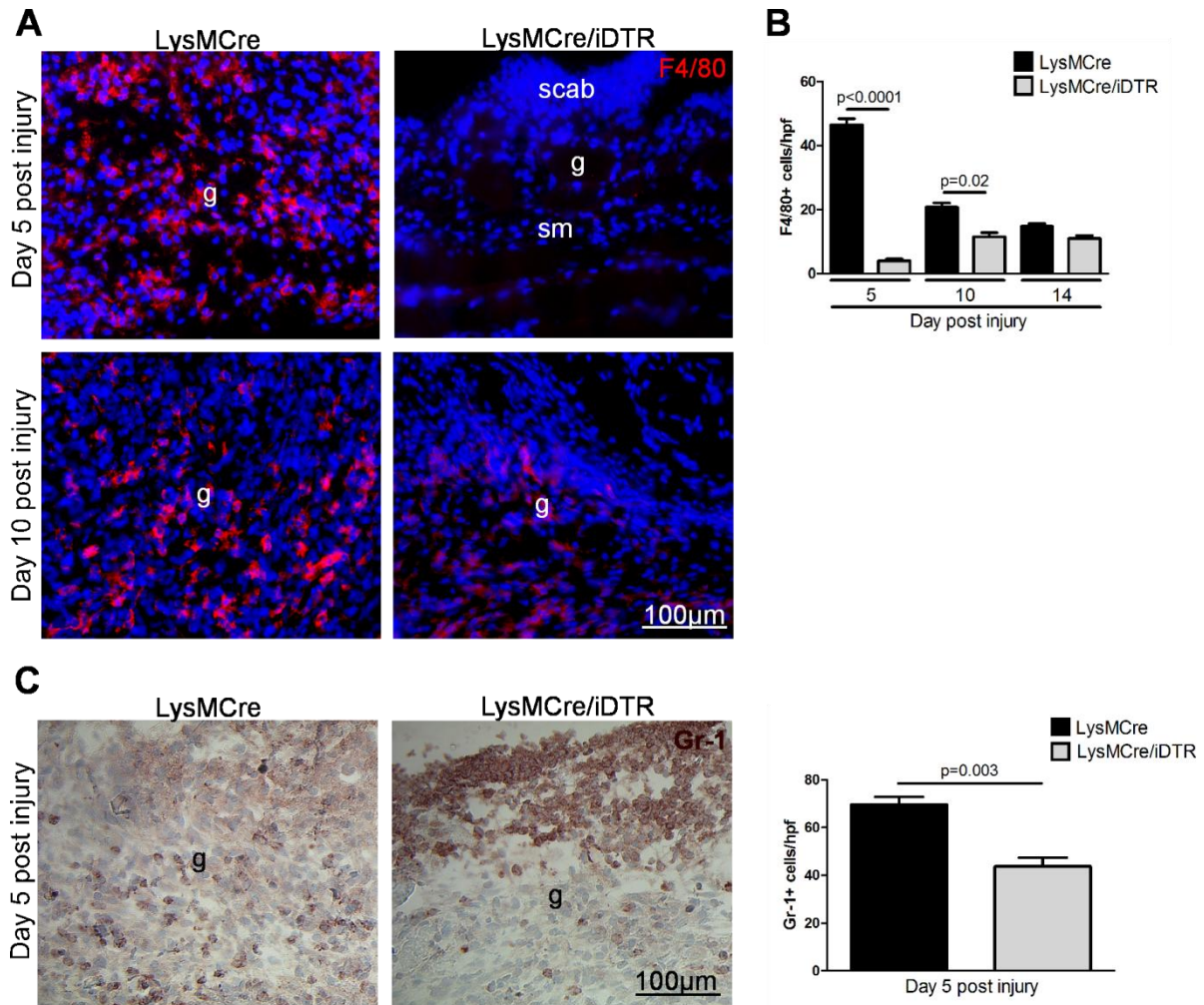


Figure 11: DT-mediated macrophage depletion in LysMCre/iDTR mice following DT injection regimen A. (A) Immunostaining for F4/80 (red) revealed the presence of numerous macrophages in the granulation tissue of control (LysMCre) wounds 5 and 10 days post injury; in LysMCre mice macrophages are absent at day 5 post injury and present 10 days post injury. **(B)** Quantification of F4/80 positive macrophages present in granulation tissue at indicated time points post injury. **(C)** Left: immunostaining for Gr-1 (brown) revealed the presence numerous neutrophils both in control and LysMCre/iDTR wounds 5 days post injury. Right: quantification of Gr-1 positive neutrophils present in granulation tissue of day 5 wounds post injury; data are expressed as mean \pm SD, $n = 3$ wounds on 3 mice for each time point and group. g, granulation tissue; sm, skeletal muscle; hpf, high power field.

Results

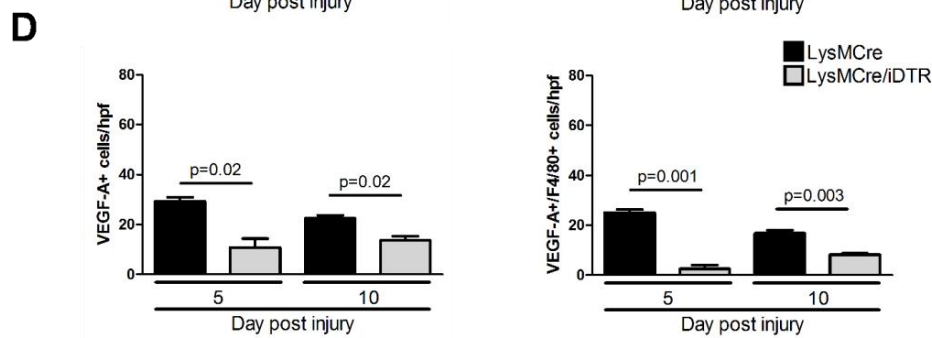
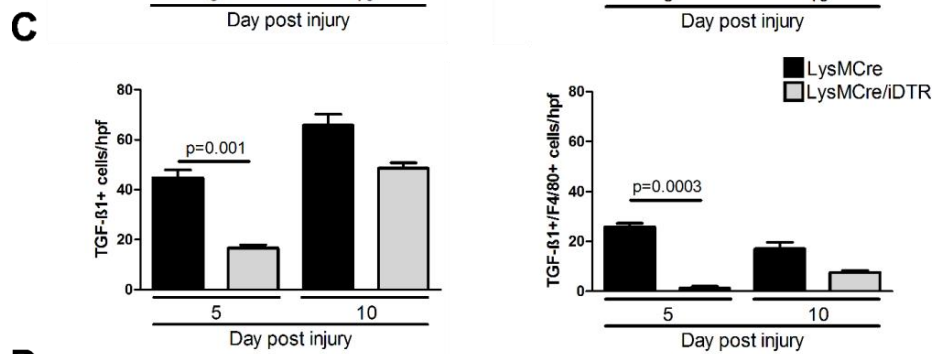
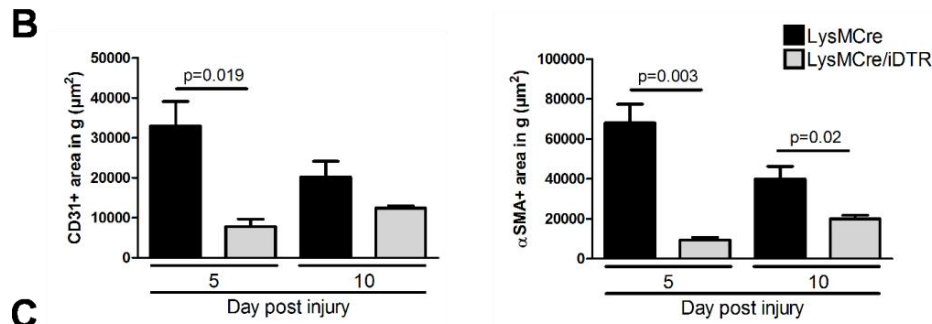
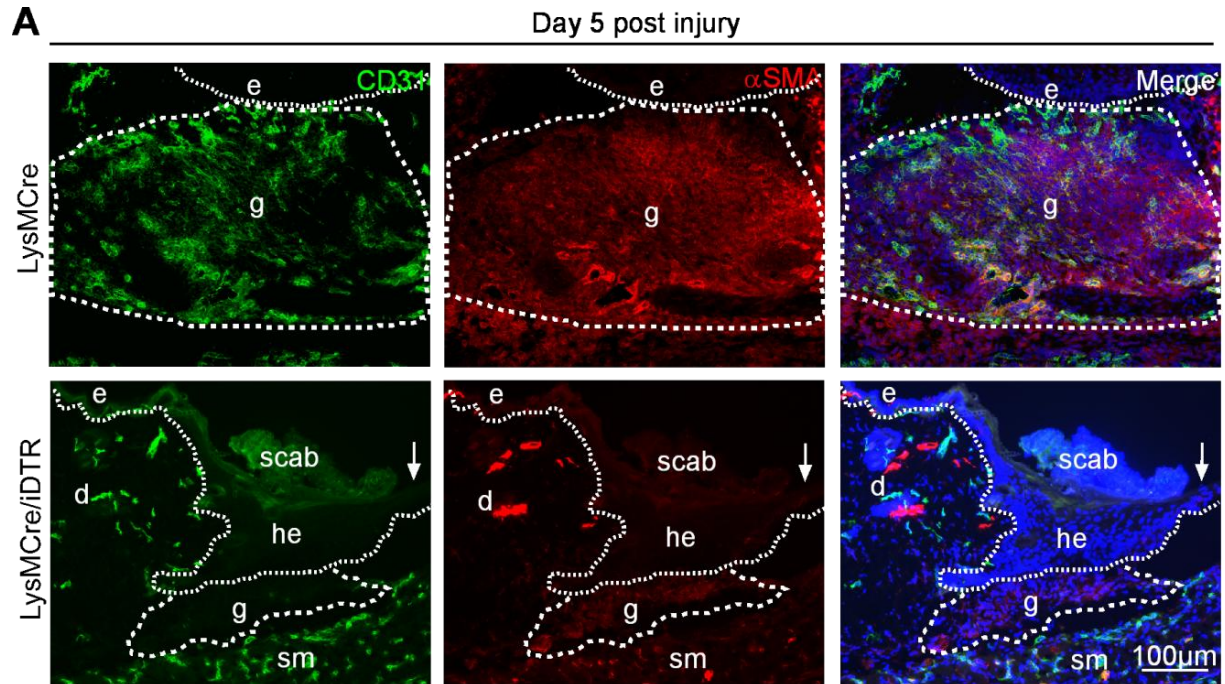
3.2.1.3 Wound vascularization and contraction is controlled by macrophage influx during the inflammatory phase of repair

To assess whether the influx of macrophages during the early stage of the repair response impacts wound angiogenesis, morphometric quantification of the expression of the endothelial cell marker CD31 within the area of granulation tissue was used as read-out for angiogenesis at the wound site. Wounds in control mice revealed a strong vascular response 5 days post injury which decreased about 30% until day 10 post injury (Figure 12 A, B left panel). In wounds of LysMCre/iDTR mice, vascular density was significantly reduced compared to control wounds 5 days post injury and slightly increased by day 10 post injury. Thereby, in LysMCre/iDTR and control mice, wound angiogenesis correlated positively with the presence of macrophages. Furthermore, to investigate whether the influx of macrophages during the phase of inflammation impacts wound contraction, the distance between the edges of the panniculus carnosus at the wound margins in LysMCre/iDTR and control mice receiving DT injections following regimen A were measured and indicated reduced wound contraction in macrophage-depleted wounds (Figure 10 D). In assessment with this, at both time points, α -SMA, a well-accepted marker for myofibroblast differentiation, was abundantly expressed throughout the entire granulation tissue (Figure 12 A, B right panel). In contrast, wounds of LysMCre/iDTR mice showed weak α -SMA staining in the scarce granulation tissue present at day 5 following injury (Figure 12 A), which slightly increased in intensity within the small amount of granulation tissue at day 10. Immunofluorescent double labeling for CD31 and α -SMA, indicated in wounds of control and LysMCre/iDTR mice a non-endothelial cell origin of the α -SMA staining and thereby the presence of myofibroblasts. This data is suggestive for attenuated myofibroblast differentiation and subsequent reduced wound contraction in the absence of macrophages during the early stage of tissue repair.

In order to identify factors that might mediate the accelerated vascular response and the myofibroblast differentiation in control mice, wound tissues were stained for TGF- β 1, a key mediator of myofibroblast differentiation [16] and for VEGF-A, one of the most potent angiogenic mediators [56]. In control wounds 5 and 10 days post injury, numerous wound cells were detected that stained positive for TGF- β 1 or VEGF-A within the granulation tissue (Figure 12 C, D left). Double staining for F4/80 and TGF- β 1 or VEGF-A indicated that macrophages represent a major fraction of TGF- β 1 or VEGF-A expressing cells (Figure 12 C, D right). Consistently, in macrophage-depleted wounds of LysMCre/iDTR mice 5 days post injury, staining for total TGF- β 1 and VEGF-A, but in particular also double staining for F4/80 and TGF- β 1 or VEGF-A was significantly reduced compared to control wounds (Figure 12 C, D left). These results suggest that macrophage-derived TGF- β 1 and VEGF-A could

Results

contribute to myofibroblast differentiation and the accelerated angiogenic response in control mice in the early phase of repair.



Results

Figure 12: Macrophage depletion during the early stage of repair attenuates angiogenesis and myofibroblast differentiation. LysMCre/iDTR and control (LysMCre) mice received DT injections following regimen A. **(A)** CD31 (green) and α -SMA (red) double immunostaining of day-5 wound tissue in control and LysMCre/iDTR mice, DAPI counterstaining of nuclei (blue); dotted line indicates basement membrane; hatched line outlines granulation tissue; e, epidermis; he, hyperproliferative epidermis; d, dermis; g, granulation tissue; sm, skeletal muscle; arrow points to the tip of epithelial tongue. **(B)** Morphometric quantification of the area within the granulation tissue which stained positive for CD31 and α -SMA at indicated time points after injury. Morphometric quantification of the area within the granulation tissue which stained positive for TGF- β 1 **(C)** and VEGF-A **(D)** at indicated time points after injury; double labeled macrophages for TGF- β 1 or VEGF-A and F4/80 were counted in high power fields (hpf). Data are expressed as mean \pm SD, $n = 3$ wounds on 3 mice for each time point and group.

3.2.1.4 Macrophage recruitment during the inflammatory phase of repair promotes alternative activation

To phenotypically characterize the macrophage infiltrate in wound tissue of LysMCre/iDTR and control mice receiving DT injections following regimen A (Figure 8), F4/80+ macrophages were analyzed for the expression of Fizz1 (found in inflammatory zone)/Relm- α and Ym1/ECF (eosinophil chemotactic factor). Expression of both factors was recently described as a reliable marker of alternatively activated macrophages [84-86]. Whereas in wound tissue of control mice at day 5 and 10 post injury, a large fraction of F4/80+ macrophages stained positive for Fizz1 (Figure 13 A-C), Ym1 was present only until day 5 post injury (Figure 13 C right). In contrast, in wounds of LysMCre/iDTR mice 5 and 10 days post injury the number of cells, that stained positive for F4/80 and Fizz1 or Ym1 was significantly reduced, even when the cells are allowed to infiltrate the wound area (Figure 13 A-C). These data indicated that the impaired healing response in LysMCre/iDTR mice receiving DT injections following regimen A (Figure 8) was not only due to reduced numbers of macrophages present at the wound site, but potentially also due to different activation states.

Results

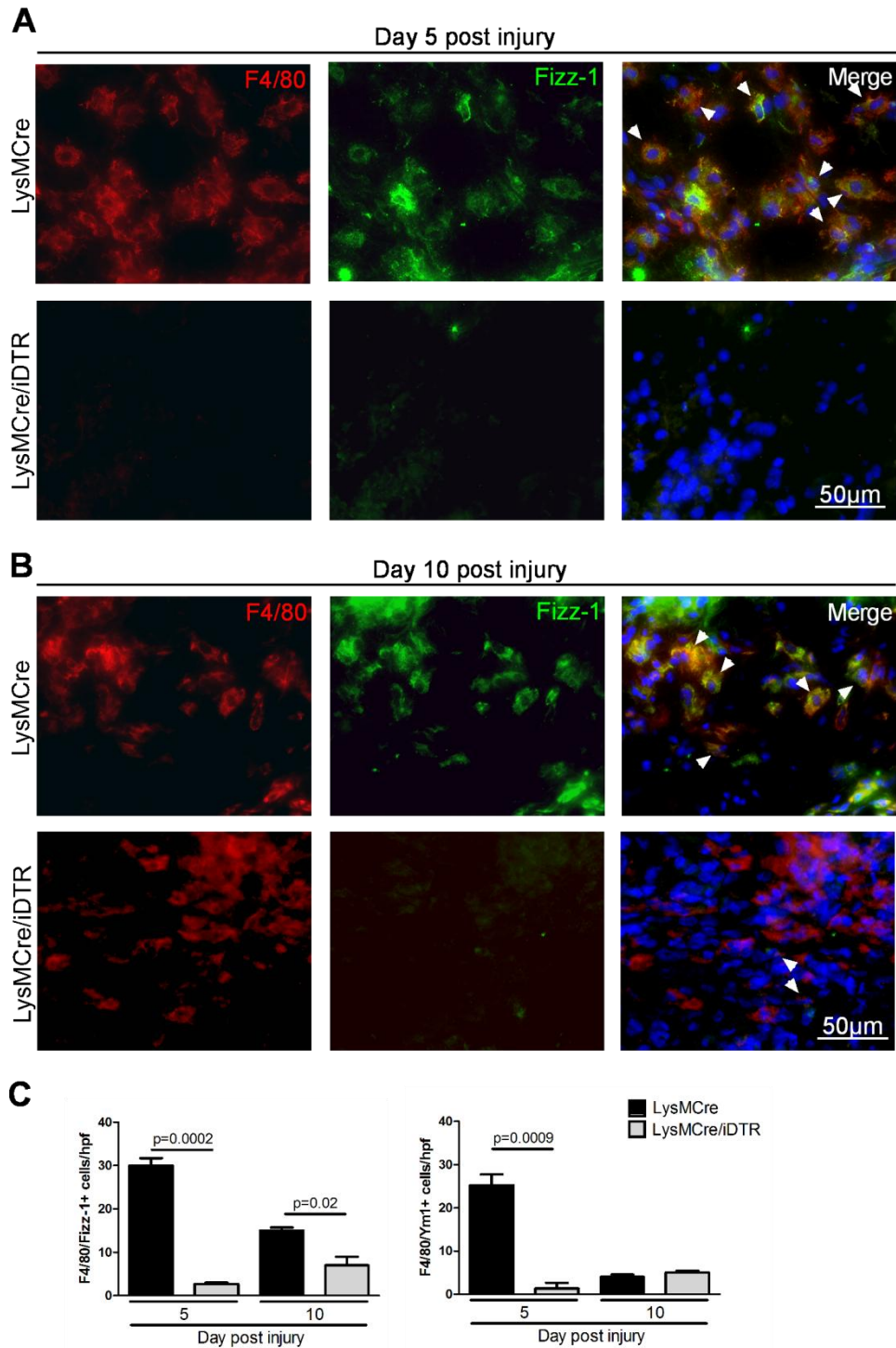


Figure 13: Fizz1- and Ym1-expressing macrophages in wound tissue of LysMCre/iDTR and control mice. LysMCre/iDTR and control (LysMCre) mice received DT injections following regimen A. **(A, B)** In granulation tissue of control mice at day 5 and 10 post injury double labeling for F4/80 (red) and Fizz1 (green) revealed expression of Fizz1 by macrophages; in contrast, in LysMCre/iDTR mice F4/80 and Fizz1 expressing cells are not detectable at day 5 post injury, in day-10 wounds F4/80 positive cells are negative for Fizz1 staining. DAPI counterstaining of nuclei (blue). **(C)** Morphometric quantification of macrophages present in granulation tissue at day 5 and 10 post injury in control and LysMCre/iDTR mice; double positive cells for F4/80 and Fizz1 or Ym1 were counted in high power fields (hpf). g, granulation tissue; arrow heads point to double positive cells; data are expressed as mean \pm SD, $n = 3$ wounds on 3 mice for each time point and group.

Results

3.2.2 Analysis of macrophage depletion during the mid stage of repair

3.2.2.1 Macrophages recruited during the inflammatory phase of tissue formation control vascular stability and the transition of granulation tissue into scar tissue

To characterize the functional impact of macrophages present in an already developed granulation tissue, skin wounds were inflicted on the back of control (LysMCre) and LysMCre/iDTR mice, which then received DT injections at day 3, 4, 6 and 9 after wounding (Figure 8, DT injection regimen B).

The macroscopic analysis of the early wound healing response in LysMCre/iDTR mice was similar to controls. However, DT-mediated macrophage depletion in LysMCre/iDTR mice during the mid stage of repair significantly delayed the subsequent wound closure rate when compared to controls (Figure 14).

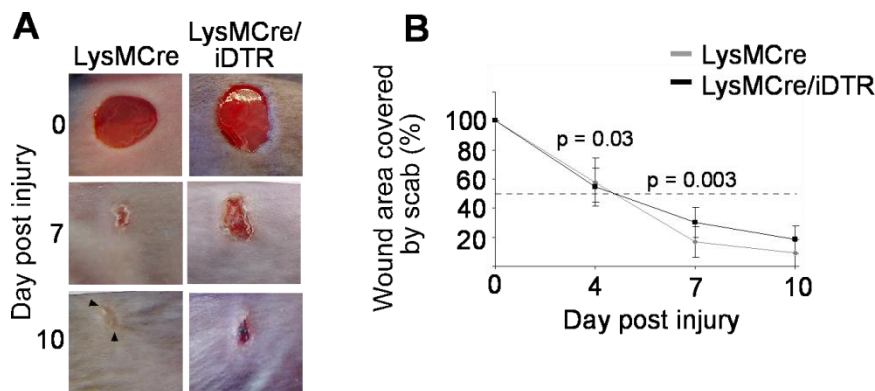


Figure 14: Macrophage depletion during the mid stage of repair delays the subsequent healing response. LysMCre/iDTR and control (LysMCre) mice received DT injections following regimen B. **(A)** Macroscopic appearance of LysMCre/iDTR wounds in which macrophages were depleted during the tissue formation phase of repair and control mice at indicated time points after injury; whereas wounds of control mice had already lost their scab, macrophage-depleted wounds still carry a firmly adherent scab 10 days after wounding. **(B)** The wound area was determined at the time points indicated using image analysis and expressed as percentage of the wound area immediately after injury. $n = 10$ wounds on 5 mice for each time point and genotype. Data are expressed as mean \pm SD.

These macroscopic findings were confirmed by histological assessment. For this purpose LysMCre/iDTR and control mice were sacrificed on day 7 and 10 after injury, and the wound tissue (4-10 wounds on 3-5 mice per time point for each group) was excised.

Results

As revealed by H&E-stained paraffin sections 7 days post injury, all wounds in control mice and six out of 10 wounds in LysMCre/iDTR mice showed complete wound closure (Figure 15 A, B). Interestingly, whereas until day 10 post injury granulation tissue in all wounds of control animals matured and showed regular transition into a scar tissue (Figure 15 A), all wounds in LysMCre/iDTR mice revealed a regression of granulation tissue maturation and appeared immature (Figure 15 A). However, the amount of granulation tissue was not affected (Figure 15 D). Immature appearance of day 10 old, macrophage-depleted granulation tissue in LysMCre/iDTR mice was reflected by severe hemorrhages, fibrin and serum exudates, which was present in all wounds analyzed (8 wounds on 4 mice). Hemorrhages were assessed by the presence of extravascular erythrocytes on H&E stained paraffin sections (Figure 15 A) as well as by immunohistochemical staining for fibrinogen/fibrin (Figure 15 E). Morphometric analysis of fibrinogen/fibrin staining revealed a significant increase in macrophage-depleted versus control mice. Furthermore, attenuated functional capacity of granulation tissue at days 7 and 10 post injury in wounds of LysMCre/iDTR mice became evident by a slightly weaker wound contraction, which however did not reach statistical significance (Figure 15 C). In addition, hypertrophic epidermal wound edges at day 5 post injury regressed into atrophic epidermal wound edges, which may contribute to the decrease in their wound closure capacity at day 10 post injury observed in LysMCre/iDTR wounds (Figure 15 B).

Staining for F4/80 revealed that the morphological and functional alterations in wounds of LysMCre/iDTR mice at day 7 and 10 post injury were characterized by a significant reduction of macrophages within the granulation tissue compared with controls (Figure 16 A, B). However, whereas in wound tissue of control mice, at both time points post injury, only few neutrophils were detected, their number was increased in macrophage-depleted wounds (Figure 16 C, D). Of interest, while hemorrhages were present in all wounds of LysMCre/iDTR mice, the number of neutrophils was only increased in those wounds with incomplete epithelialization. Overall, these data demonstrate that DT-mediated macrophage depletion in LysMCre/iDTR mice during the phase of tissue maturation severely disturbed the transition of the mid stage into the late stage of the repair response. Neutrophils appeared resistant to DT-mediated cell depletion.

Results

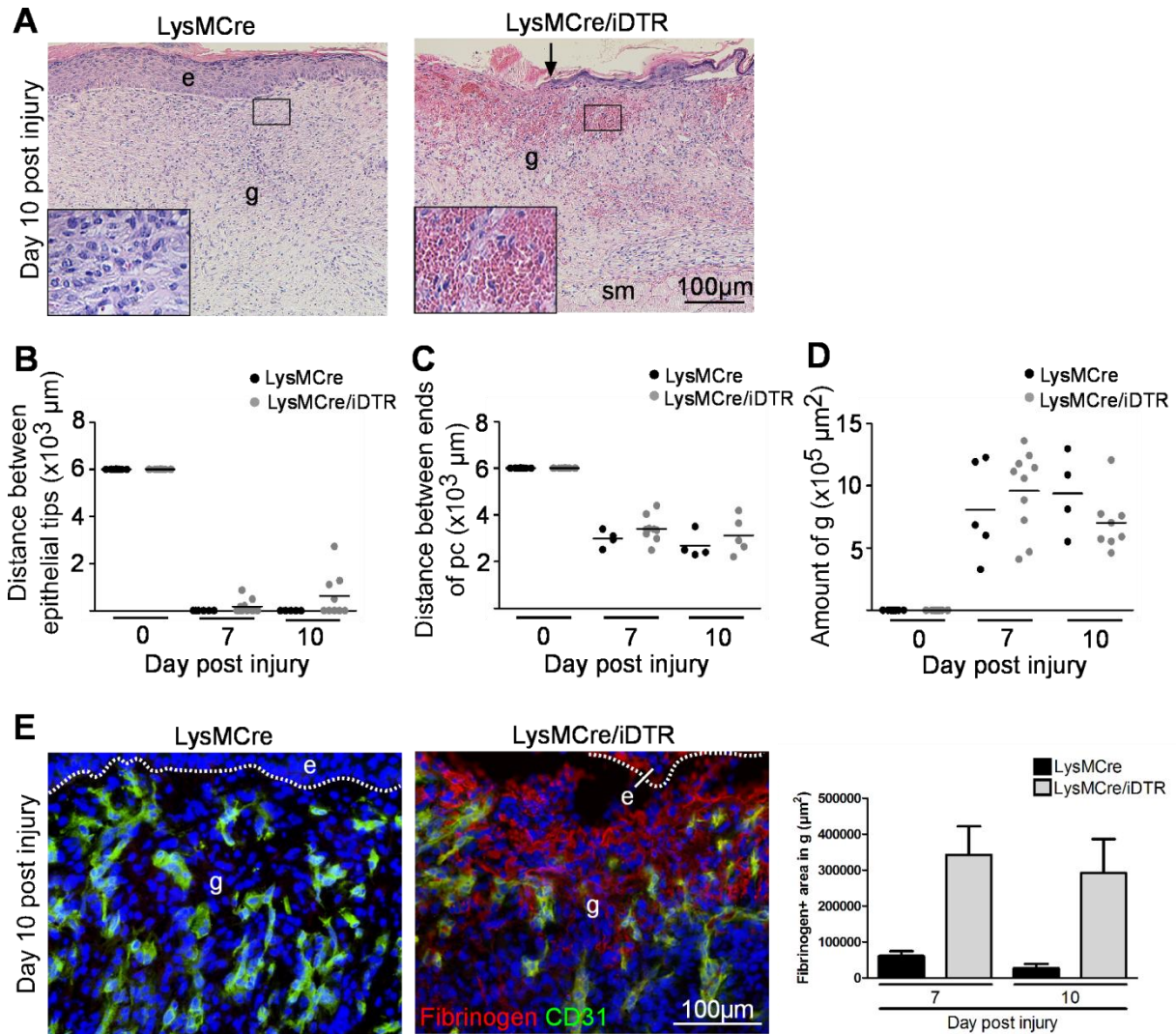


Figure 15: Macrophage depletion during the mid stage of repair abrogates the transition into the phase of tissue maturation. LysMCre/iDTR and control (LysMCre) mice received DT injections following regimen B. **(A)** H&E stainings of wounds of control and LysMCre/iDTR mice 10 days after injury. Control wounds reveal a cellular and vascular late granulation tissue covered by a closed hyperproliferative neo-epithelium. In contrast, in LysMCre/iDTR wounds severe hemorrhages, fibrin and serum exudates are present; the epithelium is not closed and the epidermal wound edge is thin and detached. **(B-D)** Morphometric analysis of wound tissue at different time points post injury: **(B)** Distance between the epithelial tips; **(C)** Distance between the edges of the panniculus carnosus; **(D)** Amount of granulation tissue. Each dot represents one wound on one mouse, horizontal bar represents the mean. **(E)** Left: immunohistochemical stainings of fibrinogen/fibrin and vessels (CD31) in wounds of control and LysMCre/iDTR mice 10 days after injury. Control wounds reveal a vascular late granulation tissue lacking fibrinogen/fibrin. In contrast, in LysMCre/iDTR wounds severe fibrinogen/fibrin exudate is present. DAPI counterstaining of nuclei (blue). Right: morphometric analysis of fibrinogen/fibrin exudate in wound tissue at indicated time points post injury. $n = 3$ wounds on three different mice per time point and group. Data are expressed as mean \pm SD. e, epidermis; sm, subcutaneous muscle layer; g, granulation tissue; pc, panniculus carnosus.

Results

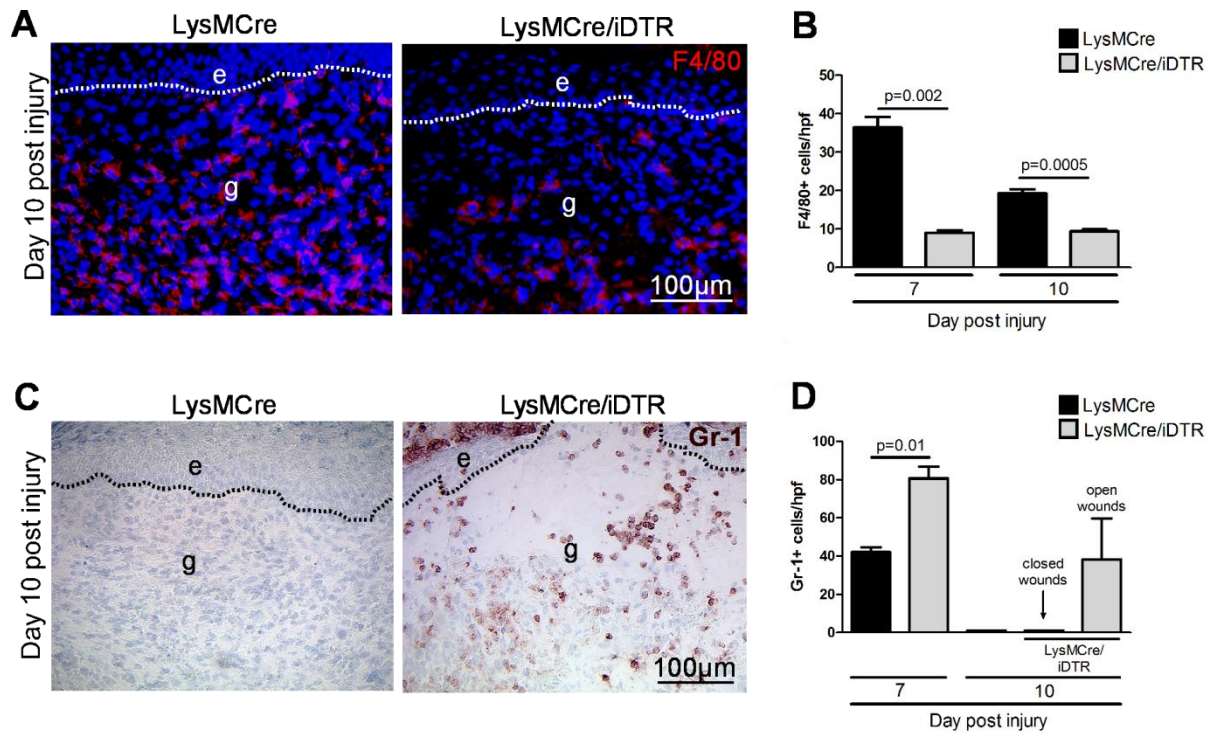


Figure 16: DT-mediated macrophage depletion in LysMCre/iDTR mice during the mid stage of repair. LysMCre/iDTR and control (LysMCre) mice received DT injections following regimen B. **(A)** Numerous macrophages (stained by F4/80, red) are present in granulation tissue of control wounds 10 days post injury, whereas macrophages are almost absent in granulation tissue of LysMCre/iDTR mice. DAPI counterstaining of nuclei (blue). **(B)** Morphometric quantification of macrophages present in granulation tissue at indicated days post injury. **(C)** Whereas neutrophils are absent in control wounds, numerous neutrophils (stained by Gr-1, brown) are present in wounds of LysMCre/iDTR mice 10 days post injury. **(D)** Morphometric quantification of neutrophils present in granulation tissue at indicated days post injury. e, epidermis; g, granulation tissue; dotted line indicates basement membrane; data are expressed as mean \pm SD, $n = 3$ wounds on 3 mice for each time point and group.

3.2.2.2 Endothelial cell damage and apoptosis in macrophage-depleted granulation tissue

To unravel the reason for the severe hemorrhages observed in macrophage-depleted granulation tissue (Figure 15 A, E), vessel maturation and endothelial cell apoptosis in LysMCre/iDTR and control (LysMCre) mice receiving DT injections following regimen B (Figure 8) was analyzed. Maturation of blood vessels in healing wounds is reflected by the presence of perivascular cells [73, 87]. Double-immunofluorescent labeling for CD31 and the pericyte marker desmin revealed that in both granulation tissue of control and LysMCre/iDTR wounds, desmin-positive cells were associated with vascular structures at day 7 and 10 post injury (Figure 17 A). To test, if the observed hemorrhages were due to endothelial cell apoptosis, co-staining for CD31 and the apoptosis marker cleaved caspase-3 were performed. This staining revealed that, whereas in granulation tissue of control wounds

Results

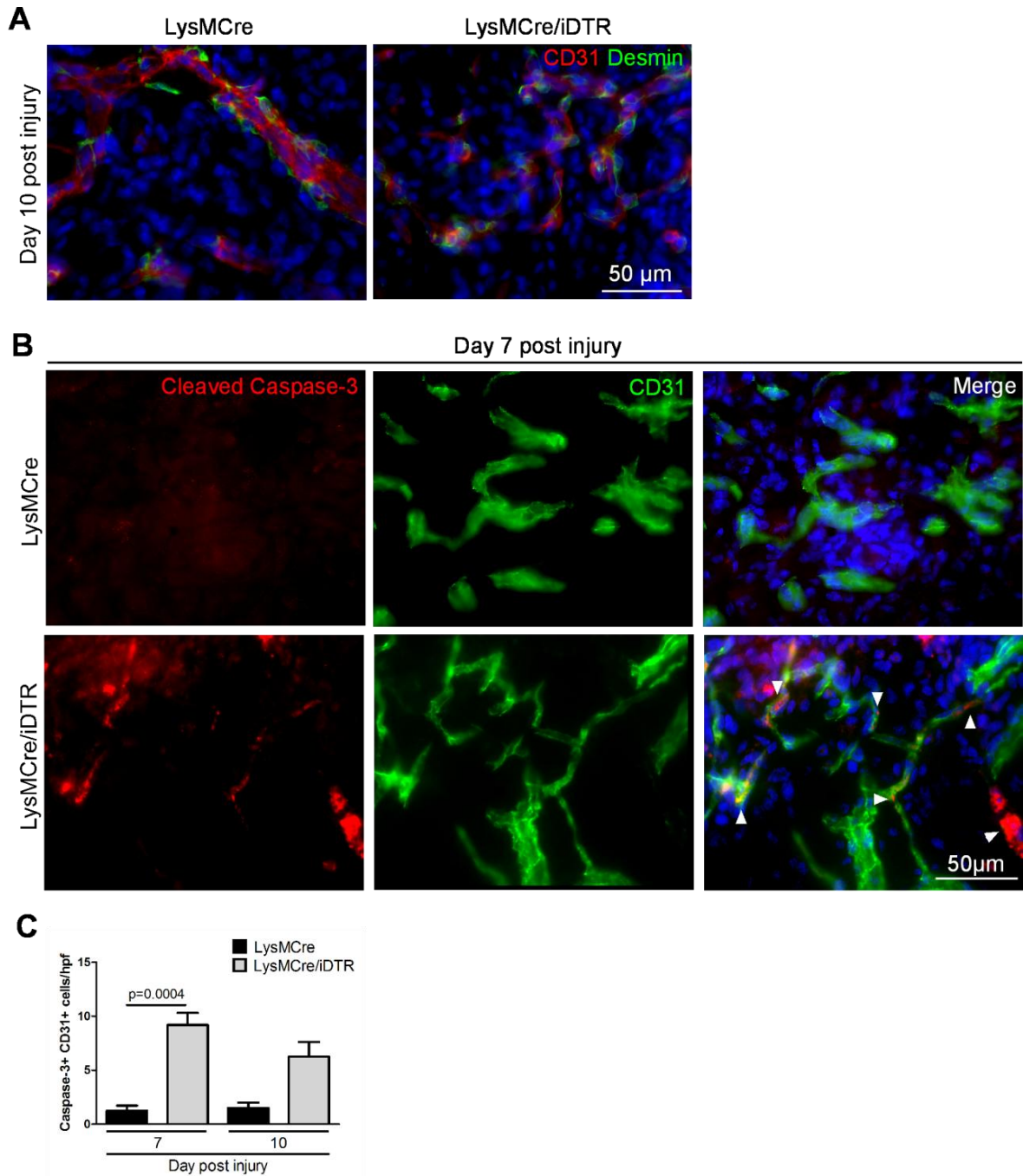


Figure 17: Macrophage depletion during the phase of tissue formation results in endothelial cell apoptosis, but does not alter pericyte recruitment. LysMCre/iDTR and control (LysMCre) mice received DT injections following regimen B. **(A)** Double labeling for desmin (green) and CD31 (red) revealed no major differences in the coverage of blood vessels by pericytes in granulation tissue of macrophage-depleted wounds 10 days post injury. **(B)** Double labeling for cleaved caspase-3 (red) and CD31 (green) revealed numerous apoptotic endothelial cells in granulation tissue of macrophage-depleted wounds, 7 days post injury; arrowheads indicate double positive cells. DAPI counterstaining of nuclei (blue). **(C)** Morphometric quantification of the area within the granulation tissue which stained positive for activated caspase-3 and CD31. Double immunolabeled cells were counted in high power fields (hpf). Data are expressed as mean \pm SD, $n = 3$ wounds on 3 mice for each time point and group.

Results

endothelial cell apoptosis was a rare event, in macrophage-depleted granulation tissue numerous apoptotic endothelial cells were present (Figure 17 C). These findings suggest that hemorrhages observed in macrophage-depleted granulation tissue in LysMCre/iDTR mice were rather caused by misscheduled apoptosis than altered vessel maturation.

3.2.3 Analysis of macrophage depletion during the late stage of repair

3.2.3.1 Macrophages present at the late stage of repair do not impact tissue maturation

To characterize the functional impact of macrophages present during the phase of tissue maturation following restoration of the epidermal barrier, skin wounds were inflicted on the back of control (LysMCre) and LysMCre/iDTR mice and DT injections were given at day 8, 9, 11 and 13 after wounding (Figure 8, DT injection regimen C).

Depletion of macrophages during the phase of tissue maturation did not result in macroscopic or microscopic alterations of the wound tissue compared to control wounds. Fourteen days post injury both macrophage-depleted and control wounds had lost their eschar and revealed similar scar tissue (Figure 18 A-C). LysMCre/iDTR and control mice were sacrificed on each of days 10 and 14 after injury and the wound tissue (4-7 wounds on 4-7 mice per time point for each group) was excised. As revealed on H&E-stained paraffin sections 14 days post injury, all wounds in control and LysMCre/iDTR mice showed complete wound closure and a slightly hyperproliferative neo-epidermis covering the scar tissue (Figure 18 B). Morphometric analysis revealed that the amount of scar tissue was similar in control and LysMCre/iDTR wounds (Figure 18 C).

Scar tissue stained for F4/80 revealed the presence of macrophages in control mice between day 10 and day 14 post injury, but macrophage numbers were significantly reduced in DT injected LysMCre/iDTR mice (Figure 19 A). Of interest, at all time points analyzed, neutrophils were absent in both control and macrophage-depleted wounds as shown by staining for Gr-1 (Figure 19 B). Furthermore, as revealed by Giemsa staining at day 14 post injury the number of mast cells present in scar tissue was similar in control and LysMCre/iDTR mice (Figure 19 C).

Results

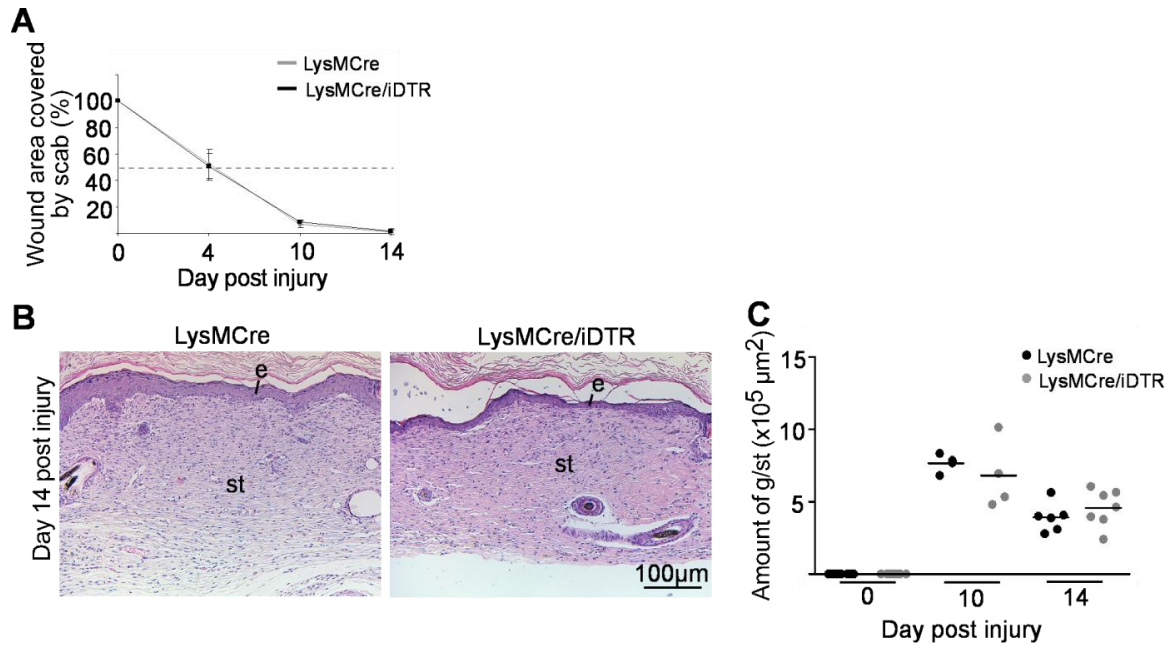


Figure 18: DT-mediated macrophage depletion during the late stage of the repair response does not impact tissue maturation. LysMCre/iDTR and control (LysMCre) mice received DT injections following regimen C. **(A)** At the time points indicated, the macroscopic wound area was determined using image analysis and expressed as percentage of the wound area immediately after injury ($n = 4$ wounds on 4 mice for each time point and genotype). **(B)** H&E stainings of wounds of control and LysMCre/iDTR mice 14 days after injury. Wounds of control and LysMCre/iDTR mice were closed and showed a similar epithelium and scar tissue. **(C)** Morphometric analysis of the amount of granulation or scar tissue 10 and 14 days post injury. Each dot represents one wound on one mouse; horizontal bar represents the mean. e, epidermis; st, scar tissue; g, granulation tissue.

Results

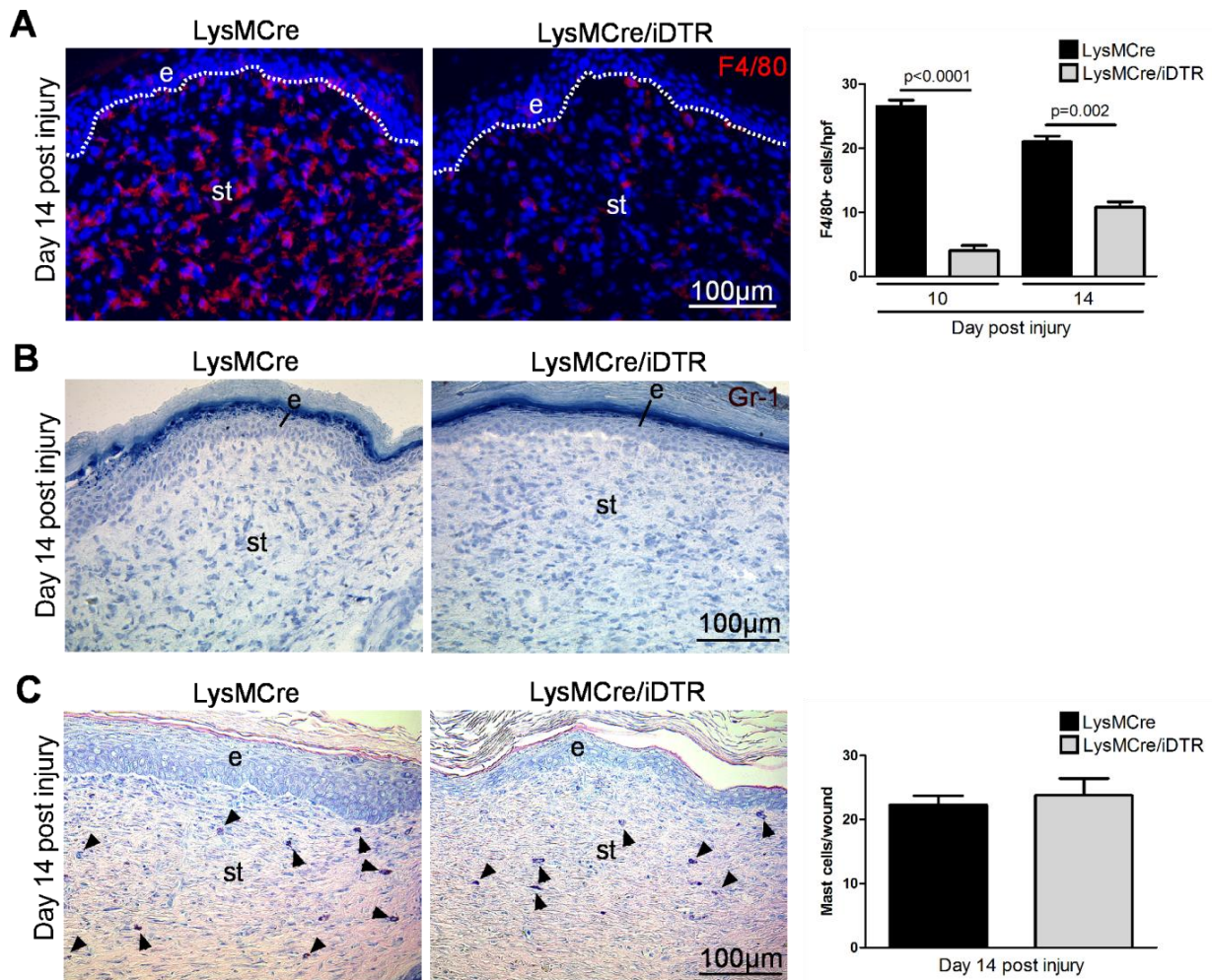


Figure 19: Macrophages and neutrophils are absent whereas mast cell numbers are similar in LysMCre/iDTR and control mice. LysMCre/iDTR and control (LysMCre) mice received DT injections following regimen C. **(A)** Left: macrophages (stained by F4/80, red) are present in scar tissue of control wounds 14 days post injury, whereas macrophages are almost absent in granulation tissue of LysMCre/iDTR mice. DAPI counterstaining of nuclei (blue). Right: quantification of F4/80 positive cells in the granulation tissue in control and LysMCre/iDTR mice at indicated time points post injury. **(B)** Neutrophils (stained by Gr-1) are absent in scar tissue of control and LysMCre/iDTR wounds 14 days post injury. **(C)** Left: mast cells (visualized by Giemsa staining) are present in scar tissue of LysMCre/iDTR and control wounds 14 days post injury. Right: quantification of positive stained cells in the scar tissue of control and LysMCre/iDTR wounds reveal similar numbers of mast cells 14 days post injury. e, epidermis; st, scar tissue; hpf, high power field; data are expressed as mean \pm SD. $n = 3$ wounds on three mice per time point and genotype.

3.3 The impact of myeloid cell-derived VEGF-A on the outcome of the wound healing response

3.3.1 Macrophages are the prevailing VEGF-A source in the early phase of tissue repair

The novel findings up to here are that macrophages have distinct functions in the different phases of skin repair, and that their impact on endothelial cell function seems to be critical. In order to identify mechanisms by which macrophages might influence endothelial cell function, the role of VEGF-A, the major regulator of endothelial cell biology and angiogenesis was investigated. VEGF-A is henceforth abbreviated as VEGF.

First, the expression pattern of VEGF in normal unwounded skin as well as in wounds at different time points post injury was analyzed. For this purpose, wild type mice were sacrificed and normal skin from unwounded mice as well as wounds on days 4, 7, and 14 post injury were analyzed for VEGF expression by quantitative real time PCR (4-10 wounds on 2 to 4 mice per time point). VEGF expression was strongly up-regulated after wounding at day 4 post injury in comparison to unwounded skin and declined during the subsequent days of healing (Figure 20 A). To further analyze the dynamics of VEGF expression in wounds and to identify different cellular compartments of VEGF expression, a reporter mouse line was used, in which both the VEGF gene expression and the lacZ reporter gene expression are under control of the murine VEGF promoter. By cloning an internal ribosome entry site in the 3'- untranslated region of the VEGF gene, a simultaneous expression of both proteins is ensured (kindly provided by Andras Nagy, [88]). Reporter mice were genotyped by PCR and VEGF-lacZ^{+wt} (VEGF-lacZ) mice were used as experimental mice (Figure 20 B). To analyze VEGF expression in these reporter mice, mice were sacrificed and normal unwounded skin as well as wounds at day 4, 7, and 14 post injury were harvested (8-12 wounds on 2-3 mice per time point). To unravel VEGF expression, wound sections were stained with X-Gal (BCIG, bromo-chloro-indolyl-galactopyranoside), a substrate for the β -galactosidase, and photographed. As a negative control to show specificity of the staining, lacZ negative littermates (VEGF-lacZ^{wt/wt}, Figure 20 B) were treated and analyzed in the same way (data not shown). Whereas unwounded skin revealed only few VEGF positive cells present within the subcutaneous fat layer, skin injury resulted in a robust increase of VEGF expressing cells within the epidermal and dermal compartment. During the early phase of repair, VEGF expressing cells were scattered throughout the granulation tissue and were present within the basal and suprabasal layers of the neo-epithelial tongue at the wound edges (Figure 20 C). As the wound healing response advanced the number of VEGF expressing cells within the granulation tissue declined, while the number of VEGF positive cells increased and their

Results

presence was sustained in the neo-epithelium (Figure 20 C). By day 14 post injury only few VEGF positive cells were detectable in both compartments (Figure 20 C).

The shift of VEGF expressing cells from macrophages predominating the early phase of repair and non-myeloid cells, most likely keratinocytes, during the later stage was corroborated by FACS analysis of single cell suspensions of wound tissue obtained from VEGF-lacZ reporter mice. VEGF expression was detected by fluorescein di- β -D-galactopyranoside (FDG) staining, a further substrate for β -galactosidase resulting in a fluorescent cleavage product. The threshold for positive FDG staining was set in relation to the wild type control (VEGF-lacZ^{wt/wt}), treated with FDG as well (negative control, data not shown). During the early phase of repair, F4/80⁺CD11b⁺ cells represented the predominant cell type expressing VEGF at the wound site accounting for 65%. Polymorphonuclear granulocytes (Gr1⁺CD11b⁺) and non-myeloid cells (F4/80⁻CD11b⁻Gr1⁻CD115⁻) constituted a minor portion of VEGF expressing cells, with 19% and 17%, respectively. Whereas the fraction of VEGF expressing F4/80⁺CD11b⁺ cells decreased over the healing time, the portion of non-myeloid cells increased (Figure 20 D). Interestingly, although F4/80⁺CD11b⁺ macrophages represented the major cell source expressing VEGF during the early phase of repair, only a small fraction of all macrophages (19.1%) present at the wound site expressed VEGF. This fraction further declined to 5.6% following wound closure (Figure 20 E). Together, these findings demonstrate a dynamic switch of VEGF expression in physiological skin wound healing between macrophages, being the major source of VEGF during the early phase and the neo-epithelium in the late phase. Furthermore, the finding that VEGF expression in macrophages is restricted to a specific population of macrophages at the wound site is in accordance with the idea of a functional heterogeneity of macrophages during skin repair.

Results

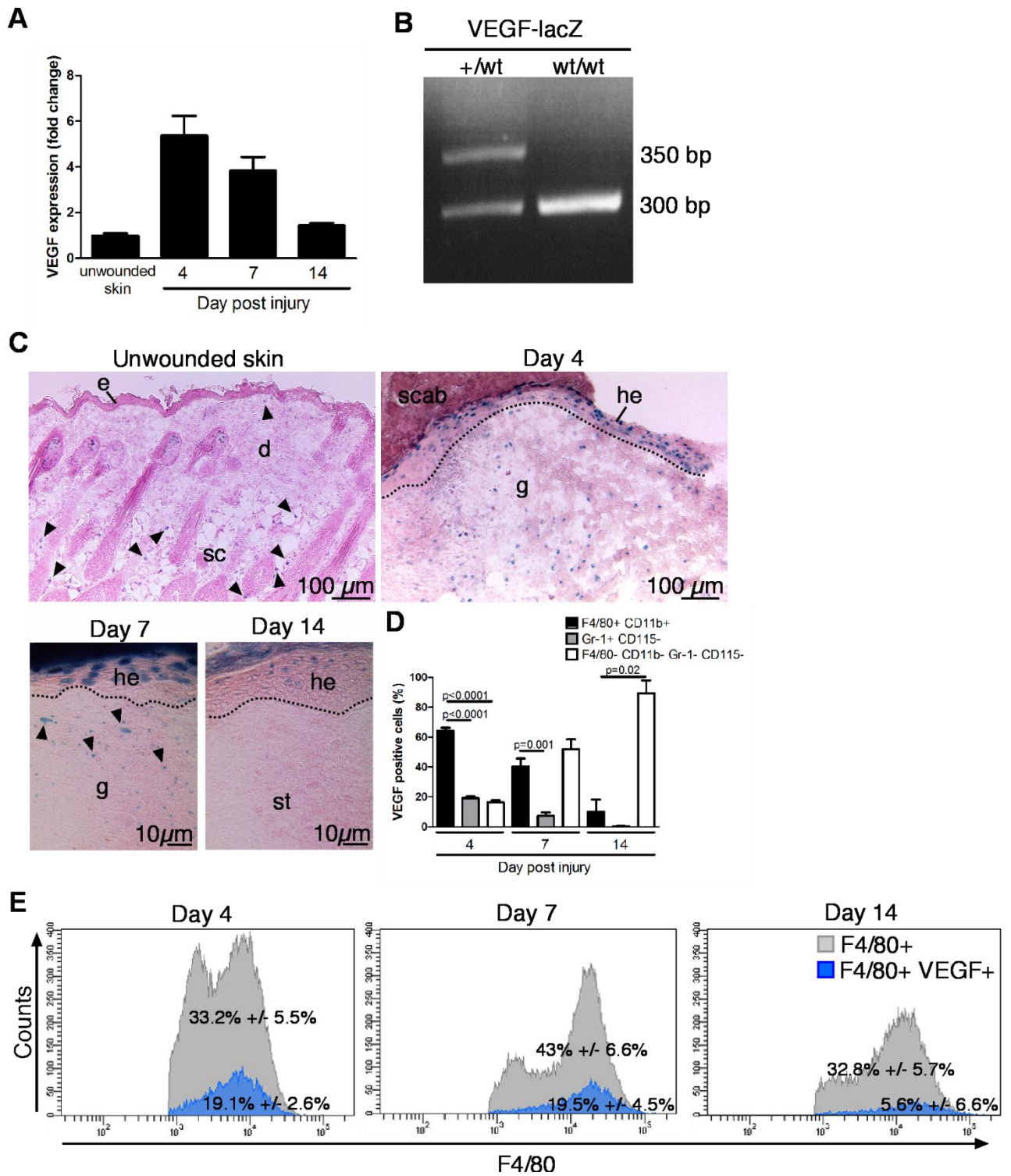


Figure 20: Macrophages express VEGF in the early phase of skin repair. (A) Real time PCR analysis for VEGF expression levels in wild type unwounded skin and wounds at day 4, 7, and 14 post injury. VEGF expression is strongly induced at day 4 post wounding and declines over the subsequent phases of healing. $n = 4-10$ wounds on 4-5 mice. (B) VEGF-lacZ mice were genotyped by PCR. The 350 bp fragment indicates the presence of one allele including the lacZ reporter gene, whereas the 300 bp fragment shows two wild type alleles. bp, base pairs. (C) X-Gal staining (blue) of unwounded skin and wounds at days 4, 7, and 14 post injury, harvested from VEGF-lacZ reporter mice. VEGF expression is nearly absent in unwounded skin. An induction of VEGF expression is shown in day-4 wounds in the hyperproliferative epithelium as well as in the granulation tissue, whereas the signal weakens at days 7 and 14 post injury. e, epidermis; d, dermis; sc, subcutaneous fat tissue; he,

Results

hyperproliferative epithelium; g, granulation tissue. Arrowheads point to positive stained cells. **(D)** FACS analysis of wound tissue 4, 7, and 14 post injury from VEGF-lacZ reporter mice. VEGF expression was unravelled by FDG staining, macrophages were identified by staining for F4/80 and CD11b and neutrophils by staining for Gr-1 and CD115 to exclude monocytes. At day 4 post wounding 65% of all wound cells stained positive for FDG and the two macrophage markers. Seven and fourteen days post wounding the portion of macrophages which stained positive for VEGF decreases and the portion of the non-myeloid cell population increases. **(E)** Histogramm of the FACS analysis, gated for F4/80 positive as well as F4/80 and FDG double positive wound cells. At day 4 post injury, only 19.1% of all F4/80 positive wound macrophages stained positive for VEGF expression, which decreases continuing for the subsequent healing phases. Grey areas reflect the macrophage portion of all wound cells at the time points indicated. Data are expressed as mean \pm SD. $n = 8-12$ wounds on 2-3 mice per time point.

3.3.2 VEGF expressing macrophages reveal a pro-inflammatory M1 phenotype

To examine the activation state of VEGF expressing macrophages infiltrating the wound site, F4/80⁺FDG(VEGF)⁺ and F4/80⁺FDG(VEGF)⁻ cells were isolated from the wound tissue of VEGF-lacZ reporter mice by FACS and analyzed for M1 and M2 gene expression profiles. VEGF expressing macrophages revealed a robust up-regulation of IL-6 and iNOS when compared to VEGF negative macrophages at day 4 post injury (Figure 21). No major differences between VEGF positive and negative macrophages were found for IL-1 β , TNF- α as well as for M2 gene signatures including Fizz-1, IL-10 and TGF- β at both time points analyzed. Even though there was a tendency of increased arginase expression in VEGF positive wound macrophages up to day 7 post injury when compared to VEGF negative macrophages, this difference was not significant (Figure 21). Together, these findings suggest that in physiological skin repair, a pro-angiogenic phenotype of macrophages is characterized rather by classical activation than by alternative activation. Similarly, as has been shown during repair of other organ systems [89, 90] and pathological conditions including tumorigenesis and macular degeneration [90].

3.3.3 Efficient VEGF gene deletion in macrophages

To analyze the functional impact of the VEGF producing macrophage population on the outcome of the wound healing response, conditional gene targeting was used to specifically deplete the VEGF gene in macrophages. To this end, a VEGF floxed mouse strain, with *loxP* sites flanking the third exon of the VEGF gene (kindly provided by Napoleone Ferrara, [53]) was crossed to the LysMCre mouse line, reported to express the *Cre* recombinase in myeloid cells [83]. Genetic recombination leads to a frameshift of the VEGF gene resulting in an early stop codon after exon 2. Both mouse lines were genotyped by PCR (Figure 6 B,

Results

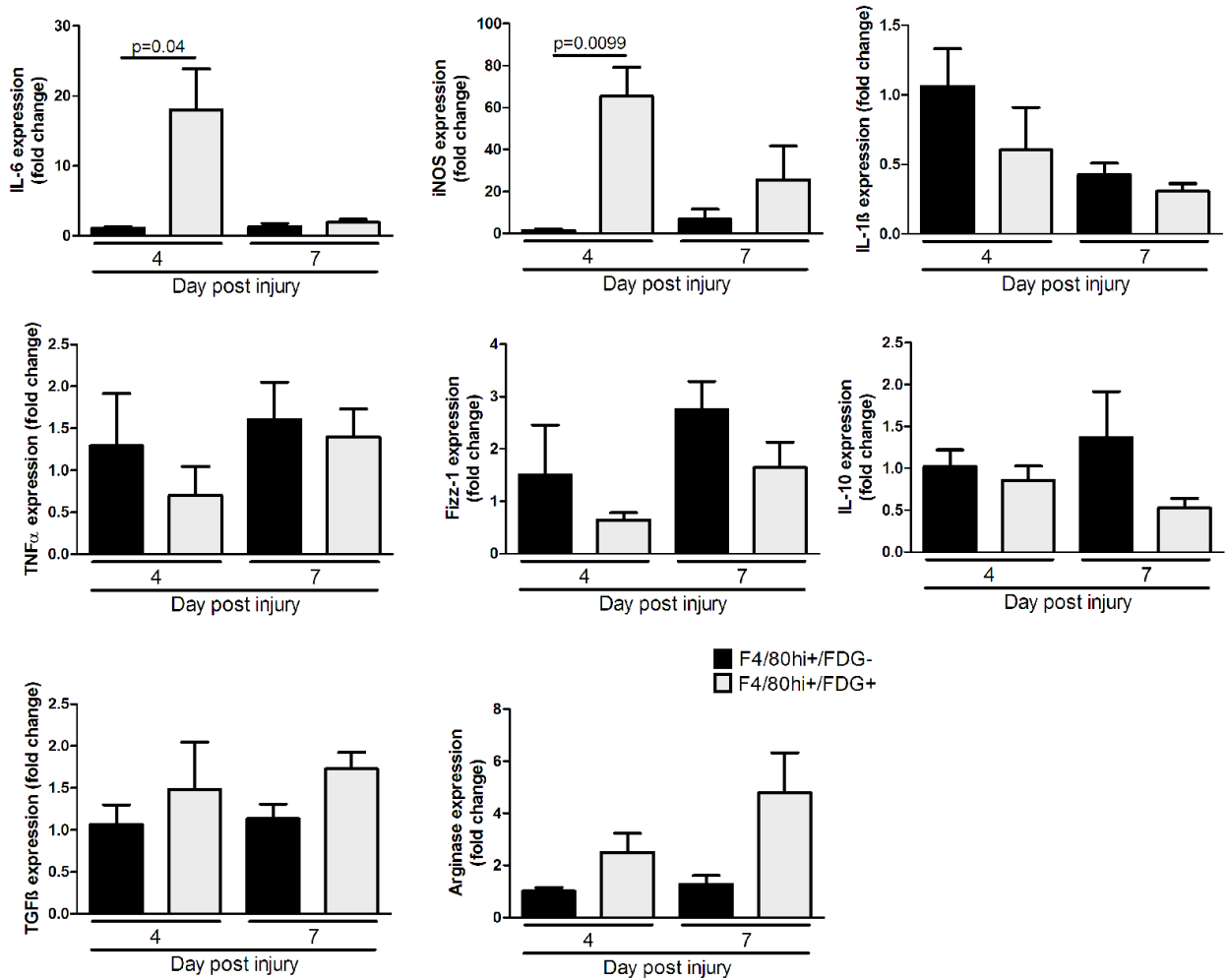


Figure 21: VEGF-expressing macrophages tend to the classically activated phenotype. Quantitative real time PCR analysis of isolated F4/80 positive wound macrophages from VEGF-lacZ reporter mice at day 4 and 7 post injury, which were either positive or negative for FDG staining, reflecting VEGF expression. Markers for the alternatively activated phenotype, such as Fizz-1, IL-10, TGF- β and arginase are equally expressed, both in macrophages positive and negative for VEGF expression. The pro-inflammatory cytokines IL-6 and iNOS are significantly up-regulated 4 days post injury in macrophages positive for VEGF expression, whereas IL-1 β and TNF- α were equally expressed. $n = 12$ wounds on 3 mice per time point. Data are expressed as mean \pm SD.

right panel and Figure 22 A) and efficient gene deletion was validated on the genomic, on the transcriptional as well as on the protein level *in vitro* (Figure 22 B-D). In order to confirm successful recombination and therefore gene deletion, primers were used flanking the floxed region, resulting in a 2.1 kb PCR fragment before recombination and in a 560 bp fragment after recombination (Figure 22 B). Furthermore, VEGF expression was measured in cultured peritoneal macrophages isolated from control (VEGF^{fl/fl}) and VEGF^{fl/fl} LysMCre mice. VEGF expression was induced in control macrophages when exposed to either hypoxia or a mixture of LPS and INF- γ in comparison to un-stimulated macrophages. Both stimulants are reported to be strong inducers of VEGF expression *in vitro* [91]. By contrast, despite

Results

stimulation with either LPS/INF- γ or hypoxia, induction of VEGF expression in VEGF^{fl/fl} LysMCre macrophages was completely absent (Figure 22 C). Additionally, efficient gene deletion was confirmed on the protein level. Cell culture supernatants of peritoneal macrophages, isolated from control and VEGF^{fl/fl} LysMCre mice were measured for secreted VEGF levels by ELISA. Control macrophages secreted VEGF after 24 and 48 hours of stimulation with LPS and INF- γ but this stimulation of VEGF release was not observed in VEGF^{fl/fl} LysMCre macrophages (Figure 22 D).

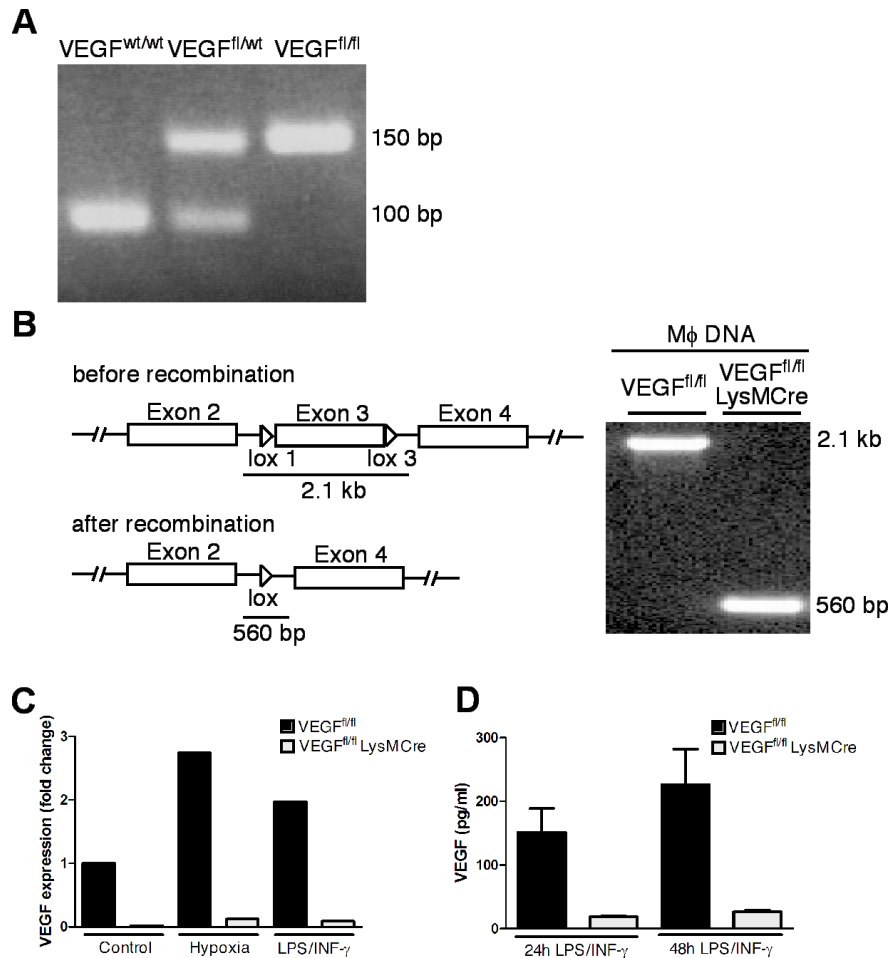


Figure 22: Efficient VEGF gene deletion in macrophages *in vitro*. (A) Genotyping PCR of VEGF floxed mice. A 150 bp fragment indicates the presence of one *loxP* site, whereas the 100 bp fragment reflects the wild type allele. (B) Left panel, scheme of the floxed VEGF gene construct with the two *loxP* sites in the two introns flanking exon 3. Bars below indicate the corresponding PCR fragment length for the gene deletion PCR (right panel). The 2.1 kb long fragment shows the allele before recombination, whereas the shorter 560 bp fragment indicates successful recombination. (C) Quantitative real time PCR analysis for VEGF expression in control (VEGF^{fl/fl}) and VEGF^{fl/fl} LysMCre peritoneal macrophages. VEGF expression is induced in control cells after exposure to either hypoxia or a mixture of LPS and INF- γ , which is in contrast blocked in VEGF^{fl/fl} LysMCre macrophages. $n = 3$ mice per genotype and condition, cells were pooled while seeding. (D) Quantitative ELISA for measurement of secreted VEGF protein levels of control and VEGF^{fl/fl} LysMCre peritoneal macrophages. Cells were stimulated with LPS and INF- γ for either 24 h or 48 h and supernatants were collected. Secreted VEGF levels were dramatically decreased in VEGF^{fl/fl} LysMCre macrophages in contrast to control cells. $n = 3$ mice per time point and genotype. Data are expressed as mean \pm SD.

Results

In order to confirm efficient gene deletion *in vivo*, F4/80 and CD11b positive wound macrophages were isolated at days 3, 5, 7, and 14 post injury from control (VEGF^{fl/fl}) and VEGF^{fl/fl} LysMCre mice by FACS. Further, for normalization CD115 and CD11b positive blood monocytes from the circulation were isolated from both groups as well. VEGF expression was strongly induced in control wound macrophages three days post injury, while VEGF expression was nearly absent in blood monocytes. VEGF expression in control wound macrophages declines from day 3 post injury on to the subsequent days of healing (Figure 23 A). In contrast VEGF expression in VEGF^{fl/fl} LysMCre wound macrophages was significantly reduced as compared to controls at all time points analyzed (Figure 23 A). In order to address the question whether the deletion of myeloid cell-derived VEGF impacts the total amount of VEGF expression in wounds, RNA was isolated from complete wound tissue of control and VEGF^{fl/fl} LysMCre wounds at days 3, 5, 7, and 14 post injury. VEGF expression induced in control mice was comparable to the expression in wild type mice in figure 20 A. In contrast, VEGF expression in VEGF^{fl/fl} LysMCre wounds was significantly reduced at day 3 post injury, indicating that myeloid cells deliver significant amounts of VEGF in early wounds (Figure 23 B).

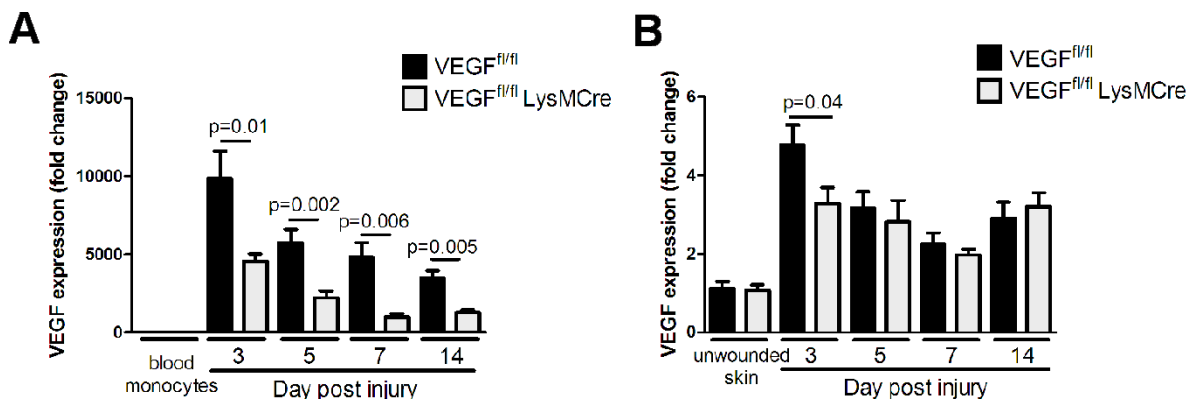


Figure 23: Efficient VEGF gene deletion in wound macrophages. (A) Quantitative real time PCR analysis for VEGF expression in F4/80 and CD11b positive wound macrophages isolated at days 3, 5, 7, and 14 post injury from control (VEGF^{fl/fl}) and VEGF^{fl/fl} LysMCre mice. VEGF expression levels were normalized to CD115 and CD11b positive blood monocytes. VEGF expression was clearly induced in control macrophages after wounding and significantly reduced in VEGF^{fl/fl} LysMCre macrophages. **(B)** Quantitative real time PCR analysis for VEGF expression in complete wound tissue of control and VEGF^{fl/fl} LysMCre mice at days 3, 5, 7, and 14 post injury, normalized to unwounded skin. VEGF expression was considerably induced after wounding in control mice and significantly reduced in VEGF^{fl/fl} LysMCre mice three days post injury. $n = 4-8$ wounds on 2-4 mice per time point and genotype. Data are expressed as mean \pm SD.

Results

3.3.4 VEGF synthesis by myeloid cells is critical for the induction of wound angiogenesis and tissue growth during the early phase of repair

To analyze the functional impact of myeloid cell-derived VEGF on the outcome of the wound healing response, control (VEGF^{fl/fl}) and VEGF^{fl/fl} LysMCre mice were sacrificed on days 4, 7, and 14 post injury, and the wound tissue (4-6 wounds on two to three mice per time point for each group) was excised and histomorphometrically analyzed. At day 4 post injury, a significantly reduced amount of granulation tissue was measured in VEGF^{fl/fl} LysMCre wounds in comparison to control wounds (Figure 24 A, B). Furthermore, cell density was distinctly impaired in VEGF^{fl/fl} LysMCre granulation tissue (Figure 24 A, upper panel). However, reduced amount of granulation tissue in the early phase of healing was recovered at days 7 and 14 post injury (Figure 24 A, B). By day 7, a cell-rich and dense granulation tissue developed in control as well as in VEGF^{fl/fl} LysMCre wounds (Figure 24 A). Despite the reduced amount of granulation tissue in early wounds of VEGF^{fl/fl} LysMCre mice, the overall healing response was not impaired. Wound closure, measured by the distance between the epithelial tips, and wound contraction, expressed as the distance between the two edges of panniculus carnosus, were not altered at all time points analyzed (Figure 24 B).

To address the question whether reduced granulation tissue formation in VEGF^{fl/fl} LysMCre wounds in the early phase of healing is accompanied by reduced angiogenesis, wound sections of VEGF^{fl/fl} (control) and VEGF^{fl/fl} LysMCre mice were stained for CD31 and desmin. Indeed, granulation tissue formation is accompanied by reduced amount of blood vessels in VEGF^{fl/fl} LysMCre mice. Whereas in control wounds a well vascularised granulation tissue has been developed 4 days post injury, VEGF^{fl/fl} LysMCre wounds show only sparse vascularisation (Figure 25 A, upper panel). At day 7 post injury, as for the granulation tissue formation, this effect was abolished in VEGF^{fl/fl} LysMCre wounds (Figure 25 A, lower panel). Interestingly, during the transition of the early to the mid stage of repair, vascularisation in wounds of VEGF^{fl/fl} LysMCre mice increased dramatically and at day 7 post injury was significantly increased over control wounds (Figure 25 B). This dynamic of an early significantly reduced but subsequently increased vascularisation of wound tissue in VEGF^{fl/fl} LysMCre mice was accompanied by a similar timely distribution of desmin positive perivascular cells (Figure 25 C). Thus, the ratio of perivascular cells to endothelial cells (desmin:CD31), reflecting the maturation of vascular structures, was similar in VEGF^{fl/fl} LysMCre and control mice (Figure 25 D). Of note, desmin coverage in VEGF^{fl/fl} LysMCre mice was significantly increased seven days post injury over controls, indicating that the delayed sprouting led to mature vessels (Figure 25 D). Certainly, the particular kinetic of increased wound angiogenesis in VEGF^{fl/fl} LysMCre mice during the mid stage of healing was

Results

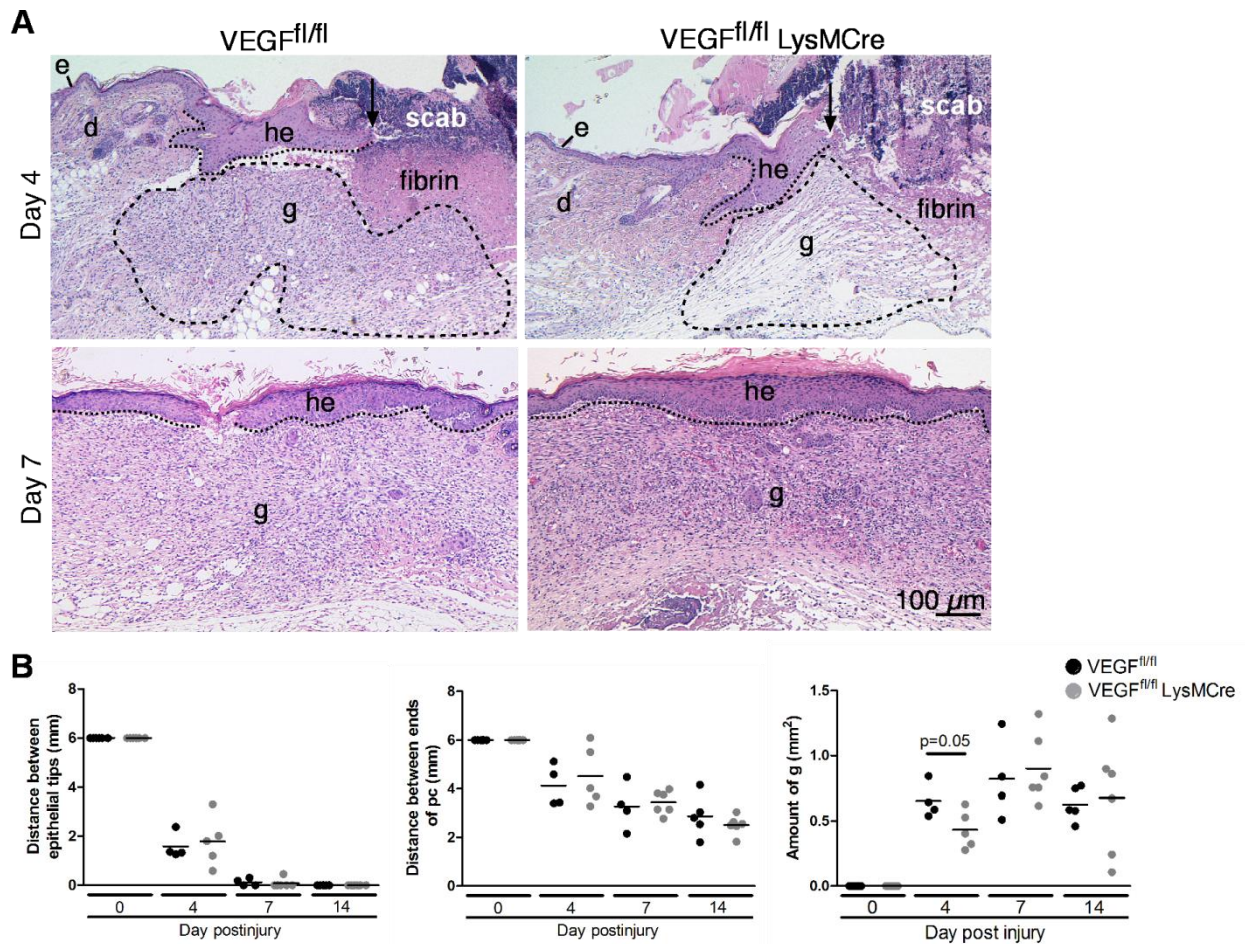
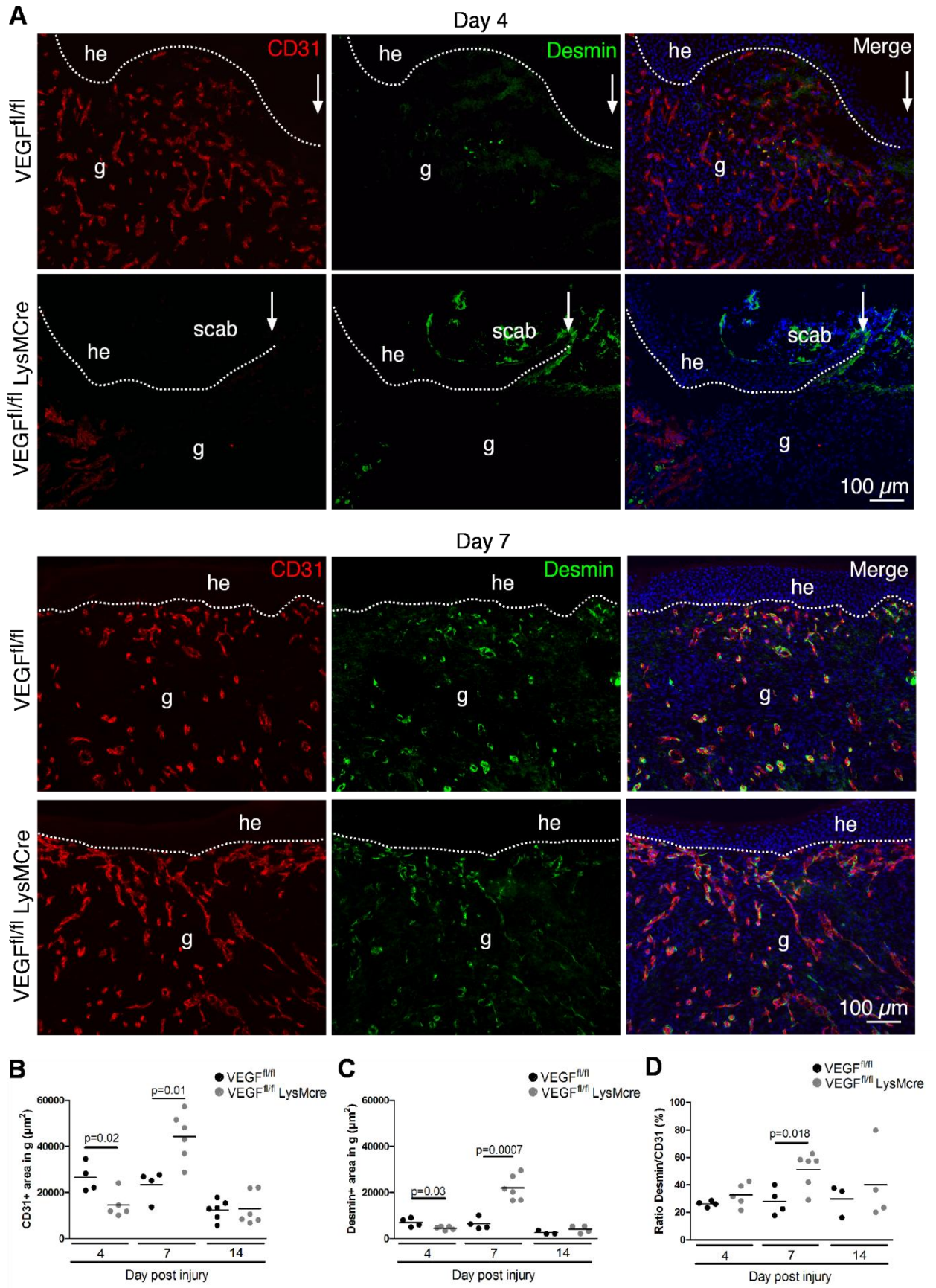


Figure 24: Myeloid cell-derived VEGF induces granulation tissue formation in the early phase of healing. (A) H&E staining of wounds in VEGF^{fl/fl} (control) and VEGF^{fl/fl} LysMCre mice at indicated time points post injury. Whereas in control mice, the day-4 wound is filled with a cell-rich granulation tissue, in VEGF^{fl/fl} LysMCre mice, only a sparse granulation tissue has formed (hatched line outlines granulation tissue; dotted line outlines hyperproliferative epithelial tongue). In day 7 wounds of control and VEGF^{fl/fl} LysMCre mice, the cell-rich granulation tissue is covered by a complete epithelium (dotted line outlines basement membrane). Arrows point to the tips of epithelial tongue. d, dermis; e, epidermis; g, granulation tissue; he, hyperproliferative epithelium. (B) Morphometric analysis of wound tissue at different time points post injury: distance between epithelial tips (left); distance between ends of panniculus carnosus (pc, middle); amount of granulation tissue (right). Each dot represents one wound and two wounds were inflicted on one mouse; horizontal bars represent the mean.

Results



Results

Figure 25: Myeloid cell-derived VEGF induces angiogenesis in the early phase of healing. (A) CD31 (red) and desmin (green) double immunostaining of day 4 and day 7 wound tissue in control and VEGF^{fl/fl} LysMCre mice; DAPI counterstaining of nuclei (blue). Dotted line indicates hyperproliferative epithelium; arrow points to the tips of epithelial tongue. he, hyperproliferative epithelium; g, granulation tissue. Morphometric quantification of the area within the granulation tissue that stained positive for CD31 **(B)** and desmin **(C)** at indicated time points post injury. **(D)** Percentage of the ratio of CD31 and desmin positive stained areas. Each dot represents one wound, two wounds on one mouse; horizontal bars represent the mean.

unexpected and suggests that wound tissue in VEGF^{fl/fl} LysMCre mice that is initially deprived of myeloid cell-derived VEGF during the early phase of repair rescues impaired angiogenesis by VEGF synthesis through other cell compartments. Indeed, quantitative reverse transcriptase PCR analysis of the entire wound tissue revealed that in VEGF^{fl/fl} LysMCre mice significantly attenuated VEGF expression was limited to the early phase of repair (Figure 23 B). At later stages, levels of VEGF expression in wound tissue were similar in mutant and control mice. Collectively, these findings provide strong evidence that myeloid cell-derived VEGF is critical for the induction of tissue angiogenesis and granulation tissue deposition during the early phase of skin repair.

3.3.5 Epidermal-derived VEGF is critical for wound angiogenesis during the late phase of tissue repair

To address the question which mechanisms might rescue wound angiogenesis as well as the deposition of granulation tissue during the late stage of repair in VEGF^{fl/fl} LysMCre mice, two hypotheses were investigated. First, if VEGF expression by another cell compartment than myeloid cells becomes critical during the late phase of repair and/or second, whether up-regulation of other pro-angiogenic mediators in VEGF deficient macrophages might rescue wound angiogenesis at later stages.

Based on the findings in wounded VEGF-lacZ mice that the neo-epithelium dominates wound VEGF expression during later stages of skin repair (Figure 20 B, C) and previous data by others, indicating that a keratinocyte-specific knock out of VEGF delays healing and reduces the amount of blood vessels in the later phases of healing [78], mice were generated which lack VEGF expression in both myeloid cells and the epidermal compartment (VEGF^{fl/fl} LysMCre K14Cre). For this purpose, VEGF^{fl/fl} LysMCre females were mated with males expressing the Cre recombinase under control of the keratinocyte-specific keratin 14 (K14) promoter, reported to be active in basal keratinocytes [92]. Efficient VEGF gene deletion was shown *in vitro* by PCR of genomic DNA from VEGF^{fl/fl} (control), VEGF^{fl/fl} LysMCre (myeloid

Results

cell-specific knock out), VEGF^{fl/fl} K14Cre (keratinocyte-specific knock out) and VEGF^{fl/fl} LysMCre K14Cre (double knock out) mice by using the same primer set described in figure 22 B. The keratinocyte-specific and the double knock out showed a strong signal for the 560 bp fragment, indicating successful recombination, while this band was absent in controls (Figure 26 A). The less efficient recombination in myeloid cell-specific knock outs derives from the fact that tail DNA was used and macrophages constitute a minor population in this tissue. Furthermore, VEGF gene deletion was evaluated by quantitative real time PCR of complete wound tissue isolated from control and VEGF^{fl/fl} LysMCre K14Cre mice. Whereas VEGF expression was strongly up-regulated in control wounds 4 and 7 days post injury, it was significantly reduced in VEGF^{fl/fl} LysMCre K14Cre wounds (Figure 26 B), indicating that both myeloid cells and keratinocytes deliver important amounts of VEGF into wound tissue. Of note, whereas at day 7 and 14 VEGF expression in wound tissue of VEGF^{fl/fl} LysMCre mice was not altered in comparison to control mice (Figure 23 B), in wound tissue of VEGF^{fl/fl} LysMCre K14Cre mice VEGF expression was significantly reduced (Figure 26 B). These findings strongly suggest that the neo-epidermis significantly contributes to the VEGF content during the late stage of skin healing.

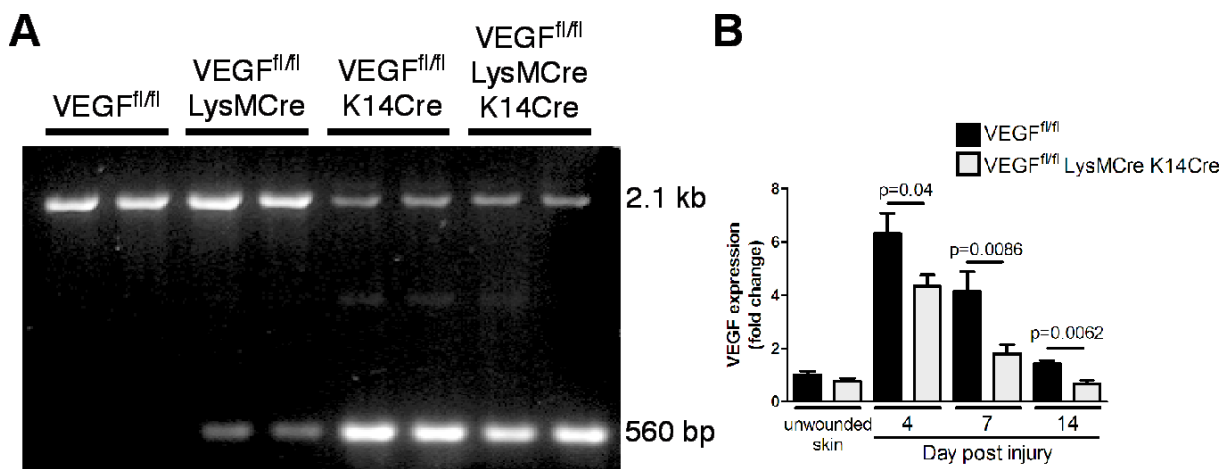


Figure 26: Efficient VEGF gene deletion in macrophages and keratinocytes in VEGF^{fl/fl} LysMCre K14Cre mice. (A) PCR of genomic DNA isolated from tail biopsies of VEGF^{fl/fl} (control), VEGF^{fl/fl} LysMCre (myeloid cell-specific knock out), VEGF^{fl/fl} K14Cre (keratinocyte-specific knock out) and VEGF^{fl/fl} LysMCre K14Cre (double knock out) mice. The 2.1 kb PCR fragment shows the floxed region before recombination and the 560 bp fragment indicates successful recombination. (B) Quantitative real time PCR analysis for VEGF expression in complete wound tissue at days 4, 7, and 14 post injury from VEGF^{fl/fl} and VEGF^{fl/fl} LysMCre K14Cre mice, normalized to VEGF expression in unwounded skin. $n = 4-8$ wounds on two to four mice per time point and genotype. Data are expressed as mean \pm SD.

Results

To examine the functional impact and the interplay of myeloid cell- and keratinocyte-derived VEGF synthesis in skin wound healing, full thickness wounds were generated on the back of VEGF^{fl/fl} LysMCre K14Cre and control (VEGF^{fl/fl}) mice and harvested at indicated time points post injury (6-8 wounds on three to four mice per time point for each group). As revealed by H&E staining, at day four post injury, a significantly reduced amount of granulation tissue was measured in VEGF^{fl/fl} LysMCre K14Cre wounds in comparison to control wounds, and this phenotype was comparable to the one shown for the myeloid cell-specific VEGF knock out (Figure 24 and 27 A). By contrast, at day 7 post injury, the time point in which the amount of granulation tissue was similar in control and in myeloid cell-specific VEGF knock outs, granulation tissue in VEGF^{fl/fl} LysMCre K14Cre wounds was still significantly reduced (Figure 27 A, B). The data indicate that keratinocyte-derived VEGF rescued the observed phenotype in myeloid cell-specific VEGF knock outs. Surprisingly, despite the dramatically impaired granulation tissue formation in VEGF double knock outs, the overall healing response was not altered. Wound closure as well as wound contraction was similar at all time points analyzed in control and in VEGF^{fl/fl} LysMCre K14Cre wounds (measured by the distance between the epithelial tips and the distance between the two edges of panniculus carnosus) (Figure 27 B).

As revealed by staining for CD31 and desmin, the reduced amount of granulation tissue at days 4 and 7 post injury in VEGF^{fl/fl} LysMCre K14Cre wounds was accompanied by an impaired angiogenic response. While control wounds show a strong angiogenic response in the granulation tissue of day 4 and day 7 wounds, granulation tissue in VEGF^{fl/fl} LysMCre K14Cre wounds was only scarcely vascularised (Figure 28 A). Morphometric analysis of the area which stained positive for CD31 in control wounds compared to VEGF^{fl/fl} LysMCre K14Cre wounds confirmed a significant decrease of the early angiogenic response in knock out wounds and also at later stages of the healing response (Figure 28 B). Also pericyte numbers, analyzed by staining for desmin, were significantly reduced at day 4 and 7 post injury in the knock outs compared to controls. In contrast, in myeloid cell-specific VEGF knock outs the ratio of CD31 to desmin positive stained area was not altered, indicating that pericyte coverage was not impaired despite the reduced amount of blood vessels (Figure 25 D), in VEGF^{fl/fl} LysMCre K14Cre wounds the ratio was significantly reduced (Figure 28 D), indicating that not only the vessel number was reduced, but also vessel maturation was impaired. These data provide strong evidence that macrophages deliver significant amounts of VEGF in the early phase of healing and that keratinocytes take over this part at later time points post injury.

Results

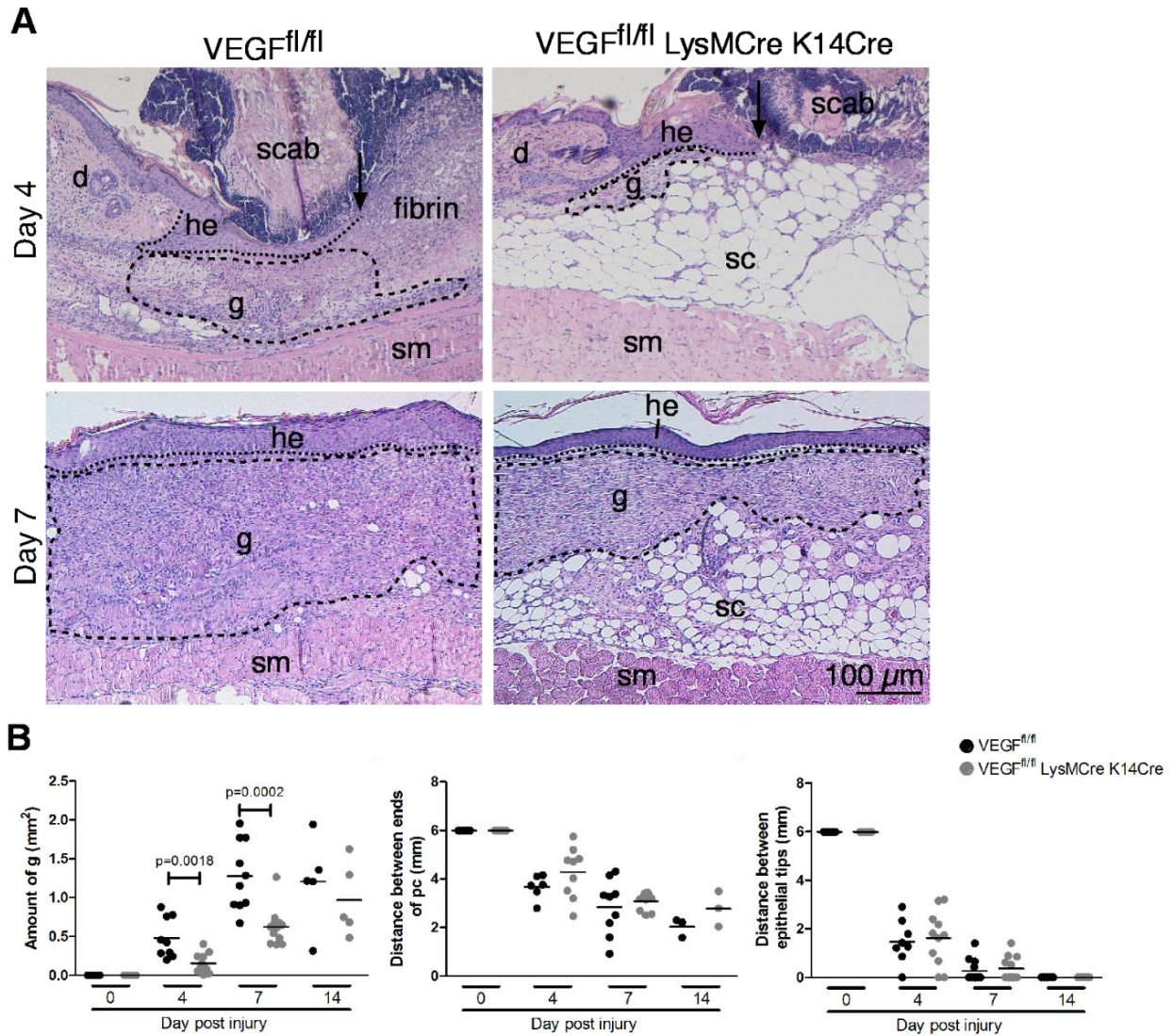


Figure 27: Both myeloid cell- and keratinocyte-derived VEGF contribute to granulation tissue formation. (A) H&E staining on wounds of VEGF^{fl/fl} (control) and VEGF^{fl/fl} LysMCre K14Cre mice at indicated time points post injury. Whereas in control mice, the day-4 wound is filled with a cell-rich granulation tissue, in VEGF^{fl/fl} LysMCre K14Cre mice, only sparse granulation tissue has formed (hatched line outlines granulation tissue; dotted line outlines hyperproliferative epithelial tongue). At day 7 post injury, wounds of VEGF^{fl/fl} LysMCre K14Cre mice show still a reduced amount of granulation tissue (dotted line outlines basement membrane). Arrows point to the tips of epithelial tongue. d, dermis; g, granulation tissue; he, hyperproliferative epithelium; sm, skeletal muscle; sc, subcutaneous fat tissue. (B) Morphometric analysis of wound tissue at different time points post injury: amount of granulation tissue (left); distance between ends of panniculus carnosus (pc, middle); distance between epithelial tips (right). Each dot represents one wound, two wounds on one mouse; horizontal bars represent the mean.

Results

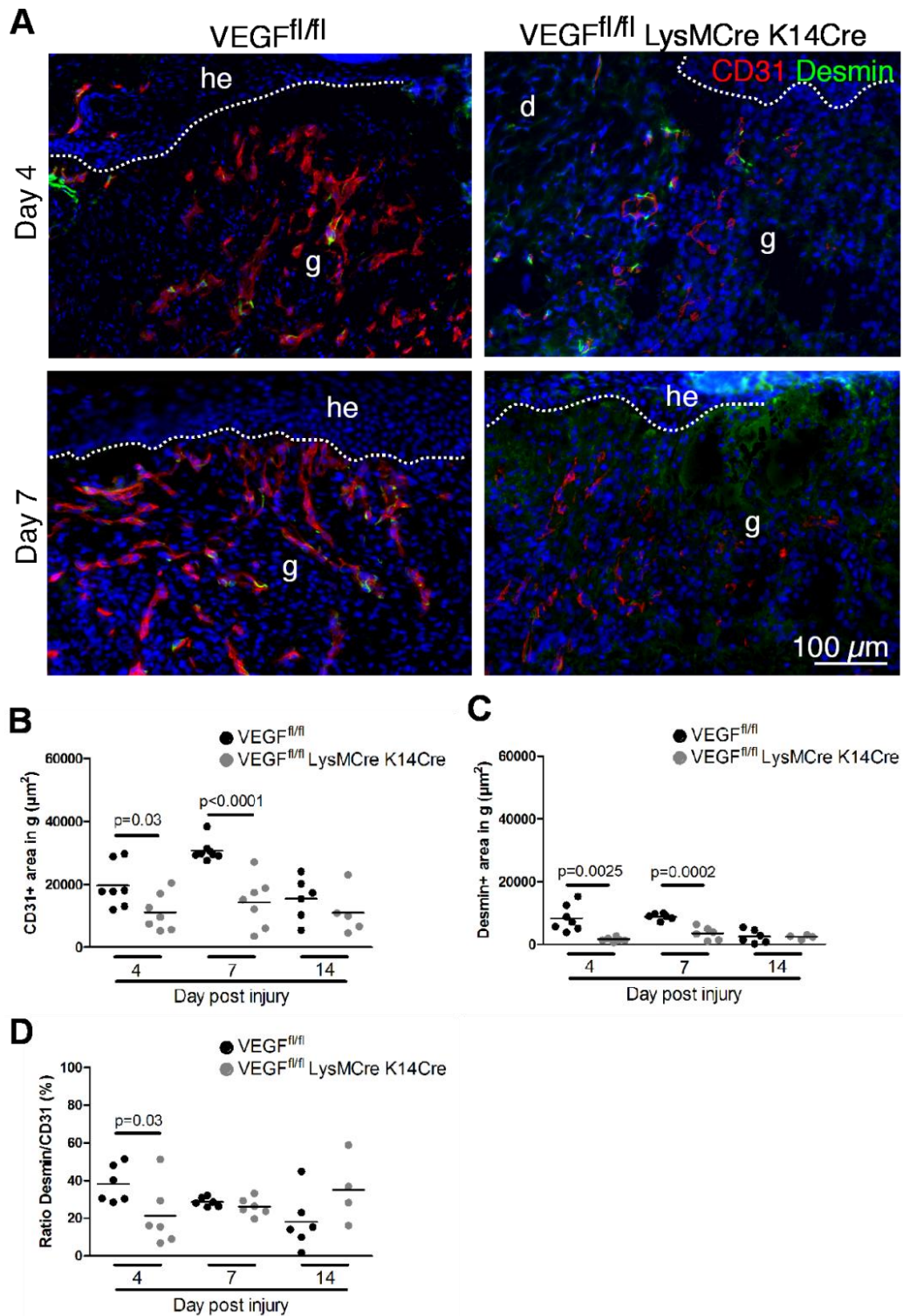


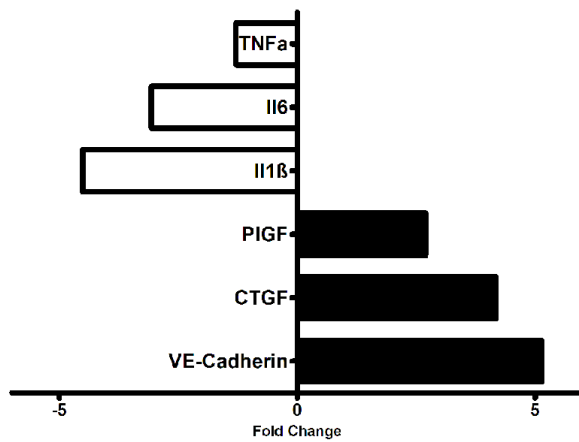
Figure 28: Myeloid cell- and keratinocyte-derived VEGF contribute to angiogenesis in wound granulation tissue. (A) CD31 (red) and desmin (green) double immunostaining of day 4 and day 7 wound tissue in control and VEGF^{fl/fl} LysMCre K14Cre mice; DAPI counterstaining of nuclei (blue). Dotted line indicates hyperproliferative epithelium; arrow points to the tips of epithelial tongue. he, hyperproliferative epithelium; g, granulation tissue; d, dermis. Morphometric quantification of the area within the granulation tissue that stained positive for CD31 **(B)** and desmin **(C)** at indicated time points post injury. **(D)** Percentage of the ratio of CD31 and desmin positive stained areas. Each dot represents one wound, two to four wounds on one mouse; horizontal bars represent the mean.

Results

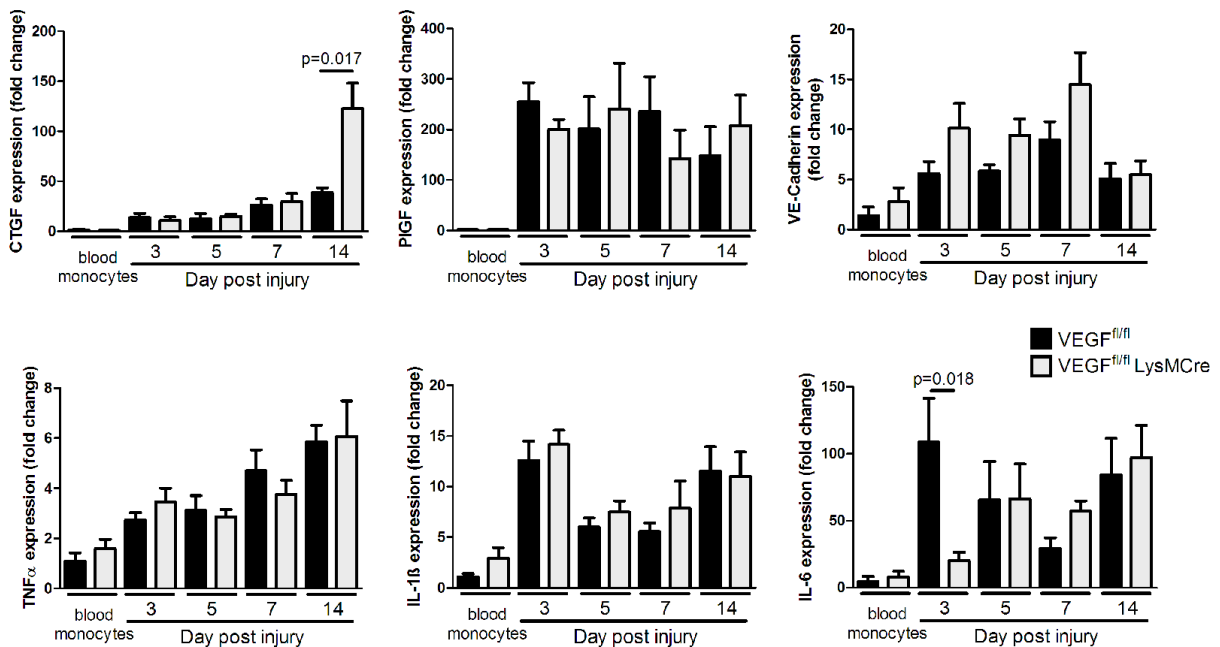
To investigate in the second hypothesis that up-regulation of other pro-angiogenic mediators in VEGF deficient macrophages might rescue wound angiogenesis at later stages, a broad real time PCR array was performed for genes differentially regulated in angiogenesis. To this end, peritoneal macrophages from control (VEGF^{fl/fl}) and VEGF^{fl/fl} LysMCre mice were isolated and exposed to hypoxia to mimic a stimulus probably participating in the activation of macrophages in the wound environment. Gene expression levels were calculated by adding cDNA from the respective genotype on a commercial well plate pre-coded with primers aiming for genes, which expression is related to angiogenesis (cells from three mice per genotype were pooled for analysis). It was shown that some pro-inflammatory cytokines were down-regulated, such as TNF- α , IL-6 and IL-1 β , whereas some pro-angiogenic mediators were up-regulated, such as PlGF, connective tissue growth factor (CTGF) and vascular endothelial cadherin (VE-cadherin) in VEGF^{fl/fl} LysMCre macrophages in comparison to control cells. These data indicate that macrophages depleted for VEGF show an altered gene expression profile *in vitro* (Figure 29 A). The expression of these differentially expressed angiogenic modulators measured *in vitro* in peritoneal macrophages from control and VEGF^{fl/fl} LysMCre mice was subsequently investigated over time in wound macrophages obtained from both groups. Whereas PlGF, TNF- α and IL-1 β expression was similar in control and VEGF knock out macrophages, CTGF was significantly up-regulated 14 days post injury (Figure 29 B). The pro-inflammatory cytokine IL-6 was significantly down-regulated at day three post injury in VEGF^{fl/fl} LysMCre macrophages (Figure 29 B). Interestingly, the endothelial cell-specific adhesion molecule VE-cadherin was up-regulated in VEGF knock out macrophages, even though it did not reach statistical significance (Figure 29 B). To address whether the significantly altered expression of CTGF and IL-6 in VEGF knock out macrophages reflected the overall expression levels in complete wound tissue, RNA was isolated from control and VEGF^{fl/fl} LysMCre wounds and the expression of CTGF and IL-6 was quantified by real time PCR. By this approach, no differences could be observed (Figure 29 C). Collectively, these data suggest that rescue of wound angiogenesis and deposition of granulation tissue during the late stages of the healing response in VEGF^{fl/fl} LysMCre mice is not due to compensatory up-regulation of other pro-angiogenic mediators. Rather, an increase of epidermal-derived VEGF expression during the late stage of repair seems to account for this effect.

Results

A



B



C

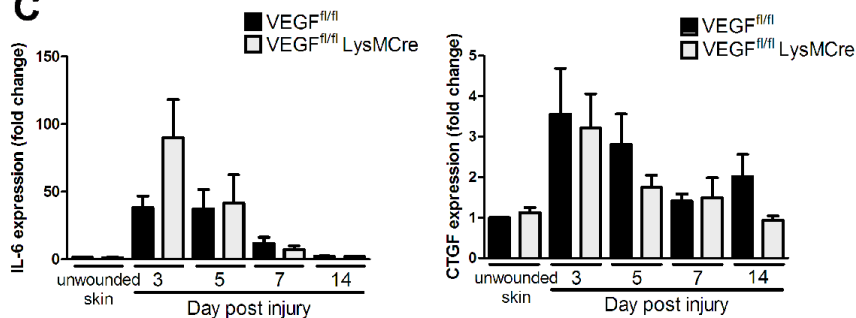


Figure 29: Macrophages deficient for VEGF expression display an altered gene expression profile. (A) Summary of real time PCR array data (commercial array for genes related to mouse angiogenesis) on cultured peritoneal macrophages isolated from control (VEGF^{fl/fl}) and VEGF^{fl/fl} LysMCre mice. Cells were stimulated under hypoxia and measured for gene expression related to angiogenesis. Cells from three mice per genotype were pooled for analysis. Bars indicate alterations of gene expression in VEGF knock out macrophages relative to the control. (B) Quantitative real time PCR analysis on isolated blood monocytes and wound macrophages from control and VEGF^{fl/fl}

Results

LysMCre mice at days 3, 5, 7, and 14 post injury for different genes as indicated. **(C)** Real time PCR analysis of unwounded skin and complete wound tissue, from control and VEGF^{fl/fl} LysMCre mice, harvested at time points as indicated. $n = 4-8$ wounds on 2-4 mice per group and time point. Data are expressed as mean \pm SD.

3.3.6 Myeloid cell-derived VEGF controls tip cell formation and the spatial association between macrophages and sprouting vessels during the early phase of tissue repair

To analyze cellular mechanisms that potentially control myeloid cell-derived VEGF mediated angiogenesis during the early phase of repair, first, the recruitment of macrophages to the site of injury in control (VEGF^{fl/fl}) and VEGF^{fl/fl} LysMCre mice was investigated. This experiment aimed to exclude, that indirectly, reduced numbers of macrophages caused diminished granulation tissue formation and angiogenesis in mice deficient for VEGF expression in myeloid cells. It is well described that macrophages express the VEGFR-1 and that VEGF is chemotactic for macrophages *in vitro* [75]. Decreased myeloid cell-derived VEGF expression may thus result in less efficient macrophage recruitment to the wound site. To this end, wound cells were isolated from control and VEGF^{fl/fl} LysMCre mice at days 4 and 7 post injury and relative numbers of macrophages, positive for the cell surface markers F4/80 and CD11b were determined. Approximately 35% of all wound cells stained positive for F4/80 and CD11b in control and in VEGF^{fl/fl} LysMCre wounds at both time points analyzed (Figure 30). Thus, indicating the recruitment of macrophages to the site of injury is not impaired in myeloid cell-specific VEGF knock outs, and myeloid cell-derived VEGF has no major impact on macrophage recruitment.

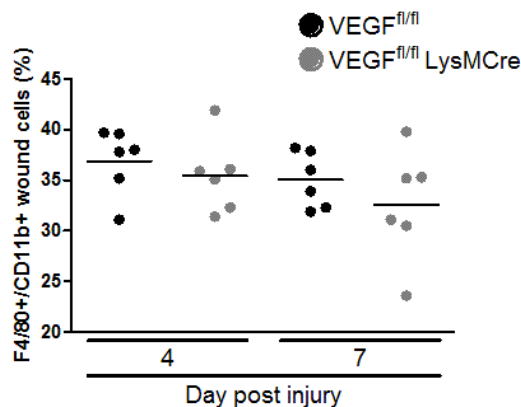


Figure 30: Myeloid cell-derived VEGF does not function as a chemoattractant for macrophages into wounds. FACS analysis of isolated wound cells from control (VEGF^{fl/fl}) and VEGF^{fl/fl} LysMCre mice at time points as indicated. Relative macrophage numbers recruited to the site of injury were quantified by staining for F4/80 and CD11b. Each dot represents one wound, two wounds on one mouse. Horizontal bars represent the mean.

Results

Second, it was examined whether myeloid cell-derived VEGF is critical for the formation of delta-like-4(Dll4)-positive tip cells. Recently it was shown that in a VEGF dependent fashion, Dll4-Notch1 signaling regulates the formation of appropriate numbers of tip cells to control vessel sprouting and branching in the mouse retina [93]. Immunostainings on wound tissue from day 4 wounds showed that in wounds of control mice the leading edge of vascular sprouts invading the provisional extracellular matrix stained positive for Dll4 and CD31 (Figure 31 A). In contrast, in wound tissue of VEGF^{fl/fl} LysMCre mice only few Dll4 positive cells were detected in the poorly vascularized granulation tissue. These findings indicate, that myeloid cell-derived VEGF is critical for the formation of delta-like-4(Dll4)-positive tip cells (which means ultimately vascular sprouts) in early granulation tissue.

Furthermore, recently it was shown during mouse development and in zebrafish, that tissue macrophages can act as important cellular chaperones for vascular anastomosis [65]. Interestingly, in brain vascularisation this process was independent of macrophage-derived VEGF. Nevertheless, motivated by the findings of Fantin et al. and due to an additional publication in which VE-cadherin was described as an interesting candidate in mediating this cell-cell contact [66] as well as accompanied by the finding of increased VE-cadherin expression in wound macrophages of VEGF^{fl/fl} LysMCre mice (although not statistically significant different when compared to control mice) the question was assessed whether potential macrophage-mediated sprout fusion in skin wounds is dependent on myeloid cell-derived VEGF. Therefore, day 4 wound tissue sections of mutant and control mice were co-stained for VE-cadherin and F4/80. In wound tissue of control mice, F4/80+ macrophages and VE-cadherin positive vascular structures showed a homogenous distribution throughout the entire depth of the granulation tissue (Figure 31 B). Using high magnification confocal microscopy at several occasions close proximity between VE-cadherin positive tube-like (resembling vascular structures) structures and F4/80 positive cells could be detected (Figure 31 C). In contrast, the distribution of VE-cadherin positive vascular structures and F4/80 positive cells within the granulation tissue of VEGF^{fl/fl} LysMCre mice was strikingly different. Staining for VE-cadherin and F4/80 was discrete and no intermingling could be detected (Figure 31 B). Whereas VE-cadherin positive vascular structures were present at the outer wound edge, F4/80 positive macrophages were concentrated within the granulation tissue at the center of the wound. Close proximity between VE-cadherin and F4/80 positive cells could hardly be detected and were significantly reduced when compared to granulation tissue of control mice (Figure 31 B, C). Therefore, these findings propose that during formation of early granulation tissue in skin wounds in mice, tip cell guidance and possibly also sprout fusion is controlled by myeloid cell-derived VEGF.

Results

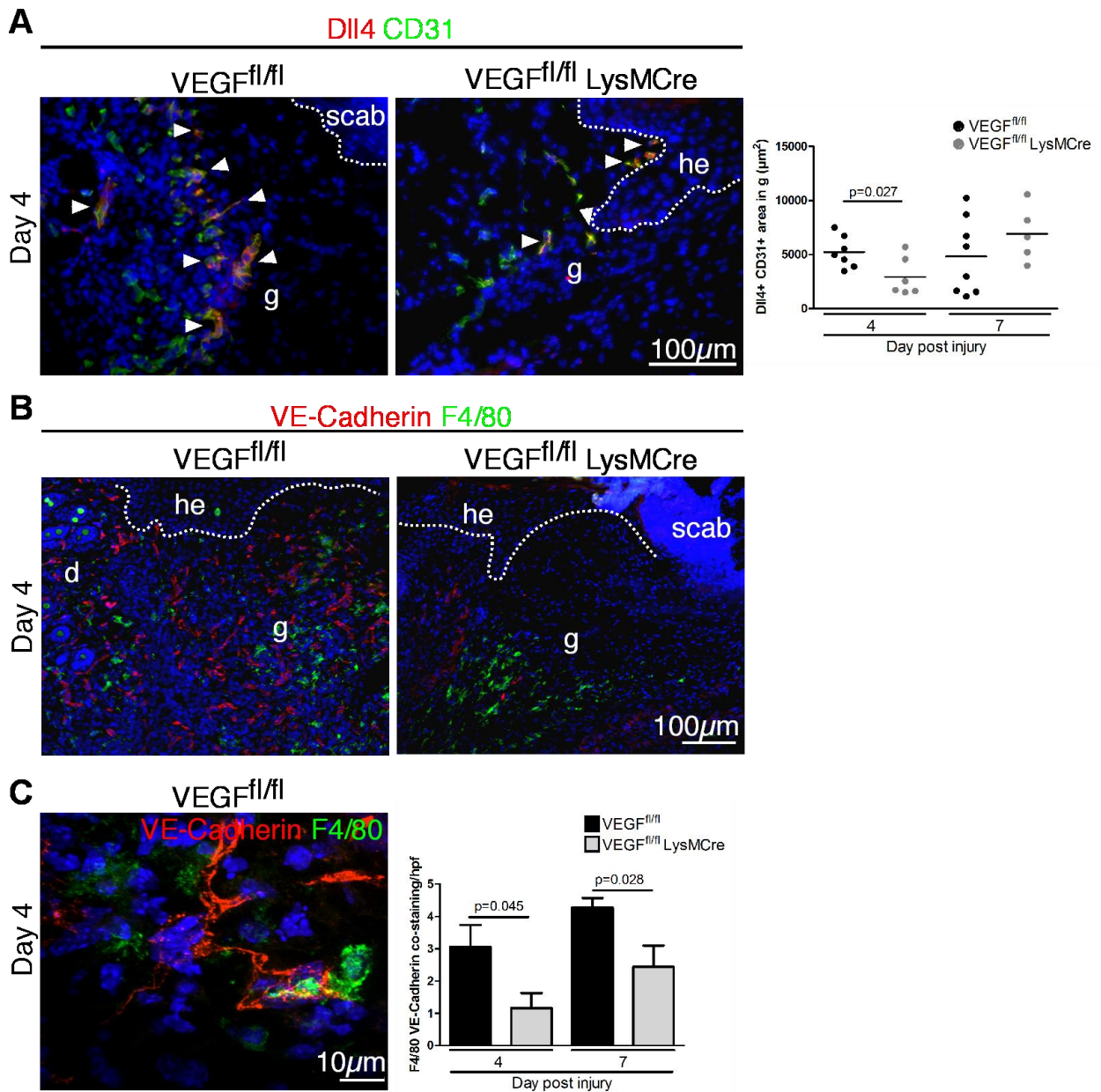


Figure 31: Macrophages are in close proximity with endothelial cells during physiological tissue repair. (A) Left: CD31 (green) and Delta-like 4 (DII4, red) double immunostaining of day 4 wound tissue in control (VEGF^{fl/fl}) and VEGF^{fl/fl} LysMCre mice. Right: Morphometric quantification of the area within the granulation tissue which were double positive for CD31 and DII4 at indicated time points post injury. Each dot represents one wound, two wounds on one mouse. Horizontal bar represents the mean. **(B)** VE-cadherin (red) and F4/80 (green) double immunostaining of day 4 wound tissue in control and VEGF^{fl/fl} LysMCre mice. **(C)** Left: High magnification confocal image to illustrate close proximity of macrophages (F4/80, green) and endothelial cells (VE-cadherin, red) in control wounds 4 days post injury. Right: Morphometric quantification of F4/80 positive macrophages and VE-cadherin positive endothelial cells, which were in close proximity to each other, counted in high power fields (hpf) in granulation tissues of control and VEGF^{fl/fl} LysMCre mice at time points as indicated. $n = 6$ wounds, two wounds on one mouse. Data are expressed as mean \pm SD. DAPI counterstaining of nuclei (blue). Dotted line indicates hyperproliferative epithelial tongue. d, dermis; he, hyperproliferative epithelium; g, granulation tissue.

4 Discussion

In this study it is shown that macrophages play a crucial role during skin repair in the adult organism and that their timely restricted depletion during distinct phases of the wound healing response has profound impact on phase-specific repair mechanisms. The results presented in this thesis show that repair mechanisms controlled by macrophages recruited during the early stage of the repair response encompass induction of granulation tissue and myofibroblast differentiation which ultimately control the degree of scar formation. Further, they induce the angiogenic response in early wounds by releasing significant amounts of VEGF (VEGF-A). During the mid stage of the repair response macrophage function is crucial for stabilization of vascular structures and transition of granulation tissue into scar tissue. But at this stage of the healing response macrophage-derived VEGF is receding in its importance and epidermal compartments take over the VEGF supply in the consecutive phases of the repair response. Finally, macrophages present at the late stage of the repair response do not impact tissue maturation and scar formation. Therefore, this study provides evidence that macrophages exert different roles at diverse stages of the repair response and that they orchestrate the natural sequence of repair phases in skin, which are essential to restore solid tissue homeostasis and integrity after injury. Overall, this study suggests a crucial and varied role for macrophages in wound healing and adds to the previous knowledge.

4.1 Eligible mouse model for inducible and timely-restricted depletion of macrophages

To assess macrophage function at distinct stages of skin repair, a mouse system was developed that allows the cell type specific and timely restricted depletion of macrophages in skin wounds. The role of macrophages during skin repair has remained a subject of debate due to their functional dichotomy as effectors of both tissue injury and repair [47]. Furthermore, in earlier studies of skin injury, macrophages have been depleted by administration of anti-macrophage serum and/or hydrocortisone, methods that have pleiotropic effects and lead to unspecific and partial cell depletion [37, 38]. To circumvent these difficulties, the transgenic LysMCre/iDTR mouse line was used, in which minute amounts of DT can efficiently, specifically as well as in a timely restricted manner deplete tissue resident and inflammatory macrophages recruited to the site of skin injury. However, it was surprising that neutrophils could not be efficiently depleted in the presented model by DT, because lysozyme M promoter activity has been reported in neutrophils [83]. Inefficient neutrophil depletion might be explained by low lysozyme M promoter activity, reduced

phagocytosis by macrophages and/or short-lived turnover of neutrophils, so that DT might fail to efficiently interfere with the high number of neutrophils that infiltrate the wound side [48, 94]. These findings are consistent with those of previous studies showing that DT treatment did not significantly affect neutrophil numbers [95, 96].

4.2 Macrophage functions during the early phase of repair

4.2.1 Macrophages recruited during the inflammatory phase of repair induce a highly vascularized granulation tissue, which results in scar formation

This study provides evidence that macrophages exert different functions during the distinct phases of skin repair. Specifically, in control mice macrophages recruited during the early stage of the repair response induce a vascularized and fibroblast-rich granulation tissue that promotes dermal as well as epidermal repair. Consistently, wound closure at day 5 post injury was significantly delayed in mice in which macrophages were depleted specifically during the early stage of repair. However, macrophage influx subsequent to their depletion rescued the delayed wound closure rate during the late stage of repair. Yet, the overall amount of granulation tissue, that developed under these conditions as well as vascularization, cellularity, contractile force and most important the extent of scar formation remained reduced when compared to control wounds. These findings demonstrate that macrophages which infiltrate the wound site immediately after injury induce a robust, highly vascularized granulation tissue associated with myofibroblast differentiation and wound contraction. These results are consistent with two recent studies published during the time when this thesis was in work [95, 96]. Although all of these events ensure rapid wound closure, they result in significant scar formation. However, a healing response that lacks specifically the initial burst of macrophage influx results in minimal scarring. Based on the findings, it is intriguing to speculate that providing a pathogen-free environment and preventing macrophage influx selectively during the early stage of repair, improves the quality of the wound healing response with less scar formation and without compromising the rate of wound closure. Certainly, it has to be proven whether minimal scarring in wounds lacking the initial influx of macrophages achieves the same quality of tensile strength of physiological scars or it is solely a cosmetic advantage with less stability. However, one should take into account that scar formation and wound contraction in mice, differs significantly to scar formation in the human system. Therefore, to validate the observations, future studies in other model systems which are more adequate to study scar formation are needed.

4.2.2 Myeloid cell-derived VEGF initiates the angiogenic response in the early phase of the wound healing response

In order to identify mediators released by macrophages which could cause the observed phenotype of reduced vascularization in macrophage-depleted wounds during the early phase of the wound healing response, conditional gene targeting was used to efficiently deplete VEGF expression specifically in myeloid cells. It was already shown by others as well that VEGF expression is induced after skin injury, mainly in keratinocytes and macrophages [71, 74], and that VEGF exerts important functions during wound angiogenesis [70, 72, 73]. Furthermore, the data provided in this thesis could demonstrate that VEGF expression in the early phase of the wound healing response is primarily macrophage mediated, whereas in later phases epidermal compartments take over the VEGF supply. By staining for the common blood vessel marker CD31 in VEGF^{fl/fl} LysMCre and VEGF^{fl/fl} LysMCre K14Cre wounds, VEGF could be identified as a factor of singular importance released by macrophages to initiate angiogenesis in the early phase of the wound healing response which is then in later phases mediated by keratinocytes. Reduced angiogenesis in wounds lacking VEGF expression either in macrophages or in macrophages and keratinocytes was interestingly accompanied by reduced amounts of granulation tissue. These findings are supported by a recently published article in which the same mouse model of a myeloid cell-specific VEGF knock out was used and analyzed for the outcome of the wound healing response [97]. Interestingly, despite reduced angiogenesis and granulation tissue formation in the early phase of the wound healing response, the overall wound healing kinetic was not altered in the punch injury model investigated. These results can be explained by a wound size-dependent effect of myeloid cell-derived VEGF on the outcome of the healing response reported by Stockmann et al. In their study they could show delayed healing in large 8 mm of diameter excisional wounds in VEGF^{fl/fl} LysMCre mice, whereas the healing kinetic was unaltered in smaller incisional wounds [97].

Furthermore, the question was addressed, if secondary effects and not directly myeloid cell-derived VEGF could cause reduced angiogenesis in myeloid cell-specific VEGF knock out wounds in the early phase of the wound healing response. To this end, first the number of macrophages recruited to the site of injury in control and VEGF^{fl/fl} LysMCre mice was evaluated by FACS analysis of wound cell suspensions stained for the common macrophage markers F4/80 and CD11b, because it is well described that macrophages express the VEGFR-1 and that VEGF is chemotactic for macrophages *in vitro* [59]. But no major differences could be observed regarding the relative number of macrophages recruited to the site of injury, indicating that myeloid cell-derived VEGF does not influence additional macrophage recruitment into wounds. These findings are further supported by two recently

Discussion

published articles in which the importance of myeloid cell-derived VEGF in a breast cancer and in a lung fibrosis model was investigated. The angiogenic response was impaired or reduced in both studies, but no differences in macrophage recruitment could be observed [80, 81]. Second, the expression pattern in macrophages depleted for VEGF expression was investigated, because VEGF could possibly stimulate a specific expression pattern in an autocrine loop, which could finally, when inhibited, lead to the observed phenotype of reduced angiogenesis in the early phase of the wound healing response. To this end, a broad real time PCR array was carried out with peritoneal macrophages from control and VEGF^{fl/fl} LysMCre mice, stimulated under hypoxia. It was found that some pro-inflammatory cytokines were down-regulated, whereas some pro-angiogenic mediators were up-regulated. When validated in *in vivo* isolated wound macrophages, only the pro-inflammatory cytokine IL-6 and the growth factor CTGF were significantly altered in VEGF^{fl/fl} LysMCre wound macrophages, however total amounts of both factors were not altered in complete wound tissue. CTGF expression was significantly up-regulated in macrophages lacking VEGF expression at day 14 post injury, a time point in which angiogenesis was similar in both control and VEGF^{fl/fl} LysMCre wounds and therefore probably not a cause for the observed phenotype in the early phase of healing. Additionally, CTGF is normally not produced by macrophages in wound tissue rather by fibroblasts and could be therefore an artifact [98]. IL-6 in contrast was significantly down-regulated at day 3 post injury, the time point when reduced angiogenesis was observed in myeloid cell-specific VEGF knock out wounds. Even though reduced IL-6 expression in VEGF^{fl/fl} LysMCre macrophages was not reflected in total expression levels in complete wound tissue, it cannot be completely excluded at this point, that local effects contributed to reduced angiogenesis. A complete knock out for IL-6 was shown to delay the cutaneous wound healing response in mice and was accompanied by reduced vascularization [99]. The pro-angiogenic effect of IL-6 is so far proposed by the induction of VEGF expression [100, 101]. If also myeloid cell-derived VEGF is able to induce IL-6 expression in macrophages in an autocrine loop via VEGFR-1 remains unresolved and needs further investigation. By usage of specific antibodies blocking VEGFR-1 signaling in macrophages, this question could be addressed. In conclusion, the data presented in this thesis propose an effect of singular importance of myeloid cell-derived VEGF for the initiation of the angiogenic response in the early phase of the wound healing response. No compensatory up-regulation of other pro-angiogenic mediators in VEGF^{fl/fl} LysMCre wounds could be detected, indicating that the observed phenotype was probably solely mediated by the lack of VEGF expression in myeloid cells. These data provide novel mechanistic insights on macrophage-mediated repair events after skin injury and potentially might identify new therapeutic targets that can promote wound angiogenesis in impaired wound healing conditions.

4.2.2.1 Myeloid cell-derived VEGF controls tip cell formation and the spatial association between macrophages and sprouting vessels during the early phase of tissue repair

Reduced vascularization in myeloid cell-specific VEGF knock out wounds was evident in this study by diminished staining for CD31 and desmin, whereas the ratio of the CD31 and desmin double positive stained area was not altered, indicating that the few developed blood vessels were qualitatively not impaired. In order to identify mechanisms which could cause reduced angiogenesis in VEGF^{fl/fl} LysMCre wounds, wound sections of controls and myeloid cell-specific VEGF knock outs were stained for CD31 and the tip cell marker Dll4 and it could be shown that reduced vascularization goes along with impaired tip cell formation. As it was shown for the mouse retina, that Dll4-Notch1 signaling regulates the formation of appropriate numbers of tip cells to control vessel sprouting and branching in the mouse retina in a VEGF dependent fashion, it can be speculated that wound angiogenesis functions with a similar mechanism [93]. The findings in this thesis provide evidence, that especially myeloid cell-derived VEGF initiates tip cell formation, because CD31 and Dll4 double positive stained tip cells were significantly reduced in VEGF^{fl/fl} LysMCre wounds.

Furthermore, the observation was made that in early wounds VE-cadherin positive stained blood vessels and macrophages show a specific distribution in which macrophages are located in the area of actively sprouting blood vessels. In contrast, in macrophage-specific VEGF knock out wounds this pattern was strikingly different and macrophages as well as blood vessels were separately located within the granulation tissue of early wounds and no intermingling was observed. It can be speculated if this impaired collocation leads to the observed phenotype of reduced angiogenesis in early wounds. Recently, it was shown during mouse development and in postnatal vascularization of the retina as well as in zebrafish that yolk sac-derived macrophages can act as important cellular chaperones for vascular anastomosis [65]. Fantin et al. could show that vessel sprouting acts in response to VEGF and that macrophages guide and prepare two tip cells for fusion. However, this process was independently of macrophage-derived VEGF. If impaired fusion of two sprouting blood vessels caused reduced angiogenesis in the mouse model used can just be speculated. On the one hand, one should take into account, that yolk sac-derived macrophages differ from adult macrophages recruited to the wound site. They do not develop from hematopoietic stem cells in the bone marrow therefore it remains unclear whether bone marrow-derived macrophages can act with a similar mechanism causing vessel fusion in adults. On the other hand in an additional article it has been described, that macrophages express the endothelial adhesion molecule VE-cadherin on a low level and that this protein could be an interesting candidate in mediating the contact between

Discussion

macrophages and endothelial cells in order to accomplish vessel fusion [66]. Interestingly, VE-cadherin was slightly up-regulated in macrophages depleted for VEGF expression and by double staining for VE-cadherin and F4/80 the observation was made that during physiological wound angiogenesis macrophages are in close proximity to endothelial cells. However, VE-cadherin and F4/80 double positive macrophages could not be detected so far and needs further investigation. Whether macrophages are indeed in a direct cell-cell contact to endothelial cells or just co-localized can only be speculated as well. Nevertheless, the findings made in this thesis provide a first evidence that myeloid cell-derived VEGF guide sprouting blood vessels into the area of granulation tissue and that macrophages might probably mediate vessel fusion. Indeed, further experiments are needed to support the mentioned hypothesis and to identify the underlying mechanisms of the angiogenic response in wounds. The questions remain unresolved, if a specific macrophage population is indeed able to express VE-cadherin and if macrophage-derived VEGF has the capability to induce and guide vessel sprouting in wounds. Regarding the first open question, the challenge is to demonstrate the weak VE-cadherin expression in macrophages, which failed so far by immunohistochemical stainings of wound tissue against VE-cadherin and F4/80, probably due to less sensitivity of the antibody. *In vitro* stainings of cultured macrophages under hypoxia could resolve this issue and might identify a specific macrophages population expressing VE-cadherin. Further, co-cultivation of macrophages and endothelial cells under hypoxia could highlight the close proximity of macrophage to endothelial cells. To finally address the question whether macrophages have in fact a direct cell-cell contact to endothelial cells via VE-cadherin, a macrophage-specific knock out for VE-cadherin is required, which should exhibit impaired vessel fusion or angiogenesis during the early phase of skin repair. Regarding the second open question, if myeloid cell-derived VEGF is indeed able to induce and guide vessel sprouting, spheroid outgrow assays or 3D cell culture systems could be suitable. By stimulation of endothelial cells with macrophage-derived VEGF or directly by co-cultivation of macrophages and endothelial cells it can be analyzed if macrophage-derived VEGF is able to induce and guide vessel sprouting.

4.2.3 Macrophage depletion during the early phase of repair attenuates alternative activation

It was also investigated whether the different repair phenotypes in control and LysMCre/iDTR mice in which macrophages were exclusively depleted during the early stage of repair, might originate in different activation states of macrophages present at the wound site. The current conceptual model of tissue macrophage activation is based on the hypothesis that

Discussion

macrophages are plastic cells and adapt their response to micro-environmental signals. Several activation states and related functions of macrophages have been described in mice and humans [27, 29, 102]. The best characterized activation states in mice encompass “classical activated macrophages” (also named M1) that exert pro-inflammatory activities, eradicate invading microorganisms and promote type I immune responses and “alternatively activated macrophages” (also termed M2), which are hyporesponsive to pro-inflammatory stimuli, are involved in debris scavenging, angiogenesis, connective tissue remodeling and resolution of inflammation (paradigm of M1/M2 polarization) [33]. The latter one is considered to exert repair and regenerative activities [86, 103]. However, conclusive evidence whether the concept of classical/alternative macrophage activation is operative at the cutaneous wound site and which of the microenvironmental cues might direct macrophage activation is still missing. Recent studies in mice report on a critical role of alternative macrophage activation for regeneration of skeletal muscle and myocardium after injury [49, 89]. However, this study reveals the presence of alternatively activated macrophages (as defined by expression of Fizz1 and Ym1) in control skin wounds particularly during the early stage of the repair response and to a lesser extent also during the mid stage of repair. In contrast, expression of both markers was absent in macrophages infiltrating the wound site, which was deprived of macrophages during the early stage of repair. These findings indicate that environmental factors which induce alternative macrophage activation are primarily present during the early stage of repair. Furthermore, a healing response, which lacks macrophage recruitment during the early stage of repair in mice is inefficient in alternative activation. In addition, these data reveal that alternative macrophage activation correlates positively with the extent of a highly vascularized and cellular granulation tissue as well as ultimately with the degree of scar formation. Contrary to the latter hypothesis, that especially M2 macrophages are pro-angiogenic, this study provides evidence that M1 macrophages present in the early phase of healing are rather pro-angiogenic in wounds and release significant amounts of VEGF. By isolation of VEGF-positive and -negative macrophages, it could be shown on transcriptional level that the pro-inflammatory cytokines IL-6 and iNOS were significantly up-regulated in macrophages expressing VEGF whereas marker for the M2 phenotype, such as arginase or Fizz1 [32] were more or less equally expressed in both macrophages negative and positive for VEGF expression. Indeed, if the early angiogenic response is solely mediated by M1-derived VEGF needs further investigation. Mouse models are needed with lack either M1 or M2 macrophage activation to completely explore the importance of both macrophage activation states and their influence during the different phases of skin repair. For instance, a mouse model is available which specifically lacks the IL-4 receptor α chain, inhibiting signaling through IL-4 and IL-13 and therefore preventing macrophages from alternative activation signals [104]. By wounding of those mice, the

Discussion

importance of alternatively activated macrophages can be analyzed. Nevertheless, besides the beneficial effect for the outcome of the wound healing response described for alternatively activated macrophages [29] this study provides strong evidence, that also M1 macrophages do not only exert harmful activities during wound healing by triggering a harsh pro-inflammatory response, they also carry out beneficial functions by releasing significant amounts of VEGF and initiating the early angiogenic response.

4.3 Macrophage depletion during the mid stage of repair abrogates transition into scar tissue and causes vessel instability

Depletion of macrophages during the mid stage of the repair response, consecutively to the development of a highly vascularized and cellular-rich granulation tissue, resulted in the abrogation or even retrogression of the physiological repair cycle. This process was evident by severe hemorrhages and fibrin exudates, suspicious for destabilization of vascular structures. Indeed, apoptosis of endothelial cells was significantly increased in macrophage-depleted granulation tissue. Furthermore, epidermal wound edges appeared atrophic and detached from the underlying granulation tissue, indicating severe disturbances in epidermal-dermal interactions. In addition, the number of neutrophils increased in macrophage-depleted wounds which had not yet completed re-epithelialization. During physiological skin repair in the used model, the number of neutrophils declines within the initial 5 days post injury [94]. Thus, high numbers of neutrophils present in macrophage-depleted granulation tissue at day 7 and 10 post injury is abnormal. Whether macrophage recruitment during the late phase of repair by discontinuing DT injection could rescue the impaired and retrogressive healing conditions observed in macrophage depleted wounds during the mid stage of healing remains elusive. Regarding this question later time points have to be investigated to analyze if wound closure occurs and if a stable scar tissue develops resulting in tissue maturation and restoration of skin homeostasis.

Several mechanisms underlying the morphological and functional changes associated with macrophage depletion during the mid stage of the repair response might be discussed. Sudden withdrawal of several growth factors by macrophage depletion from the metabolically highly active granulation tissue might result in severe alterations in tissue homeostasis. For example, withdrawal of VEGF and TGF- β , both of which are potent survival factors for endothelial cells, might explain endothelial cell apoptosis and vessel destabilization observed in macrophage-depleted wounds [56, 105]. However, a single withdraw of myeloid cell-derived VEGF in the conditional knock out mouse model used did not result in hemorrhages

Discussion

as observed in DT treated LysMCre/iDTR wounds, indicating that the described phenotype was not a result of the withdrawal of this growth factor alone. Moreover, it could be shown that myeloid cell-derived VEGF is receding in its importance during the phase of tissue formation. By contrast, epidermal compartments take over VEGF supply at this stage of the wound healing response, because vessels could grow normally during the mid phase in VEGF^{fl/fl} LysMCre mice despite a lack of myeloid cell-derived VEGF, which was however not the case in double knock outs for VEGF in myeloid cells and keratinocytes. The double knock out showed a prolonged delay in the angiogenic response indicating a dynamic switch of the importance of macrophage- and keratinocyte-derived VEGF on the outcome of the angiogenic response in wounds. Interestingly, even the double knock out for VEGF in both keratinocytes and macrophages does not cause vessel instability and hemorrhages, indicating that keratinocyte- and myeloid cell-derived VEGF during wound angiogenesis might not be an important survival signal for endothelial cells. These findings are further supported by another study in which VEGF expression was exclusively depleted in keratinocytes [78]. The wounds in these mice showed indeed reduced vascularization particularly during later phases of the skin repair response but did not exhibit hemorrhages. Whether VEGF amounts coming from other cell compartments present at the wound site or VEGF expressed by endothelial cells themselves is sufficient for vessel stability during wound angiogenesis needs to be further investigated. Indeed, autocrine VEGF derived by endothelial cells is required for the homeostasis of blood vessels in the adult [54] and could also be sufficient enough for vessel stabilization during wound angiogenesis. Yet, by usage of an inducible complete knock out mouse model for VEGF, the overall function of VEGF in wound angiogenesis and vessel stabilization could be identified.

As mentioned above, TGF- β released by macrophages is another interesting candidate in mediating endothelial cell survival during wound angiogenesis [105]. In a knock out model which lacks the TGF- β receptor type II exclusively in macrophages [106], showed reduced amounts of TGF- β in wounds (TGF- β amplifies its expression in an autocrine loop [107]) and displayed the same hemorrhages within the granulation tissue during the tissue formation phase (personal communication R. Ranjan, [108]). Yet, to identify macrophage-derived TGF- β as an important factor for vessel stability during wound angiogenesis, a macrophage-specific knock out directly for TGF- β is needed. Furthermore, it can be discussed that the sudden withdrawal of TGF- β as a potent immunosuppressive mediator [109] might be responsible for the increased influx of neutrophils into the macrophage-depleted granulation tissue. In turn, neutrophils are rich in highly active tissue degrading proteases and reactive oxygen species, which could contribute to the severe endothelial cell damage observed [110]. Although, at this stage we cannot exclude neutrophil-mediated vascular cell damage, we consider it an unlikely event, because hemorrhages and endothelial cell apoptosis were

also present in macrophage-depleted granulation tissue which did not present increased numbers of neutrophils. Overall, our data clearly illustrate that macrophages present in an already developed granulation tissue are crucial for the progression of the mid stage of the repair response into the late stage characterized by tissue maturation.

4.4 Macrophages present at the late stage of repair do not impact tissue maturation

Finally, depletion of macrophages during the late stage of repair did not cause significant morphological changes, indicating a minor role of macrophages present during the phase of tissue maturation and scar formation. Indeed, as outlined above, macrophages recruited during the early stage of repair significantly control the degree of scar formation. Furthermore, absence of morphological alterations in macrophage-depleted day 14 wounds of LysMCre/iDTR mice, demonstrates that DT-mediated macrophage apoptosis itself does not inevitably cause cellular changes in the wounded tissue. Therefore, in our model the altered healing response observed in macrophage-depleted wounds during the early or mid stage of repair is a consequence of macrophage deficiency and not a sequela of their apoptosis.

4.5 Model: Macrophages as sentinels directing the quality of skin repair

In conclusion, this study adds to previous knowledge on the function of macrophages in skin repair [38, 95, 96], but also uncovers several novel aspects. First, the findings substantiate previous work, demonstrating a crucial role of macrophages in healing skin wounds in the adult organism to achieve tissue homeostasis. Secondly, repair mechanisms were identified that are dependent or independent from macrophage function. Third, it was revealed that macrophages exert distinct functions during the diverse phases of skin repair which are however complementary to restore skin integrity. Finally, the findings suggest that different macrophage functions in skin repair can originate in different macrophage activation states. Overall, our findings delineate cellular and molecular mechanisms that control the kinetics of skin repair and links macrophage function as the critical force to the dynamics of wound repair. Future studies will analyze whether selective modulation of macrophage activation and function during specific stages of repair might be an effective therapeutic strategy to

Discussion

normalize tissue regeneration in pathological healing conditions. However, one has to take into account that skin repair in mice differs significantly to the human system. Therefore, it is suggested that additional experimental studies in mice and/or other model organisms, should be paralleled by analysis of macrophage activation and function during wound repair in the human system. Figure 32 illustrates the proposed model for macrophage function during the different phases of the cutaneous wound healing response.

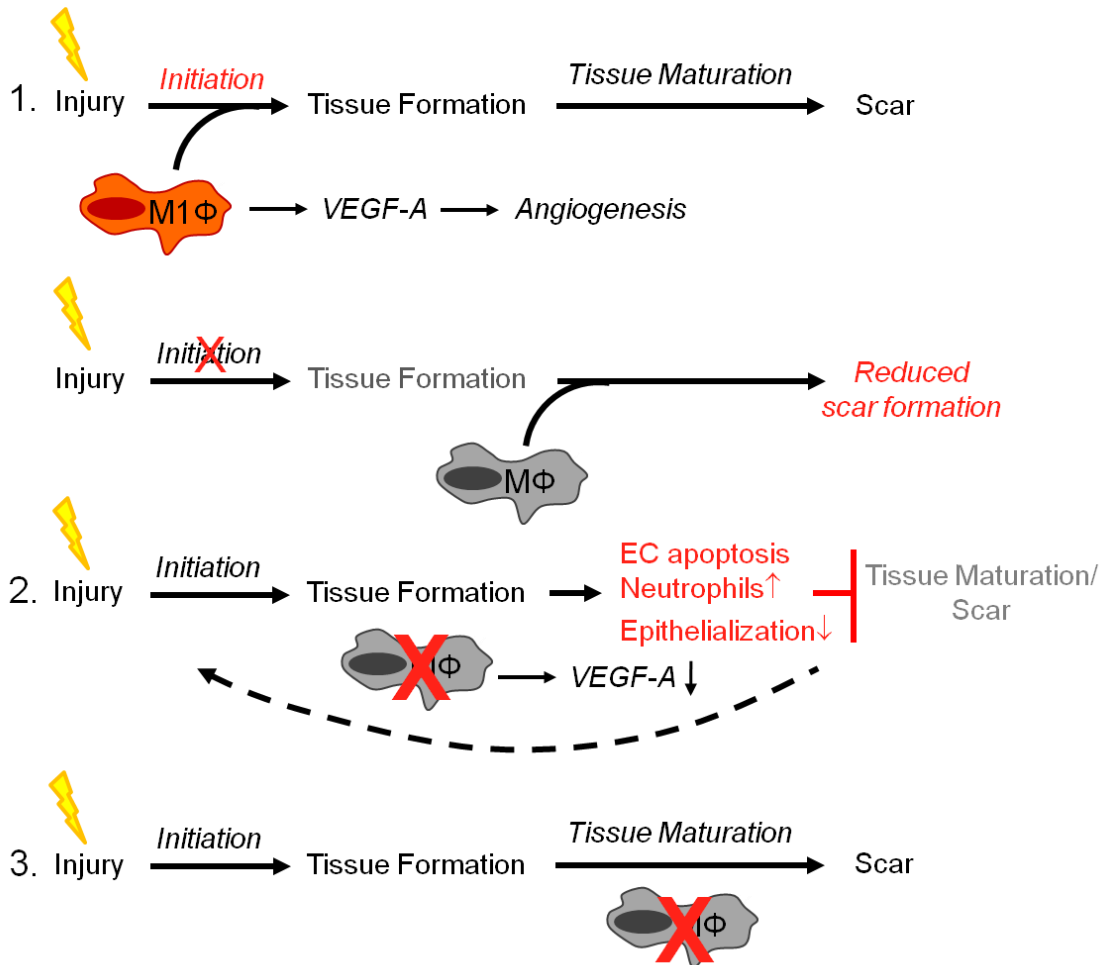


Figure 32: Model for macrophage functions during the different phases of the cutaneous wound healing response. First, influx of macrophages during the early phase of healing is crucial to induce a highly vascularized granulation tissue, which however leads to scar formation. Macrophage-derived VEGF-A initiates this angiogenic response and there is evidence that these pro-angiogenic macrophages show a rather pro-inflammatory M1 phenotype. Macrophage recruitment at later stages reaches wound closure and interestingly scar formation is reduced. Second, it could be shown that the presence of macrophages in an already developed granulation tissue is important for the transition of granulation tissue into a stable scar tissue and therefore for the restoration of skin homeostasis. Third, macrophages present in the late phase of repair after re-epithelialization is completed do not impact scar formation and tissue maturation.

5 Material and Methods

5.1 Material

5.1.1 Chemicals and enzymes

Unless otherwise specified, all standard chemicals were purchased from Roth (Karlsruhe, Germany), Merck Bioscience (Schwalbach, Germany), Serva (Heidelberg, Germany) or Sigma-Aldrich (St. Louis, MO, USA). Used chemical solutions and buffers were prepared with deionized water at room temperature. Taq polymerase including the respective buffers was obtained from Bio Budget (Krefeld, Germany), proteinase K from Sigma-Aldrich, Liberase Blendzyme from Roche Applied Science (Mannheim, Germany), Power SYBR[®] Green from Applied Biosystems (Carlsbad, CA, USA) and RT² SYBR Green/ROX qPCR Master Mix from SABioscience (a Qiagen Company, Hilden, Germany).

5.1.2 Buffers used

PBS: 10 mM Na₂HPO₄, 1.5 mM KH₂PO₄; 2.6 mM KCl, 136 mM NaCl, pH 7.4

TE buffer: 10 mM TrisHCl (pH 8.0), 1 mM EDTA

TAE buffer: 40 mM TrisHCl (pH 8.0), 20 mM NaAc, 1 mM EDTA

5x loading dye: 40% Glycerol, 0.04% bromphenol blue, 0.2% orange G, 1 mM EDTA

Tail lysis buffer: 100 mM Tris-HCl (pH 8.0), 5 mM EDTA, 0.2% (w/v) SDS, 0.2 M NaCl, 500 mg/ml proteinase K

FACS buffer: 1% BSA, 2 mM EDTA in PBS

Anticoagulation buffer: 1 mM EDTA in PBS supplemented with Heparin (1:4000, Heparin-Natrium-25,000-ratiopharm[®], Ratiopharm GmbH, Ulm, Germany)

ACK lysis buffer: 150 mM NH₄Cl, 10 mM KHCO₃, 0.1 mM EDTA

5.1.3 Kits

Following commercial kits were used within this work: RNeasy Plus Mini Kit, RNeasy Plus Micro Kit, RNeasy Fibrous Tissue Kit (all from Qiagen, Hilden, Germany), mouse VEGF Quantikine[®] ELISA Kit (R&D Systems, Minneapolis, MN, USA), High Capacity cDNA Reverse Transcription Kit (Applied Biosystems, Carlsbad, CA, USA), RT² First Strand Kit (SABioscience, a Qiagen Company, Hilden, Germany) and RT² Profiler[™] PCR Array for genes related to mouse angiogenesis (PAMM-024, SABioscience, a Qiagen Company, Hilden, Germany).

Material and Methods

5.1.4 Oligonucleotides

Table 1: Oligonucleotides used in this thesis were purchased from Sigma-Aldrich (St. Louis, MO, USA). Lyophilized primers were dissolved in TE buffer (see section 5.1.2).

No.	Name	Sequence
P1	Lys1	5' CTTGGGCTGCCAGAATTTCTC
P2	Lys2	5' TTACAGTCGGCCAGGCTGAC
P3	Cre8	5' CCCAGAAATGCCAGATTACG
P4	K14Cre Up	5' GATGAAAGCCAAGGGGAATG
P5	K14Cre Down	5' CATCACTCGTTGCATCGACC
P6	iDTR 1	5' CCAAAGTCGCTCTGAGTTGTTATC
P7	iDTR 2	5' GCGAAGAGTTTGTCTCAACC
P8	iDTR 3	5' GGAGCGGGAGAAATGGAT
P9	muVEGF419.F	5' CCTGGCCCTCAAGTACACCTT
P10	muVEGF567.R	5' TCCGTACGACGCATTTCTAG
P11	lacZex8	5' TGGCGATTTAGCAGCAGATA
P12	lacZ WT	5' ATGTGACAAGCCAAGGCGGTG
P13	lacZ5'	5' GGTAGGGTTTTTTCACAGAC
P14	VEGFc5R.2	5' ACATCTGCTGTGCTGTAGGAAG
P15	VEGF322.F	5' ACTTCATGGACAGGCTTCGG
P16	Cdh5for	5' CCGCTGATCGGCACTGTGGT
P17	Cdh5rev	5' TGGAGTACCCGATGCTGCGCT
P18	CTGFfor	5' CCTCCGTCGCAGGTCCCATCA
P19	CTGFrev	5' CCATAGCAGGCCGGGTGCAG
P20	IL-1 β for	5' GGACCCCAAAGATGAAGGGCTGC
P21	IL-1 β rev	5' GCTCTTGTGATGTGCTGCTGCG
P22	PIGFfor	5' ACTCAACAGAAGTGGAAGTGGTGCC
P23	PIGFrev	5' TCAGAAGGACACAGGACGGACTGAA
P24	VEGFfor	5' TGTACCTCCACCATGCCAAGT
P25	VEGFrev	5' CGCTGGTAGACGTCCATGAA
P26	IL-6for	5' ACACATGTTCTCTGGGAAATC
P27	IL-6rev	5' AAGTGCATCATCGTTGTTTCATACA
P28	iNOSfor	5' CCACCTTGGTGAAGGGACTGAGCT
P29	iNOSrev	5' AGGGGCAAGCCATGTCTGAGACT
P30	TNFafor	5' GACCCTCACACTCAGATCATCTTCT
P31	TNFarev	5' CCTCCACTTGGTGGTTTGCT

Material and Methods

P32	Arg1for	5'	GCTTCGGAACCTCAACGGGAGGG
P33	Arg1rev	5'	ACCAGAAAGGAACTGCTGGGATACA
P34	IL-10for	5'	AGCCGGGAAGACAATAACTG
P35	IL-10rev	5'	CATTTCCGATAAGGCTTGG
P36	S18for	5'	GATCCCAGACTGGTTCCTGA
P37	S18rev	5'	GTCTAGACCGTTGGCCAGAA
P38	TGF- β for	5'	TGGAGCAACATGTGGAACCTC
P39	TGF- β rev	5'	GTCAGCAGCCGGTTACCA
P40	Fizz1for	5'	TATGAACAGATGGGCCTCCT
P41	Fizz1rev	5'	GGCAGTTGCAAGTATCTCCAC

5.1.5 Antibodies

As primary antibodies for immunohistochemistry, monoclonal rat antibodies against F4/80 (Dianova BMA AG, Augst, Switzerland), CD31 (Pecam-1, BD Pharmingen, Heidelberg, Germany), Ki67 (DakoCytomation Inc., Carpinteria, CA, USA), Gr-1 (Ly-6G, BD Pharmingen, Heidelberg, Germany) or CD144 coupled to biotin (VE-cadherin, eBioscience Inc., San Diego, CA, USA) were used; further, monoclonal mouse antibodies against Desmin (DakoCytomation Inc., Carpinteria, CA, USA) or α -SMA coupled to Cy-3 (Sigma-Aldrich, St. Louis, MO, USA), polyclonal rabbit antibodies against Fizz1 (Peprotech, Paris, France), VEGF-A (A-20) (Santa Cruz Biotechnology Inc., Santa Cruz, CA, USA) or fibrinogen/fibrin (DakoCytomation Inc., Carpinteria, CA, USA), monoclonal goat antibodies against Dll4 (Delta-like protein 4, R&D Systems, Minneapolis, MN, USA), Ym1 (R&D Systems, Minneapolis, MN, USA) or TGF- β 1 (R&D Systems, Minneapolis, MN, USA) and a monoclonal rabbit antibody against cleaved caspase-3 (Asp175) (Cell Signaling Technology Inc., Boston, MA, USA). Bound primary antibodies were detected by incubation with corresponding Alexa-conjugated secondary antibodies (Invitrogen, Darmstadt, Germany). For flow cytometry direct labeled antibodies to either Fluoresceinisothiocyanat (FITC), Phycoerythrin (PE) or Allophycocyanin (APC) were used against F4/80 (AbD Serotec, Düsseldorf, Germany), Gr-1 (Miltenyi, Bergisch Gladbach, Germany), CD11b (Mac-1, Miltenyi, Bergisch Gladbach, Germany), CD115 (eBioscience Inc., San Diego, CA, USA) or CD19 (Miltenyi, Bergisch Gladbach, Germany). Further details are listed in table 3, 4 and 5.

Material and Methods

5.1.6 Special technical equipment

Microscopes: Leica DM 4000B (Leica Camera AG, Solms, Germany), Nikon eclipse E 800 (Nikon, Melville, NY, USA), Nikon A1 (Nikon, Melville, NY, USA).

PCR machines: 7300 Real Time PCR system (Applied Biosystems, Carlsbad, CA, USA), T3000 Thermocycler (Biometra, Göttingen, Germany).

Flow Cytometers: FACS Canto (BD, Heidelberg, Germany), FACS Aria III (BD, Heidelberg, Germany).

5.1.7 Software

Statistical analyses were performed by using GraphPad Prism5 (GraphPad Software, Inc., San Diego, CA, USA), FACS data were analysed with FACSDiva (BD, Heidelberg, Germany), light microscopy images were taken and analyzed with Diskus 4.50 Software (Diskus, Königswinter, Germany), fluorescent microscopy images with NIS-Elements AR 2.30 Software (Nikon, Melville, NY, USA) and confocal fluorescent images with Velocity Software (Nikon, Melville, NY, USA) and analysed with either ImageJ (Image Processing and Analysis in Java, Wayne Rasband, National Institute of Mental Health, Bethesda, MD, USA) or Adobe Photoshop 7.0 (Adobe Systems Inc., Dublin, Ireland).

5.2 Standard molecular biology methods

5.2.1 RNA extraction, RT PCR and quantitative real time PCR

Total RNA from wound tissue was extracted using the Qiagen RNeasy Fibrous Tissue Kit (Qiagen, Hilden, Germany) and total RNA from isolated monocytes or macrophages using either the RNeasy Mini or Micro Kit, depending on the cell number (Qiagen, Hilden, Germany). 500-1000 ng of each RNA sample was reversely transcribed using the High Capacity cDNA RT Kit (Applied Biosystems, Carlsbad, CA, USA) according to manufacturer's protocols. Amplification reactions, each in triplicates, were set up using PowerSYBR Green PCR Master Mix (Applied Biosystems, Carlsbad, CA, USA). Real time PCR was validated with the 7300 Real Time PCR system (Applied Biosystems, Carlsbad, CA, USA). The comparative method of relative quantification ($2^{-\Delta\Delta Ct}$) [111] was used to calculate expression level of the target gene normalized to the house keeping gene S18. Note, in case that no expression in blood monocyte samples for the normalization was detectable, the Ct value was set to 40 corresponding to the last cycle of the PCR run. All used oligonucleotides are listed in table 1 (P16-P41). Primer were designed with the NCBI

Material and Methods

Primer-BLAST tool and were, if possible, exon-exon spanning. Primers were tested for specificity by analyzing a dissociation curve, resulting in one single curve in case of one specific PCR product and by loading the PCR fragments on an agarose gel (see section 5.2.4) and calculating the corresponding fragment length. The amplified PCR fragments were not longer than 250 bp and the annealing temperature was always $60^{\circ}\text{C} \pm 1^{\circ}\text{C}$.

5.2.1.1 Mouse angiogenesis real time PCR array

RNA was isolated out of cultured macrophages, stimulated under hypoxia as described above and in section 5.5. For cDNA generation the RT² First Strand Kit (SABioscience, a Qiagen Company, Hilden, Germany) was used according to the manufacturer's instructions. Primers for qPCR were pre-coated by the company on a 96-well plate for a RT² ProfilerTM PCR Array for genes related to mouse angiogenesis (PAMM-024; SABioscience, a Qiagen Company, Hilden, Germany). Amplification reactions were set up using RT² SYBR Green/ROX qPCR Master Mix (SABioscience, a Qiagen Company, Hilden, Germany) according to the manufacturer's instructions and real time PCR was validated as described above.

5.2.2 RNA quantification

The concentration of RNA was determined by measuring absorption at 260 nm and 280 nm (A_{260} and A_{280}). An A_{260} of 1 corresponds to a concentration of approximately 40 $\mu\text{g}/\text{ml}$ of RNA. The purity of the RNA can be assessed by calculating the ratio of A_{260}/A_{280} with 2 reflecting pure RNA. A ratio below or above 2 indicates protein or genomic DNA contamination, respectively.

5.2.3 Isolation of genomic DNA

Mouse tail biopsies (~5 mm) or isolated peritoneal cells (see section 5.3.3.1) were incubated in tail lysis buffer (see section 5.1.2) in a thermo mixer (Eppendorf, Hamburg, Germany) at 56°C over night. DNA was then precipitated from the solution by adding an equivalent of isopropanol, centrifuged and the pelleted DNA was washed with the same volume of 70% ethanol. After an additional centrifugation step, the DNA pellet was dried at room temperature for ~1 hour and resuspended in 125 μl (in case of tail biopsies) or 30 μl (in case of cultured cells) 1x TE buffer (see section 5.1.2).

Material and Methods

5.2.4 Polymerase chain reaction (PCR)

PCR was mainly used for genotyping. In a standard protocol 10-100 ng template DNA (conforms to 1 μ l of isolated tail DNA resuspended in 125 μ l TE buffer) was amplified in a reaction batch containing 1x reaction buffer, 2 mM MgCl₂, 200 nM each primer, 200 μ M dNTP mix and 0.05 U/ μ l Taq-Polymerase (Bio Budget, Krefeld, Germany; except primers). For most applications the template DNA was denatured at 95°C for 5 min followed by 30-35 cycles of 45 sec at 95°C, 1 min at the appropriate annealing temperature and 1 min per kb DNA to be amplified at synthesis temperature (72°C). Amplification was completed with a final synthesis step at 72°C for 7 min. The optimal annealing temperature of the primers was estimated with the following formula: $T_A=59.9+0.41(\text{GC}\%)-600/L$ (GC%, GC content in percent, L, total number of base pairs). All primers used for genotyping are listed in table 1 (P1-P15). PCR-amplified DNA fragments were mixed with 5x loading dye (see section 5.1.2) and applied to 1% - 2% (w/v) agarose gels (1x TAE, 0.5 mg/ml ethidium bromide) and electrophoresed at 120 V.

5.2.5 VEGF-specific ELISA

A commercial VEGF sandwich ELISA from R&D (Quantikine[®] Mouse VEGF immunoassay, R&D Systems, Minneapolis, MN, USA) was used for the determination of secreted VEGF protein of cultured peritoneal macrophages (see section 5.5) in comparison to a VEGF-standard curve following the manufacturer's manual.

5.3 Mice

5.3.1 Mouse strains

All mouse strains were maintained and bred under standard pathogen-free conditions. To generate mice in which macrophages can be depleted in a temporally controlled manner, iDTR mice (C57Bl/6 background) [82] were bred with mice expressing the *Cre* recombinase (C57Bl/6 background) from the myeloid cell specific lysozyme M promoter [83]. To generate mice in which VEGF-A is specifically depleted in either macrophages or keratinocytes and macrophages, FVB/N VEGF^{fl/fl} mice [53] were bred with mice expressing *Cre* (C57Bl/6 background) from the LysM promoter or from the keratinocyte specific keratin 14 promoter (K14Cre, C57Bl/6 background) [92], respectively. Mice were backcrossed to the FVB/N background for at least six generations. To analyze VEGF expression in tissues a VEGF-lacZ reporter mouse line (CD-1/129 mixed background) was used in which both the VEGF

Material and Methods

and the LacZ gene is expressed under the control of the murine VEGF promoter [88]. 8- to 12-week-old iDTR (control), iDTR/LysMCre (inducible macrophage-depleted mice, heterozygous or homozygous for the *DTR* gene), VEGF^{fl/fl} (control), VEGF^{fl/fl} LysMCre (myeloid cell-specific knock out), VEGF^{fl/fl} LysMCre K14Cre (double knock out) or VEGF-lacZ^{+/wt} (reporter) mice were used for the experiments. In each and every case the *Cre* recombinase was used heterozygously. All experiments were done according to institutional guidelines.

5.3.2 Genotyping

Tail biopsies were taken from mice with three weeks of age and DNA was isolated (see section 5.2.3). Mice were genotyped by PCR using the standard PCR program (see section 5.2.4) with varying annealing temperatures (T_A) and cycle numbers (Table 2). Primers used for genotyping are listed in table 1.

Table 2: Protocols for genotyping by PCR, the corresponding primer sequences are listed in table 1 under the respective primer numbers.

Strain/PCR	Primer	PCR product	T_A and cycle number
iDTR	P6-8	wt: 600 bp	$T_A = 54^\circ\text{C}$, 12 cycles
		iDTR: 300 bp	$T_A = 51^\circ\text{C}$, 18 cycles
LysMCre	P1-3	wt: 350 bp	$T_A = 56^\circ\text{C}$, 12 cycles
		LysMCre: 750 bp	$T_A = 52^\circ\text{C}$, 18 cycles
VEGFflox	P9-10	wt: 100 bp	$T_A = 55^\circ\text{C}$, 30 cycles
		flox: 150 bp	
K14Cre	P4-5	K14Cre: 250 bp	$T_A = 60^\circ\text{C}$, 32 cycles
VEGFlacZ	P11-13	wt: 300 bp	$T_A = 55^\circ\text{C}$, 35 cycles
		lacZ: 350 bp	
VEGFDel	P14-15	before recombination: 2.1 kb after recombination: 560 bp	$T_A = 58^\circ\text{C}$, 30 cycles

5.3.3 Administration of diphtheria toxin

The 1 mg/ml stock solution of the diphtheria toxin (DT, Merck Bioscience, Schwalbach, Germany) in pyrogen free ddH₂O was aliquoted and stored at -80°C . Fresh aliquots were thawed on ice for each treatment. The working concentration was 5 $\mu\text{g/ml}$, diluted in sterile PBS and LysMCre/iDTR mice (hetero- or homozygous for the *iDTR* gene as indicated) and

Material and Methods

control mice (LysMCre) received DT (25 ng/g bodyweight) injections intraperitoneally or intravenously at indicated time points. For wound-phase-restricted depletion of macrophages LysMCre/iDTR and control mice were injected with DT according to three regimens outlined in Figure 8. For macrophage depletion during the inflammatory phase mice were injected with DT 2 and 1 days prior wounding as well as 2 and 4 days post wounding (regimen A), the phase of tissue formation mice were injected with DT 3, 4, 6 and 8 days post injury (regimen B), and the phase of maturation mice were injected with DT 8, 9, 11, and 13 days post injury (regimen C).

5.3.4 Thioglycolate-induced peritonitis

For thioglycolate-mediated peritonitis a 4% thioglycolate brew (Sigma-Aldrich, St. Louis, MO, USA) in PBS was prepared, autoclaved and matured in the bottle for at least one month in the dark before use. Mice were then injected intraperitoneally with 2 ml 4% thioglycolate and peritoneal cells were isolated 4 days thereafter for FACS analysis, as described in section 5.4.3.2. For LysMCre/iDTR and control mice, mice were injected additionally prior thioglycolate administration two times with DT (25 ng/g bodyweight) i.v. and afterwards three times i.p.

4.3.5 Wounding

Mice were anesthetized by intraperitoneal injection of Ketanest/Rompun (Ketanest S: Park Davis GmbH, Karlsruhe, Germany; Rompun 2%: Bayer, Leverkusen, Germany). The back was shaved and two (iDTR mouse strain) to four (VEGFflox mouse strain and reporter mice) 6-mm diameter full thickness wounds were generated using a standard biopsy puncher (Stiefel, Offenbach, Germany). For histological analysis, wound cell isolation or RNA extraction, wounds were excised at indicated time points post injury. For histological analysis wounds were bisected in caudocranial direction and the tissue was either fixed overnight in 4% paraformaldehyde or embedded in OCT compound (Tissue Tek, Miles, Elkhart, IN, USA) for immunohistochemical stainings. Histological analysis was performed on serial sections from the central portion of the wound. For wound cell isolation, tissues were processed immediately as described in section 5.4.3.3 and for RNA extraction wounds were stored in RNA^{later}® at -20°C (Ambion, Applied Biosystems, Carlsbad, CA, USA) until isolation was performed (see section 5.2.1).

5.4 Flow cytometrie

5.4.1 Single cell suspensions

5.4.1.1 Peritoneal lavage

Mice were sacrificed, the skin was removed from the peritoneum as far as possible and the peritoneal cavity was flushed with around 8 ml ice-cold FACS buffer (see section 5.1.2). Cells were centrifuged at 300 g for 8 min at 4°C and the pellet was resuspended in 1 ml FACS buffer before counting with a Neubauer counting chamber.

5.4.1.2 Blood leukocyte cell suspension

Mice were sacrificed and the thorax was opened as far as possible. Blood was taken by dissecting the heart and collected in 5 ml anticoagulation buffer (see section 5.1.2). After centrifugation at 300 g for 8 min at 4°C blood leukocytes were purified by hypotonic lysis of erythrocytes with 5 ml ACK lysing buffer (two times for 8 min) (see section 5.1.2), the reaction was stopped by adding 45 ml of ice-cold FACS buffer (see section 5.1.2). The suspension was poured over a 70 µm cell strainer (BD, Heidelberg, Germany) and centrifuged. Cells were resuspended in 1 ml FACS buffer and counted.

5.4.1.3 Wound cell suspension

Wounds at indicated time points post injury were excised and minced thoroughly using a scalpel. The wound mush was further digested enzymatically with Liberase blendzyme (0.15 U/ml) (Roche Applied Science, Mannheim, Germany) in DMEM (Dulbecco's modified eagle medium, Invitrogen, Darmstadt, Germany) for 90 min at 37°C and 1000 rpm in a thermo mixer (Eppendorf, Hamburg, Germany). After enzymatical digestion, wounds were additionally disrupted mechanically by using the BD™ Medimachine System (BD Bioscience, Heidelberg, Germany) for 5 min at room temperature in PBS containing 10% FCS (fetal calf serum, PAA, Pasching, Austria). Cells were collected through a 70 µm cell strainer and centrifuged at 300 g for 8 min at 4°C. The cell suspension was then resuspended in PBS/2 mM EDTA and poured additionally through a 40 µm strainer, centrifuged and resuspended in 1 ml FACS buffer (see section 5.1.2) before counting.

Material and Methods

5.4.2 FACS staining

Cells of interest in the different cell suspensions (described above) were identified by staining for cell surface markers. Unspecific binding of antibodies to Fc receptors via their invariable part of the heavy chain was avoided by blocking with anti-CD16/32 (eBioscience Inc., San Diego, CA, USA) directed against the FcγIII and the FcγII receptor, respectively. Subsequently, cells were incubated with the antibodies listed in table 3 in 50-100 μl FACS buffer (see section 5.1.2) for 20-30 min on ice in the dark. After two washing steps with 1 ml FACS buffer, 7-Amino-Actinomycin D (7-AAD, 1:20, eBioscience Inc., San Diego, CA, USA) was added 10 min before analysis for the detection of dead cells. The samples were analyzed in a BD FACS Canto or sorted in a BD FACS Aria III with the appropriate laser using the BD FACS Diva Software.

Table 3: Monoclonal antibodies used for flow cytometry. Antibodies were conjugated with fluorescein isothiocyanate (FITC), phycoerythrin (PE) or allophycocyanin (APC).

Specificity	Target cells	Host/Isotype	Clone	Dye	Final dilution	Commercial source
F4/80	Macrophages	Rat IgG2a κ	BM8	FITC, PE	1:100	AbD Serotec
CD11b/ Mac-1	Macrophages, DCs, NK cells, neutrophils	Rat IgG2b κ	M1/70	PE, APC	1:100	BD- Pharmingen
CD115	Monocytes	Rat IgG2a κ	AFS98	APC	1:250	eBioscience
Gr-1	Neutrophils, monocytes	Rat IgG2b κ	RB6- 8C5	PE	1:10	BD- Pharmingen
CD19	B cells	Rat IgG2a κ	1D3	APC	1:100	BD- Pharmingen

5.4.2.1 FDG staining

β-Gal activity in wound cell suspensions harvested from the VEGF-lacZ reporter mouse strain was unraveled by fluorescein di-β-D-galactopyranoside (FDG) (Invitrogen, Darmstadt, Germany) incubation and always done after cell surface staining. The 10 mM stock solution of FDG in DMSO was aliquoted and stored at -20°C. Fresh aliquots were thawed for each treatment, diluted with ddH₂O to a working concentration of 2 mM and immediately used to avoid spontaneous degradation in water, which leads to a high background and a false positive signal. For the staining procedure cells were resuspended in 40 μl FACS buffer (see

Material and Methods

section 5.1.2) and for the hypotonic shock 1:1 diluted with water containing 2 mM FDG for exactly 20 sec at 37°C. The hypotonic shock was stopped by adding immediately 1 ml ice-cold FACS buffer. FDG incubation within the cells lasted up to 1 hour. The threshold for FDG positive cells was set related to the wild type control (VEGF-lacZ^{wt/wt}), treated with FDG as well.

5.5 Cultivation of macrophages

Primary macrophages were isolated under sterile conditions from the peritoneal cavity (see section 5.4.1.1) and seeded in either 6-well or 24-well plates (0.5×10^6 cells/cm²) (BD, Heidelberg, Germany) in DMEM (Dulbecco's Modified Eagle Medium, Invitrogen, Darmstadt, Germany) supplemented with 10% FCS (PAA, Pasching, Austria) and Penicillin-Streptomycin (100 U/ml penicillin, 0.1 mg/ml streptomycin (final concentrations, Biochrom AG, Berlin, Germany)) (1×10^6 cells/ml). Cells were cultured in a 5% CO₂ atmosphere at 37°C. Macrophages were enriched by plastic adhesion for 4 h, washed twice with fresh medium and cultured over night. Thereafter cells were stimulated with either a mixture of LPS (1 mg/ml; Sigma Aldrich, St. Louis, MO, USA) and recombinant mouse INF- γ (0.1 mg/ml; R&D Systems, Minneapolis, MN, USA) in DMEM supplemented with 1% FCS for 24 h and 48 h or under hypoxia (1% O₂, 5% CO₂, 37°C) in DMEM supplemented with 1% FCS for 8 h. For measurements of secreted VEGF protein amounts supernatants were harvested, centrifuged at high speed for 1 min and stored at -80°C until analysis (see section 5.2.5). For RNA isolation cells were lysed and processed as indicated in section 5.2.1.

5.6 Histology

5.6.1 Histochemistry

Skin samples were fixed in 4% formalin over night and embedded in paraffin. 6 μ m sections were stained with hematoxylin/eosin (H&E), Giemsa stain, and Sirius Red stain following standard protocols in a routine histology laboratory. H&E staining was used for an overview and quantification of common wound healing parameters (see section 5.6.3). In this case eosin stains eosinophilic structures like cytoplasm and protein pink, and erythrocytes red. Hematoxylin stains basophilic structures such as nucleic acids purple. Giemsa staining was used to identify in particular mast cells by means of their dark purple cytoplasmic granules.

Material and Methods

Sirius Red stain was used to analyze collagen fibers, which when examined through polarized light appear bright pink or orange on a dark background.

5.6.2 Immunohistochemistry

For immunohistochemical stainings 10 µm cryosections were fixed either in 4% PFA (7 min) or in ice-cold acetone (2 min, air-dried) and blocked with 10% normal goat serum (DakoCytomation Inc., Carpinteria, CA, USA) or with 10% fetal calf serum (FCS; PAA, Pasching, Austria) in PBS containing 5% BSA to reduce nonspecific antibody binding (at least 1 h at room temperature). Sections were then incubated either 1-2 hours at room temperature or overnight at 4°C with the primary antibodies diluted in the respective blocking buffer. Primary antibodies used in this thesis are listed in table 4. Bound primary antibody was detected by incubation with respective Alexa-conjugated (Invitrogen, Darmstadt, Germany) or peroxidase-conjugated (Southern Biotechnology, Birmingham, AL, USA) secondary antibodies for 1 hour at room temperature (see table 5), followed by counterstaining with DAPI (mainly, 1 µg/ml final concentration) or propidium iodide (in case of the Ki67 staining, 1 µg/ml final concentration) (both Invitrogen, Darmstadt, Germany).

Please note, for the anti CD144/VE-cadherin antibody it is recommend using PBS containing magnesium and calcium for all steps to protect the protein from shedding. For the usage of biotin labeled primary antibodies endogenous biotin was blocked with the DakoCytomation Biotin Blocking System according to the manufacturer's protocol (DakoCytomation Inc., Carpinteria, CA, USA) before incubation of the primary antibody. By usage of a peroxidase-conjugated secondary antibody endogenous peroxidase was inactivated with PBS containing 0.03% H₂O₂ and 0.15 mol/L NaN₃ for 20 min at room temperature and aminoethyl carbazole (AEC substrate solution, DakoCytomation Inc., Carpinteria, CA, USA) was used as a substrate for peroxidase activity by adding some drops on the sections and incubation of 5-20 min at room temperature (depending on the signal intensity). In this case sections were counterstained with hematoxylin.

5.6.3 X-Gal staining

For X-Gal (BCIG, bromo-chloro-indolyl-galactopyranoside) staining 20 µm cryosections from VEGF-lacZ wound tissues were fixed with 0.5% glutaraldehyde for 30 min at room temperature and washed three times with PBS containing 0.02% NP-40 and 0.2 mM MgCl₂. X-Gal staining solution contained 0.5 mg/ml X-Gal (Fermentas, St. Leon-Rot, Germany), 10 mM K₃[Fe(CN)₆], 10 mM K₄[Fe(CN)₆] and 0.2 mM MgCl₂. Sections were incubated for 4-6 hours at 37°C (depending on the signal intensity). After washing with PBS/0.02%

Material and Methods

NP-40/0.2 mM MgCl₂, sections were counterstained with a nuclear fast red aluminum sulphate solution (Roth, Karlsruhe, Germany) for 30 sec at room temperature.

Table 4: Primary monoclonal or polyclonal antibodies used for immunohistochemistry

Specificity	Host/Isotype	Clone	Final dilution	PrimaryAb incubation	Commercial Source
F4/80	Rat IgG _{2a} , monoclonal	BM8	1:200	2 h, RT	Dianova
CD144/VE-cadherin*	Rat IgG ₁ , monoclonal	BV13	1:1000	o.n., 4°C	eBioscience
CD31/Pecam-1	Rat IgG _{2a} κ, monoclonal	MEC 13.3	1:1000	1 h, RT	BD Pharmingen
Gr-1	Rat IgG _{2b} κ, monoclonal	RB6-8C5	1:10	o.n., 4°C	BD Pharmingen
Fizz1/Relm-α	Rabbit, polyclonal		1:50	o.n., 4°C	Peprotech
VEGF-A	Rabbit IgG, polyclonal	sc-152-G	1:100	2 h, RT	Santa Cruz
Fibrinogen/Fibrin	Rabbit, polyclonal		1:8000	1 h, RT	DakoCytomation
Ym1/ECF-L	Goat IgG, polyclonal		1:50	o.n., RT	R&D Systems
Cleaved caspase-3	Rabbit, monoclonal		1:200	o.n., 4°C	Cell Signaling
α-SMA**	Mouse IgG _{2A} , monoclonal	1A4	1:250	1 h, RT	Sigma-Aldrich
DII4	Goat IgG, monoclonal		1:50	o.n., 4°C	R&D Systems
TGF-β*	Goat IgG, polyclonal		1:30	o.n., 4°C	R&D Systems
Desmin	Mouse IgG ₁ κ, monoclonal	D33	1:100	o.n., 4°C	DakoCytomation
Ki67	Rat IgG _{2a} , monoclonal	TEC-3	1:50	1 h, RT	DakoCytomation

* Coupled to biotin, ** coupled to Cy-3

Material and Methods

Table 5: Secondary antibodies used for immunohistochemistry were purchased from Invitrogen (Darmstadt, Germany) or Southern Biotech (Birmingham, AL, USA)

Secondary Antibody	Dye	Final dilution	Commercial source
Goat anti-rabbit IgG (H+L)	Alexa Fluor [®] 488, 568	1:500	Invitrogen
Goat anti mouse IgG₁ (y1)	Alexa Fluor [®] 488, 594	1:500	Invitrogen
Chicken anti goat IgG (H+L)	Alexa Fluor [®] 488	1:500	Invitrogen
Goat anti rat IgG (H+L)	Alexa Fluor [®] 488, 594	1:500	Invitrogen
Donkey anti goat IgG (H+L)	Alexa Fluor [®] 594	1:1000	Invitrogen
Streptavidin	Alexa Fluor [®] 555	1:500	Invitrogen
Goat anti-rat IgG+M (H+L)	HRP	1:250	Southern Biotech

5.6.4 Morphometric analysis

5.6.4.1 Quantification of wound healing parameters

The macroscopic wound area was quantified by processing of photographs taken at various time points, and was calculated as the percentage of the wound area immediately after surgery using the software ImageJ (Image Processing and Analysis in Java, Wayne Rasband, National Institute of Mental Health, Bethesda, MD, USA). For scale setting a ruler next to the wounds was photographed as well. The microscopic wound area was quantified on H&E stained paraffin sections using a light microscope and the corresponding software (Leica DM4000B, Leica Microsystems, Wetzlar, Germany; Diskus 4.50 Software, Diskus, Königswinter, Germany). The extent of epithelialization was determined by measuring the distance between the two epithelial tips and the distance between the edges of the panniculus carnosus was determined as a measure of wound contraction. Finally, dermal repair was estimated by measuring the area of granulation tissue.

5.6.4.2 Quantification of histochemical stainings

Organization and maturation of collagen bundles was assessed on paraffin sections of day 14 wounds stained with Sirius Red and analyzed by polarized light microscopy (Leica DM4000B, Leica Microsystems, Wetzlar, Germany). Numbers of mast cells were determined by counting cells in the entire area of giemsa stained scar tissues (Leica DM4000B, Leica Microsystems, Wetzlar, Germany; Diskus 4.50 Software, Diskus, Königswinter, Germany).

5.6.4.3 Quantification of immunohistochemical stainings

Immunofluorescence microscopy was conducted at indicated magnifications (Microscope Eclipse 800E; Nikon, Melville, NY, USA). Morphometric analysis was performed on digital images using Imaging Software NIS-Elements AR 2.3 (Nikon, Melville, NY, USA). Numbers of macrophages, neutrophils and cells positive for activated caspase-3, VEGF-A or TGF- β 1 and also macrophages in close proximity to blood vessels were determined by counting cells in 2-3 representative rectangles of 200 x 160 μm^2 (defined as high power fields, hpf) in the granulation tissue of wound sections at indicated time points post injury. Ki67 positive cells were determined by counting positively stained cells in 2 representative rectangles of 200 x 160 μm^2 (hpf) within the hyperproliferative epidermal wound margins. For quantitative analysis of CD31, α -SMA, Desmin and Dll4 expression as well as for fibrinogen/fibrin excudate, the area in parts of the granulation tissue, which stained positive for the respective antibodies were calculated by using the ImageJ software (Image Processing and Analysis in Java, Wayne Rasband, National Institute of Mental Health, Bethesda, MD, USA). F4/80 positive cells in close proximity to VE-cadherin positive blood vessels were further analyzed with confocal fluorescence microscopy using a Nikon A1 confocal microscope and the corresponding Velocity software (Nikon, Melville, NY, USA).

5.7 Statistical analysis

Statistical analyses were performed using GraphPad Prism5 (GraphPad Software, Inc., San Diego, CA, USA). Significance of difference was analyzed using unpaired student t-test. All data presented as mean \pm SD. $P \leq 0.05$ was considered significant.

References

6 References

1. Koster, M.I., *Making an epidermis*. Ann N Y Acad Sci, 2009. **1170**: p. 7-10.
2. Breitkreutz, D., N. Mirancea, and R. Nischt, *Basement membranes in skin: unique matrix structures with diverse functions?* Histochem Cell Biol, 2009. **132**(1): p. 1-10.
3. Delavary, B.M., et al., *Macrophages in skin injury and repair*. Immunobiology, 2011.
4. Martin, P., *Wound healing--aiming for perfect skin regeneration*. Science, 1997. **276**(5309): p. 75-81.
5. Gurtner, G.C., et al., *Wound repair and regeneration*. Nature, 2008. **453**(7193): p. 314-21.
6. Babcock, D.T., et al., *Circulating blood cells function as a surveillance system for damaged tissue in Drosophila larvae*. Proc Natl Acad Sci U S A, 2008. **105**(29): p. 10017-22.
7. Niethammer, P., et al., *A tissue-scale gradient of hydrogen peroxide mediates rapid wound detection in zebrafish*. Nature, 2009. **459**(7249): p. 996-9.
8. Chen, Y., et al., *C/EBPalpha initiates primitive myelopoiesis in pluripotent embryonic cells*. Blood, 2009. **114**(1): p. 40-8.
9. Eming, S.A., T. Krieg, and J.M. Davidson, *Inflammation in wound repair: molecular and cellular mechanisms*. J Invest Dermatol, 2007. **127**(3): p. 514-25.
10. DiPietro, L.A., et al., *MIP-1alpha as a critical macrophage chemoattractant in murine wound repair*. J Clin Invest, 1998. **101**(8): p. 1693-8.
11. Werner, S. and R. Grose, *Regulation of wound healing by growth factors and cytokines*. Physiol Rev, 2003. **83**(3): p. 835-70.
12. Eming, S.A., et al., *Regulation of angiogenesis: wound healing as a model*. Prog Histochem Cytochem, 2007. **42**(3): p. 115-70.
13. Roy, R., B. Zhang, and M.A. Moses, *Making the cut: protease-mediated regulation of angiogenesis*. Exp Cell Res, 2006. **312**(5): p. 608-22.
14. Brooks, P.C., R.A. Clark, and D.A. Chersesh, *Requirement of vascular integrin alpha v beta 3 for angiogenesis*. Science, 1994. **264**(5158): p. 569-71.
15. Hinz, B., *Formation and function of the myofibroblast during tissue repair*. J Invest Dermatol, 2007. **127**(3): p. 526-37.
16. Tomasek, J.J., et al., *Myofibroblasts and mechano-regulation of connective tissue remodelling*. Nat Rev Mol Cell Biol, 2002. **3**(5): p. 349-63.
17. Werner, S., T. Krieg, and H. Smola, *Keratinocyte-fibroblast interactions in wound healing*. J Invest Dermatol, 2007. **127**(5): p. 998-1008.
18. Gipson, I.K., S.J. Spurr-Michaud, and A.S. Tisdale, *Hemidesmosomes and anchoring fibril collagen appear synchronously during development and wound healing*. Dev Biol, 1988. **126**(2): p. 253-62.
19. Braiman-Wiksmann, L., et al., *Novel insights into wound healing sequence of events*. Toxicol Pathol, 2007. **35**(6): p. 767-79.
20. Lovvorn, H.N., 3rd, et al., *Relative distribution and crosslinking of collagen distinguish fetal from adult sheep wound repair*. J Pediatr Surg, 1999. **34**(1): p. 218-23.
21. Levenson, S.M., et al., *The Healing of Rat Skin Wounds*. Ann Surg, 1965. **161**: p. 293-308.
22. Geissmann, F., S. Jung, and D.R. Littman, *Blood monocytes consist of two principal subsets with distinct migratory properties*. Immunity, 2003. **19**(1): p. 71-82.
23. Randolph, G.J., et al., *Differentiation of phagocytic monocytes into lymph node dendritic cells in vivo*. Immunity, 1999. **11**(6): p. 753-61.
24. Cecchini, M.G., et al., *Role of colony stimulating factor-1 in the establishment and regulation of tissue macrophages during postnatal development of the mouse*. Development, 1994. **120**(6): p. 1357-72.
25. Grage-Griebenow, E., H.D. Flad, and M. Ernst, *Heterogeneity of human peripheral blood monocyte subsets*. J Leukoc Biol, 2001. **69**(1): p. 11-20.
26. Sunderkotter, C., et al., *Subpopulations of mouse blood monocytes differ in maturation stage and inflammatory response*. J Immunol, 2004. **172**(7): p. 4410-7.

References

27. Martinez, F.O., L. Helming, and S. Gordon, *Alternative activation of macrophages: an immunologic functional perspective*. *Annu Rev Immunol*, 2009. **27**: p. 451-83.
28. Gordon, S. and F.O. Martinez, *Alternative activation of macrophages: mechanism and functions*. *Immunity*, 2010. **32**(5): p. 593-604.
29. Mosser, D.M. and J.P. Edwards, *Exploring the full spectrum of macrophage activation*. *Nat Rev Immunol*, 2008. **8**(12): p. 958-69.
30. Qian, B.Z. and J.W. Pollard, *Macrophage diversity enhances tumor progression and metastasis*. *Cell*, 2010. **141**(1): p. 39-51.
31. Guruvayoorappan, C., *Tumor versus tumor-associated macrophages: how hot is the link?* *Integr Cancer Ther*, 2008. **7**(2): p. 90-5.
32. Loke, P., et al., *IL-4 dependent alternatively-activated macrophages have a distinctive in vivo gene expression phenotype*. *BMC Immunol*, 2002. **3**: p. 7.
33. Gordon, S., *Alternative activation of macrophages*. *Nat Rev Immunol*, 2003. **3**(1): p. 23-35.
34. Eming, S.A., et al., *Interrelation of immunity and tissue repair or regeneration*. *Semin Cell Dev Biol*, 2009. **20**(5): p. 517-27.
35. Loots, M.A., et al., *Differences in cellular infiltrate and extracellular matrix of chronic diabetic and venous ulcers versus acute wounds*. *J Invest Dermatol*, 1998. **111**(5): p. 850-7.
36. Martin, P. and S.J. Leibovich, *Inflammatory cells during wound repair: the good, the bad and the ugly*. *Trends Cell Biol*, 2005. **15**(11): p. 599-607.
37. Simpson, D.M. and R. Ross, *The neutrophilic leukocyte in wound repair a study with antineutrophil serum*. *J Clin Invest*, 1972. **51**(8): p. 2009-23.
38. Leibovich, S.J. and R. Ross, *The role of the macrophage in wound repair. A study with hydrocortisone and antimacrophage serum*. *Am J Pathol*, 1975. **78**(1): p. 71-100.
39. Redd, M.J., et al., *Wound healing and inflammation: embryos reveal the way to perfect repair*. *Philos Trans R Soc Lond B Biol Sci*, 2004. **359**(1445): p. 777-84.
40. Martin, P., et al., *Wound healing in the PU.1 null mouse--tissue repair is not dependent on inflammatory cells*. *Curr Biol*, 2003. **13**(13): p. 1122-8.
41. Nagaoka, T., et al., *Delayed wound healing in the absence of intercellular adhesion molecule-1 or L-selectin expression*. *Am J Pathol*, 2000. **157**(1): p. 237-47.
42. Peters, T., et al., *Wound-healing defect of CD18(-/-) mice due to a decrease in TGF-beta1 and myofibroblast differentiation*. *EMBO J*, 2005. **24**(19): p. 3400-10.
43. Subramaniam, M., et al., *Role of endothelial selectins in wound repair*. *Am J Pathol*, 1997. **150**(5): p. 1701-9.
44. Mori, R., et al., *Impairment of skin wound healing in beta-1,4-galactosyltransferase-deficient mice with reduced leukocyte recruitment*. *Am J Pathol*, 2004. **164**(4): p. 1303-14.
45. Ishida, Y., J.L. Gao, and P.M. Murphy, *Chemokine receptor CX3CR1 mediates skin wound healing by promoting macrophage and fibroblast accumulation and function*. *J Immunol*, 2008. **180**(1): p. 569-79.
46. Han, M., et al., *Development and regeneration of the neonatal digit tip in mice*. *Dev Biol*, 2008. **315**(1): p. 125-35.
47. Duffield, J.S., *The inflammatory macrophage: a story of Jekyll and Hyde*. *Clin Sci (Lond)*, 2003. **104**(1): p. 27-38.
48. Duffield, J.S., et al., *Selective depletion of macrophages reveals distinct, opposing roles during liver injury and repair*. *J Clin Invest*, 2005. **115**(1): p. 56-65.
49. Arnold, L., et al., *Inflammatory monocytes recruited after skeletal muscle injury switch into antiinflammatory macrophages to support myogenesis*. *J Exp Med*, 2007. **204**(5): p. 1057-69.
50. Senger, D.R., et al., *Tumor cells secrete a vascular permeability factor that promotes accumulation of ascites fluid*. *Science*, 1983. **219**(4587): p. 983-5.
51. Ferrara, N. and W.J. Henzel, *Pituitary follicular cells secrete a novel heparin-binding growth factor specific for vascular endothelial cells*. *Biochem Biophys Res Commun*, 1989. **161**(2): p. 851-8.

References

52. Ferrara, N., et al., *Heterozygous embryonic lethality induced by targeted inactivation of the VEGF gene*. *Nature*, 1996. **380**(6573): p. 439-42.
53. Gerber, H.P., et al., *VEGF is required for growth and survival in neonatal mice*. *Development*, 1999. **126**(6): p. 1149-59.
54. Lee, S., et al., *Autocrine VEGF signaling is required for vascular homeostasis*. *Cell*, 2007. **130**(4): p. 691-703.
55. Ferrara, N., *Vascular endothelial growth factor: basic science and clinical progress*. *Endocr Rev*, 2004. **25**(4): p. 581-611.
56. Olsson, A.K., et al., *VEGF receptor signalling - in control of vascular function*. *Nat Rev Mol Cell Biol*, 2006. **7**(5): p. 359-71.
57. Tischer, E., et al., *The human gene for vascular endothelial growth factor. Multiple protein forms are encoded through alternative exon splicing*. *J Biol Chem*, 1991. **266**(18): p. 11947-54.
58. Holmes, K., et al., *Vascular endothelial growth factor receptor-2: structure, function, intracellular signalling and therapeutic inhibition*. *Cell Signal*, 2007. **19**(10): p. 2003-12.
59. Hiratsuka, S., et al., *Flt-1 lacking the tyrosine kinase domain is sufficient for normal development and angiogenesis in mice*. *Proc Natl Acad Sci U S A*, 1998. **95**(16): p. 9349-54.
60. Folkman, J. and M. Klagsbrun, *Angiogenic factors*. *Science*, 1987. **235**(4787): p. 442-7.
61. Potter, M.D., S. Barbero, and D.A. Cheresh, *Tyrosine phosphorylation of VE-cadherin prevents binding of p120- and beta-catenin and maintains the cellular mesenchymal state*. *J Biol Chem*, 2005. **280**(36): p. 31906-12.
62. Marin-Padilla, M., *Early vascularization of the embryonic cerebral cortex: Golgi and electron microscopic studies*. *J Comp Neurol*, 1985. **241**(2): p. 237-49.
63. Gerhardt, H., et al., *VEGF guides angiogenic sprouting utilizing endothelial tip cell filopodia*. *J Cell Biol*, 2003. **161**(6): p. 1163-77.
64. Blum, Y., et al., *Complex cell rearrangements during intersegmental vessel sprouting and vessel fusion in the zebrafish embryo*. *Dev Biol*, 2008. **316**(2): p. 312-22.
65. Fantin, A., et al., *Tissue macrophages act as cellular chaperones for vascular anastomosis downstream of VEGF-mediated endothelial tip cell induction*. *Blood*, 2010. **116**(5): p. 829-40.
66. Schmidt, T. and P. Carmeliet, *Blood-vessel formation: Bridges that guide and unite*. *Nature*, 2010. **465**(7299): p. 697-9.
67. Suchting, S., et al., *The Notch ligand Delta-like 4 negatively regulates endothelial tip cell formation and vessel branching*. *Proc Natl Acad Sci U S A*, 2007. **104**(9): p. 3225-30.
68. Lobov, I.B., et al., *Delta-like ligand 4 (Dll4) is induced by VEGF as a negative regulator of angiogenic sprouting*. *Proc Natl Acad Sci U S A*, 2007. **104**(9): p. 3219-24.
69. von Tell, D., A. Armulik, and C. Betsholtz, *Pericytes and vascular stability*. *Exp Cell Res*, 2006. **312**(5): p. 623-9.
70. Frank, S., et al., *Regulation of vascular endothelial growth factor expression in cultured keratinocytes. Implications for normal and impaired wound healing*. *J Biol Chem*, 1995. **270**(21): p. 12607-13.
71. Lauer, G., et al., *Expression and proteolysis of vascular endothelial growth factor is increased in chronic wounds*. *J Invest Dermatol*, 2000. **115**(1): p. 12-8.
72. Lauer, G., et al., *Generation of a novel proteolysis resistant vascular endothelial growth factor165 variant by a site-directed mutation at the plasmin sensitive cleavage site*. *FEBS Lett*, 2002. **531**(2): p. 309-13.
73. Roth, D., et al., *Plasmin modulates vascular endothelial growth factor-A-mediated angiogenesis during wound repair*. *Am J Pathol*, 2006. **168**(2): p. 670-84.
74. Brown, L.F., et al., *Expression of vascular permeability factor (vascular endothelial growth factor) by epidermal keratinocytes during wound healing*. *J Exp Med*, 1992. **176**(5): p. 1375-9.
75. Barleon, B., et al., *Migration of human monocytes in response to vascular endothelial growth factor (VEGF) is mediated via the VEGF receptor flt-1*. *Blood*, 1996. **87**(8): p. 3336-43.
76. Fukumura, D., et al., *Tumor induction of VEGF promoter activity in stromal cells*. *Cell*, 1998. **94**(6): p. 715-25.

References

77. Kishimoto, J., et al., *In vivo detection of human vascular endothelial growth factor promoter activity in transgenic mouse skin*. Am J Pathol, 2000. **157**(1): p. 103-10.
78. Rossiter, H., et al., *Loss of vascular endothelial growth factor activity in murine epidermal keratinocytes delays wound healing and inhibits tumor formation*. Cancer Res, 2004. **64**(10): p. 3508-16.
79. Xiong, M., et al., *Production of vascular endothelial growth factor by murine macrophages: regulation by hypoxia, lactate, and the inducible nitric oxide synthase pathway*. Am J Pathol, 1998. **153**(2): p. 587-98.
80. Stockmann, C., et al., *Deletion of vascular endothelial growth factor in myeloid cells accelerates tumorigenesis*. Nature, 2008. **456**(7223): p. 814-8.
81. Stockmann, C., et al., *Loss of myeloid cell-derived vascular endothelial growth factor accelerates fibrosis*. Proc Natl Acad Sci U S A, 2010. **107**(9): p. 4329-34.
82. Buch, T., et al., *A Cre-inducible diphtheria toxin receptor mediates cell lineage ablation after toxin administration*. Nat Methods, 2005. **2**(6): p. 419-26.
83. Clausen, B.E., et al., *Conditional gene targeting in macrophages and granulocytes using LysMcre mice*. Transgenic Res, 1999. **8**(4): p. 265-77.
84. Raes, G., et al., *Differential expression of FIZZ1 and Ym1 in alternatively versus classically activated macrophages*. J Leukoc Biol, 2002. **71**(4): p. 597-602.
85. Nair, M.G., D.W. Cochrane, and J.E. Allen, *Macrophages in chronic type 2 inflammation have a novel phenotype characterized by the abundant expression of Ym1 and Fizz1 that can be partly replicated in vitro*. Immunol Lett, 2003. **85**(2): p. 173-80.
86. Loke, P., et al., *Alternative activation is an innate response to injury that requires CD4+ T cells to be sustained during chronic infection*. J Immunol, 2007. **179**(6): p. 3926-36.
87. Benjamin, L.E., I. Hemo, and E. Keshet, *A plasticity window for blood vessel remodelling is defined by pericyte coverage of the preformed endothelial network and is regulated by PDGF-B and VEGF*. Development, 1998. **125**(9): p. 1591-8.
88. Miquerol, L., et al., *Multiple developmental roles of VEGF suggested by a LacZ-tagged allele*. Dev Biol, 1999. **212**(2): p. 307-22.
89. Nahrendorf, M., et al., *The healing myocardium sequentially mobilizes two monocyte subsets with divergent and complementary functions*. J Exp Med, 2007. **204**(12): p. 3037-47.
90. Kelly, J., et al., *Senescence regulates macrophage activation and angiogenic fate at sites of tissue injury in mice*. J Clin Invest, 2007. **117**(11): p. 3421-6.
91. Ramanathan, M., A. Giladi, and S.J. Leibovich, *Regulation of vascular endothelial growth factor gene expression in murine macrophages by nitric oxide and hypoxia*. Exp Biol Med (Maywood), 2003. **228**(6): p. 697-705.
92. Hafner, M., et al., *Keratin 14 Cre transgenic mice authenticate keratin 14 as an oocyte-expressed protein*. Genesis, 2004. **38**(4): p. 176-81.
93. Hellstrom, M., et al., *Dll4 signalling through Notch1 regulates formation of tip cells during angiogenesis*. Nature, 2007. **445**(7129): p. 776-80.
94. Kim, M.H., et al., *Dynamics of neutrophil infiltration during cutaneous wound healing and infection using fluorescence imaging*. J Invest Dermatol, 2008. **128**(7): p. 1812-20.
95. Mirza, R., L.A. DiPietro, and T.J. Koh, *Selective and specific macrophage ablation is detrimental to wound healing in mice*. Am J Pathol, 2009. **175**(6): p. 2454-62.
96. Goren, I., et al., *A transgenic mouse model of inducible macrophage depletion: effects of diphtheria toxin-driven lysozyme M-specific cell lineage ablation on wound inflammatory, angiogenic, and contractive processes*. Am J Pathol, 2009. **175**(1): p. 132-47.
97. Stockmann, C., et al., *A wound size-dependent effect of myeloid cell-derived vascular endothelial growth factor on wound healing*. J Invest Dermatol, 2011. **131**(3): p. 797-801.
98. Barrientos, S., et al., *Growth factors and cytokines in wound healing*. Wound Repair Regen, 2008. **16**(5): p. 585-601.
99. McFarland-Mancini, M.M., et al., *Differences in wound healing in mice with deficiency of IL-6 versus IL-6 receptor*. J Immunol, 2010. **184**(12): p. 7219-28.

References

100. Huang, S.P., et al., *Interleukin-6 increases vascular endothelial growth factor and angiogenesis in gastric carcinoma*. J Biomed Sci, 2004. **11**(4): p. 517-27.
101. Hashizume, M., et al., *IL-6/sIL-6R trans-signalling, but not TNF-alpha induced angiogenesis in a HUVEC and synovial cell co-culture system*. Rheumatol Int, 2009. **29**(12): p. 1449-54.
102. Gordon, S. and P.R. Taylor, *Monocyte and macrophage heterogeneity*. Nat Rev Immunol, 2005. **5**(12): p. 953-64.
103. Pull, S.L., et al., *Activated macrophages are an adaptive element of the colonic epithelial progenitor niche necessary for regenerative responses to injury*. Proc Natl Acad Sci U S A, 2005. **102**(1): p. 99-104.
104. Brombacher, F., et al., *Analyzing classical and alternative macrophage activation in macrophage/neutrophil-specific IL-4 receptor-alpha-deficient mice*. Methods Mol Biol, 2009. **531**: p. 225-52.
105. ten Dijke, P. and H.M. Arthur, *Extracellular control of TGFbeta signalling in vascular development and disease*. Nat Rev Mol Cell Biol, 2007. **8**(11): p. 857-69.
106. Cazac, B.B. and J. Roes, *TGF-beta receptor controls B cell responsiveness and induction of IgA in vivo*. Immunity, 2000. **13**(4): p. 443-51.
107. McCartney-Francis, N., et al., *TGF-beta regulates production of growth factors and TGF-beta by human peripheral blood monocytes*. Growth Factors, 1990. **4**(1): p. 27-35.
108. Lucas, T., et al., *Differential roles of macrophages in diverse phases of skin repair*. J Immunol, 2010. **184**(7): p. 3964-77.
109. Li, M.O., et al., *Transforming growth factor-beta regulation of immune responses*. Annu Rev Immunol, 2006. **24**: p. 99-146.
110. Kumin, A., et al., *Peroxiredoxin 6 is required for blood vessel integrity in wounded skin*. J Cell Biol, 2007. **179**(4): p. 747-60.
111. Pfaffl, M.W., *A new mathematical model for relative quantification in real-time RT-PCR*. Nucleic Acids Res, 2001. **29**(9): p. e45.

7 Abbreviations

7-AAD	7-aminoactinomycin D
APC	allophycocyanin
α -SMA	α -smooth muscle actin
bFGF	basic fibroblast growth factor
bp	base pairs
BSA	bovine albumin
CCL2	chemokine (C-C motif) ligand 2
CD	cluster of differentiation
Cdh-5	cadherin 5
cDNA	copy deoxyribonucleic acid
Csf-1	colony stimulating factor
CTGF	connective tissue growth factor
d	dermis
DAPI	4',6-diamidino-2-phenylindole
DC	dendritic cell
Dll4	delta-like 4 protein
DMEM	dulbecco's modified eagle medium
DNA	deoxyribonucleic acid
DT	diphtheria toxin
e	epidermis
Ecf	eosinophil chemotactic factor
ECM	extracellular matrix
EDTA	ethylenediaminetetraacetic acid
EGF	epidermal growth factor
ELISA	enzyme-linked immunosorbent assay
FACS	fluorescence activated cell sorting
FCS	fetal calf serum
FDG	fluorescein di- β -D-galactopyranoside

Abbreviations

FITC	fluoresceinisothiocyanat
Fizz1	found in inflammatory zone
fl	floxed
Flk-1	fetal liver kinase-1
Flt-1	fms-related tyrosine kinase-1
g	granulation tissue
he	hyperproliferative epithelium
H&E	hematoxylin and eosin stain
HIF-1 α	hypoxia inducible factor-1 α
hpf	high power field
HSC	hematopoietic stem cell
ICAM	intercellular adhesion molecule
INF- γ	interferon- γ
i.p.	intraperitoneal
i.v.	intravenous
iDTR	inducible diphtheria toxin receptor
IL	interleukin
iNOS	inducible nitric oxide synthase
K14	keratin 14
kb	kilo base pairs
KDR	kinase insert domain receptor
KGF	keratinocyte growth factor
LPS	lipopolysaccharide
LysM	lysozyme M
M Φ	macrophage
MCP-1	monocyte chemotactic protein-1
MIP-1 α	macrophage inflammatory protein
MMP	matrix metalloprotease
NK cells	natural killer cells
Nrp	Neuropilin
p	p-value

Abbreviations

PBS	phosphate buffer saline
pc	panniculus carnosus
PCR	polymerase chain reaction
PDGF	platelet-derived growth factor
PE	phycoerythrin
PECAM	platelet endothelial cell adhesion molecule
PFA	paraformaldehyde
PIGF	placenta growth factor
PMN	polymorphonuclear
qPCR	quantitative polymerase chain reaction
Relm- α	resistin-like molecule- α
RNA	ribonucleic acid
ROS	reactive oxygen species
rp	red pulp
RT PCR	reverse transcriptase polymerase chain reaction
sc	subcutaneous fat tissue
SD	standard deviation
sm	skeletal muscle
st	scar tissue
sVEGFR-1	soluble vascular endothelial growth factor receptor-1
T _A	annealing temperature
TAM	tumor-associated macrophages
TAE	Tris base acetic acid EDTA
TE	Tris base EDTA
TGF	transforming growth factor
TNF- α	tumor necrosis factor- α
Th1	T helper 1 cells
Th2	T helper 2 cells
TLR	toll-like receptor
Tris	tris(hydroxymethyl)aminomethane
UV	ultraviolet

Abbreviations

VE-cadherin	vascular endothelial cadherin
VEGF	vascular endothelial growth factor
VEGFR	vascular endothelial growth factor receptor
VPF	vascular permeability factor
wp	white pulp
wt	wild type

Acknowledgements

I would like to thank Professor Matthias Hammerschmidt and Dr. Roswitha Nischt for reviewing my thesis. Further I would like to thank Professor Thomas Krieg for providing me the opportunity to join his department.

My sincere thanks to my supervisor Professor Sabine Eming who gave me the opportunity to join her group. I am very grateful for her professional support, for her motivating enthusiasm and also for giving me the opportunity to present my data on various international congresses.

I also wish to thank all members of the lab for creating this friendly atmosphere.

At this point I would like to thank our technicians Margot Junker and Michael Piekarek for cutting and staining tons of paraffin- and cryosections. Further, I have to thank Micha for his great computer skills, which rescued me quite a lot of times. I thank Sebastian Willenborg for establishing the wound cell isolation protocol and for helping me with this complicated FDG staining. I thank Johanna Knipper for helpful discussion and for her sunny disposition every day. I thank Rajeev Ranjan for taking the best wound pictures ever and for his great indian chicken. Finally, I would like to thank Daniel Hoffmann and Stephanie Traub for helpful discussion and developing of new ideas regarding the angiogenesis stuff. I have to thank Stephie also for her valuable time helping me several hours with the confocal microscope and for reading my manuscript.

I had a good time with you guys.

I would like to thank Gundula Grimberg and Anna Riese for helping me quite a lot with the qPCR and for providing me several primers. I have to thank Anna also for the good team work and the funny atmosphere in our office. I thank Jan Zamek for helping me always with the Nikon microscope in case of emergency.

Further, I would like to thank some former members of the department, Dr. Julia Scholten and Bettina Maar, for helping me with the first experiments and for teaching me all the mice stuff.

My sincere thanks to Christian Fork for his great support, sympathy and being a friend in need. Also many thanks to my family for their support during my whole studies.

I thank you for every single thing.

Erklärung

Ich versichere, dass ich die von mir vorgelegte Dissertation selbständig angefertigt, die benutzten Quellen und Hilfsmittel vollständig angegeben und die Stellen der Arbeit – einschließlich Tabellen, Karten und Abbildungen –, die anderen Werken im Wortlaut oder dem Sinn nach entnommen sind, in jedem Einzelfall als Entlehnung kenntlich gemacht habe; dass diese Dissertation noch keiner anderen Fakultät oder Universität zur Prüfung vorgelegen hat; dass sie – abgesehen von unten angegebenen Teilpublikationen – noch nicht veröffentlicht worden ist sowie, dass ich eine solche Veröffentlichung vor Abschluss des Promotionsverfahrens nicht vornehmen werde. Die Bestimmungen der Promotionsordnung sind mir bekannt. Die von mir vorgelegte Dissertation ist von Prof. Dr. Sabine Eming betreut worden.

Köln, den 09. Mai 2011

Tina Lucas

Teilpublikation:

Lucas, T., Waisman, A., Ranjan, R., Roes, J., Krieg, T., Müller, W., Roers, A. and Eming, S. (2010) Differential roles of macrophages in diverse phases of skin repair. *J Immunol*, 184(7):3964-77.

Curriculum vitae

Name Tina Lucas
Date of birth 4th October 1982
Place of birth Krefeld, Germany
Nationality german

Education

August 2007 - present *University of Cologne, Department of Dermatology.*
PhD student in Natural Sciences
Supervisor: Prof. Dr. Sabine Eming
Dissertation: Dynamics, regulation and function of macrophages in skin repair

**August 2006 -
June 2007** *University of Cologne, Institute of Pharmacology.*
Diploma thesis
Supervisor: Prof. Dr. Dirk Gründemann
Titel: „Der humane Transporter SLC22A14: Klonierung und Substratsuche“

**October 2002 -
July 2006** *University of Cologne, Studies in biology*
Diploma examinations: Genetics, Developmental biology and Pharmacology

June 2002 **Gesamtschule am Kaiserplatz, Krefeld**
Abitur

Poster

Tina Lucas, Ari Waisman, Thomas Krieg, Sabine A. Eming: Selective depletion of myeloid cells reveals distinct roles during the early and late phase of skin repair. 39th Annual Meeting of the European Society for Dermatological Research (ESDR), 2009, Budapest, Hungary

Tina Lucas, Ari Waisman, Thomas Krieg, Sabine A. Eming: Macrophages as sentinels directing the quality of skin repair. 38. Jahrestagung der Arbeitsgemeinschaft Dermatologischer Forschung (ADF), 2011, Tübingen, Germany

Oral Presentations

Macrophages as sentinels directing the quality of skin repair. Plenary Session at the 40th Annual Meeting of the European Society for Dermatological Research (ESDR), 2010, Helsinki, Finland

Differential roles of macrophages in diverse phases of skin repair. The work was awarded with the Young Investigator Award, 20th Annual Meeting of the European Tissue Repair Society (ETRS), 2010, Gent, Belgium

Differential roles of macrophages in diverse phases of skin repair. Young Investigator Award Session at the 21st Annual Meeting of the Wound Healing Society (WHS), 2011, Dallas, Texas, USA

Awards

European Tissue Repair Society (ETRS) Young Investigator Award 2010, Gent, Belgium

Publications

Tina Lucas, Ari Waisman, Rajeev Ranjan, Jürgen Roes, Thomas Krieg, Werner Müller, Axel Roers and Sabine Eming (2010) Differential roles of macrophages in diverse phases of skin repair. *J Immunol*, 184(7):3964-77.

Stephanie Traub, **Tina Lucas**, Daniel Hoffmann, Thomas Krieg, and Sabine A. Eming. Design of a novel Protease-resisten vascular endothelial growth factor-A Protein for angiogenic therapy. (Yearbook of the American Wound Healing Society 2010; Advances in wound care:Vol 1, chapter 58)

Anke Batsch, Andrea Noetel, Christian Fork, Anita Urban, Daliborka Lazic, **Tina Lucas**, Julia Pietsch, Andreas Lazar, Edgar Schömig and Dirk Gründemann (2008) Simultaneous fitting of real-time PCR data with efficiency of amplification modeled as Gaussian function of target fluorescence. *BMC Bioinformatics*, 9:95.

